Ministry of Higher Education &

Scientific Research

University of Babylon

College of Science / Chemistry Department

Estimation and Adsorption of Chloramphenicol and Clonazepam on the Surface of Hydrogel / CNT/ZnO Nanocomposite

A Thesis Submitted to the Council of College of Science

University of Babylon in Partial Fulfillment of the Requirements

for the Degree of Doctor Philosophy in Chemistry

By

Lubna Abd Al-Hussain Abd Al-Ameer Al-Shik

B. Sc. University of AL-Nahrain / 2004

M. Sc. University of AL-Nahrain / 2007

Supervised By

Prof. Dr. Abbas Noor Mohammed Al-Sharify

Prof. Dr. Ayad Fadhil Mohammed Alkaim

2023 A.D **1444 A.H**

Supervisor Declaration

I certify that this thesis **" Estimation and Adsorption of Chloramphenicol and Clonazepam on the Surface of Hydrogel / CNT/ZnO Nanocomposite"** has been prepared under my supervision at Chemistry Department –College of Science/Babylon University, as a partial requirement for the degree of philosophy doctor in analytical chemistry.

Signature:

Supervisor: Prof. Dr. Abbas Noor Mohammed Al-Sharify

Date: / /2023

Signature:

Supervisor: Prof. Dr. Ayad Fadhil Alkaim

Date: / /2023

Forwarding for debate

In view of the available recommendations, I forward this thesis for debate by the examining committee.

Signature:

Name: Prof. Dr. Abbas Jasim Atiyah

Title: Head of Chemistry Department - College of Science/Babylon University

Date: / /2023

Dedications

- To my parents, the most sacrifices

- To the light that enlight my way and with him the difficulties are eased; my husband

- To my Sons

- To my brothers and sister

-To all the honest

To all of them, I dedicate this work.

Lubna

Acknowledgments

First, I would like to thank Allah for his merciful and his continuous help over all the period of my life.

I would like to express my great appreciation to my supervisors Prof. Dr. ***Abbas Noor Alshirify*** and Prof. Dr. ***Ayad Fadhil Alkaim*** for their supervision, encouragement, helpful advice and their suggestion subject of the thesis.

I would like to express my gratitude to Assit. Prof. Dr. ***Aseal Mushtaq Aljeboree*** for their generous help, assistance and support during my study.

I thank the University of Babylon and College of Sciences for Girls, for giving me this great opportunity to achieve my goal in completing my PhD degree.

Finally, and most importantly, I must thank my dearest family for giving me the support and encouragement that only a family can give.

Lubna

Summary:

The current study is divided into two sections. **Part one:** To determine the presence of clonazepam (CLZ) and chloramphenicol (CHL) in pharmaceutical formulations, the first step entails developing and validating a straightforward, quick, and sensitive spectrophotometric approach. The procedure is based on the azo coupling process, which transforms a diazotized medication into a stable pinkish-red azo molecule that exhibits maximum absorption at wavelengths of max 453 nm and 532 nm for CHL and CLZ, respectively, in an alkali solution. The factors that affect the stability and growth of the reaction product were carefully examined and optimized. Beer's law is obeyed by the suggested approach in the concentration ranges of (0.5-17) and (1.2-26) g mL^{-1} with correlation coefficients of R^2(0.9982) and (0.9989) for CHL and CLZ , with molar absorption coefficients of $3.57*10^4$ and $2.56*10^4$ $L.mol^{-1}.cm^{-1}$ for CHL and CLZ , Sandell's sensitivities were discovered to be 0.013 and 0.0184 $g.cm^2$ for CHL and CLZ , limits of quantitation (LOQ) were found to be 0.355 and 0.908 g mL^{-1} and limits of detection (LOD) to be 0.117 and 0.299 g mL^{-1}, respectively.

Part Two: Synthesis of a new (Sodium alginate g- poly (Acrylic acid –co Acryl amid)/Zinc oxide-carbon nanotube, (SA-g-P(Ac-co-AM)/ZnO-CNT) hydrogel composite. N,N'-Methylenebisacrylamide (MBAA) is used as a cross-linking agent in the synthesis in accordance with the free radical polymerization of acrylic acid for sequestration of two drugs clonazepam (CLZ) and chloramphenicol (CHL) . Through the use of thermogravimetric analysis (TGA), scanning electron microscopy (SEM), transmission electron microscopy (TEM), X-ray diffraction (XRD), Surface Area Analyzer (BET) and EDX analysis. hydrogel composite was characterized. Due to their great adsorption capability, the synthetic

hydrogel composite was used to remove the (CLZ) and (CHL) drugs from the genuine sample. The factors that determine adsorption efficiency, such as initial drugs concentration, pH solution, adsorbent dose, and contact time, were thoroughly investigated and adjusted. When comparing isotherm Freundlich and Langmuir models, the results of the adsorption isotherms revealed that there is a very strong agreement in the Freundlich model. The hydrogel composite effective adsorption capability for the elimination of both drugs and organic contaminants was in the range of 78–83%. In addition, the understanding of the regeneration, recovery, and reuse of hydrogel-based adsorbent materials provides a detailed explanation of the synthesis and adsorption mechanisms. Therefore, a long-term solution for drug removal may be offered by the economical, simple, adaptable, and biodegradable hydrogel. Also comparative adsorption between different surfaces to removal two drugs a comparison of CNT/ZnO, hydrogel, and hydrogel composite surfaces was conducted. The order of increasing hydrogel composite > hydrogel > CNT/ZnO .

List of Contents

List of Tables

List of Figures

List of Abbreviations

Shorten	Full name
T	Absolute temperature
Abs	Absorbance
pH	Acidic function
q_e	Amount of adsorbate per unit weight of adsorbent at equilibrium
BET	Brunauer-Emmett-Teller
ΔH	Change of enthalpy
ΔS	Change of entropy
Conc.	Concentration
R^2	Correlation coefficient
K_e	Distribution coefficients
EDX	Energy Dispersive X-Ray
K_{eq}	Equilibrium constant
C_e	Equilibrium dye concentration
FE-SEM	Field emission scanning electron microscopy
FT-IR	Fourier Transform Infrared
K_f	Freundlich constant
ΔG	Gibbs free energy
Q	Heat of adsorption
C_o	Initial Concentration
k_L	Langmuir constant
M	Mass of adsorbent
Q_m	Maximum adsorbed
X_m	Maximum adsorption
q_m	Maximum Adsorption Capacity

λ_{max}	Maximum wavelength
NP	Nanoparticles
PEI	Poly Ethylene Imine
E%	Removal percent
q_t	The amount of adsorbent at a given time
k_1	The pseudo-first-order rate constant
K_2	The pseudo-second-order rate constant
TGA	Thermal gravimetric analysis
T	Time
TEM	Transmission electron microscopy
UV–Vis	Ultraviolet-Visible Spectroscopy
R	Universal gas constant
XRD	X-ray diffraction spectroscopy
C_t	Concentration after different time of irradiation
CB	Conduction band
e^-/h^+ pair	Electron-hole pair
eV	Electron Volt
E_g	Energy gap
AOPs	Advanced Oxidation Processes

Chapter One

Introduction

1.1 General Introduction

The most pervasive significant issue that has led to an ecosystem defect and is also a risk to human life is pollution. As a result, it is challenging to find clean water where there is a lot of wastewater. It has been discovered that all industrialized nations have an elevated rate of water contamination that negatively impacts human health [1]. Heavy metals, oils, and dyes are the substances that pose the greatest risk. Particularly, organic dyes are produced in numerous local industries, including textile, paper, plastic, leather, food, and cosmetics [2]. Even at incredibly low concentrations, textile dyes provide vibrant color. These colors are stable to light, biological, and chemical treatments, non-degradable, and bioaccumulative in living things. Additionally [3, 4]. exhibit high levels of biotoxicity and have the potential to cause cancer and mutagenesis [5]. Water dye pollution tends to block light from penetrating, which has a significant negative impact on photosynthesis. Due to their intricate structure and manufacture, many dyes are challenging to remove from contaminated water solutions. Using conventional methods to remove these dyes is ineffective .Ion exchange, coagulation/flocculation, adsorption, chemical oxidation, ozone treatment, membrane filtering, sono-chemical and electrochemical procedures, photocatalysis, etc. are a few techniques that can be utilized to remove these colors with great efficiency[6-9]. Adsorption is regarded as an innovative technology among them because of its great effectiveness, simple construction, and cost-efficiency. Researchers have given nanotechnology a lot of attention during the last few decades. This interest may be seen in the enormous rise in the production of nanomaterials worldwide[10]. Nanotechnology is defined as the study of understanding, manipulating, and using materials with dimensions

between one and one hundred nanometers. A large-scale initiative called nanotechnology aims to minimize materials, tools, and equipment. This method greatly attempted to improve the properties of nanoparticles and create new nanomaterials with distinctive qualities in addition to reducing the size of the nanomaterials generated [11]. It is noteworthy that chemistry controls the stages of the formation and dissolution of linkages between atoms in chemical reactions, which plays a significan;;;;;t role in the development of nanotechnology. They have developed mastery over chemical processes and the ability to create materials as nanoparticles of various sizes and forms, including metal oxide nanoparticles, nanosuspension, and nanocomposite [12].

pharmaceuticals used in agriculture, animal care, and human health promotion applications. Drugs known as antibiotics are frequently used to treat or prevent microbial illnesses [13] Through pharmaceutical and wastewater treatment facilities, they are discharged into the water. Pharmaceuticals are characterized as bio-accumulative contaminants that can affect terrestrial or aquatic ecosystems [14] . Antibiotics cannot be completely eliminated by oxidation processes since they are slow and difficult. Because of its great effectiveness, simplicity, and economics, adsorption as a physical approach is the most suitable and effective treatment option for eliminating organic pollutants [15, 16]

1.2. Pharmaceutical removal in water treatment methods

Several of the methods used to remove pharmaceutical pollutants are illustrated below.

1.2.1 The Conventional Removal Methods

Microorganisms as a therapy are ineffective because of the complicated composition and low concentration of organic chemicals in water, with fewer than 10% of contaminants being eliminated. While chlorine dioxide is a safer alternative to chlorine, it reacts only with phenoxides and tertiary amine, making chlorine the most common source of toxic chlorinated compounds in drinking water. Ozone is more powerful than oxygen at oxidizing drugs [17].

1.2.2 Technologies Based on Advanced Oxidation Process(AOPs)

These reactions rely on the production of free radicals, where the extremely reactive hydroxyl radical (•OH) can destroy the majority of organic compounds. Numerous photo-catalytic AOPs can completely destroy a variety of pharmaceuticals [18].

1.2.2.1 Ozonation

Ozone is a potent oxidant that breaks down in water to produce hydroxyl radicals, which then cause some functional groups of organic molecules to indirectly oxidize. In addition, therapy is improved when hydrogen peroxide is added [19].

1.2.2.2 Fenton Oxidation

As more hydroxyl radicals are produced (homogeneous photo-catalysis), the reaction between ferrous ions and hydrogen peroxide, in

which ferrous iron serves as the catalyst, is enhanced. This process has the potential to mineralize a significant portion of contaminants, reducing their toxicity and increasing the effluent's susceptibility to biological post-treatments [20].

1.2.2.3 UV Radiation

Due to the presence of aromatic rings, heteroatoms, and other functional groups, the majority of medicines absorb light and are photodegradable. Water disinfection and the treatment of pharmaceutically contaminated wastewater are both accomplished with UV light [21].

1.2.2.4 Photo electrocatalysis

Numerous studies have revealed that TiO_2 is the most prevalent photo catalytic catalyst that effectively eliminates pharmaceutical residues [22, 23].

1.3 Adsorption

Adsorption is a phenomenon on surfaces when molecules, ions, or even whole atoms of one substance stick to the surface of another. An "adsorbent" is a substance on which deposition or adsorption takes place, as opposed to a "adsorbate," which is the substance that is deposited or adsorbed. Adsorption is known as monolayer adsorption when the adsorbate only forms a single layer on the surface of the adsorbent. Adsorption is known as multimolecular adsorption when many layers are deposited. Desorption is the process by which an absorbed substance is liberated from the surface of an adsorbent [24-26].

According to the way substances attach to the absorbent surface, there are two different types of absorption processes. (Fig. 1.1) [27]:

A. Physical Adsorption (Physisorption): Van der Waal's force, a mild physical force, causes the absorbate substance to stick to the surface of the absorbent in this form of absorption.

B. Chemical adsorption, also known as chemisorption, happens when the solid absorbent has an electron-unsaturated surface that forms a covalent bond with the absorbate material.

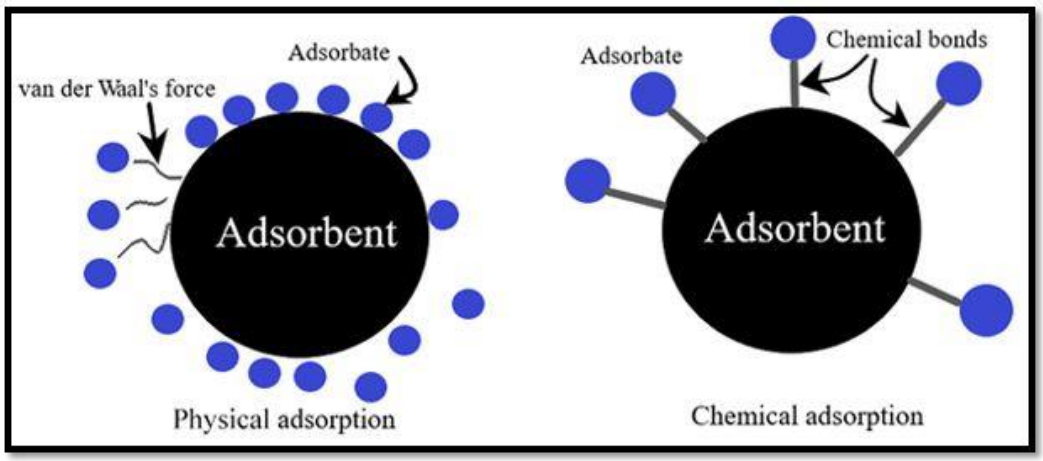

Figure 1.1 Physical adsorption versus chemical adsorption.

Since the start of the industrial revolution, the amount of pollution in the world has risen yearly as a result of the construction of numerous factories in numerous nations around the world in a variety of industries, including medicine, agriculture, textiles, and the military [28].

Scientists all over the world, particularly in industrialized and developed nations, have tended to pay attention to this topic and to establish worldwide committees for environmental preservation as a result of the major growth in pollution concerns in recent decades. They concentrate on creating procedures to lessen or handle pollution caused by or after manufacturing. Large amounts of hospital waste and pharmaceutical factories include high concentrations of pharmacetical

compounds and raw materials for medication manufacture in medicine. (Fig. 1.2) *[29-32]*.

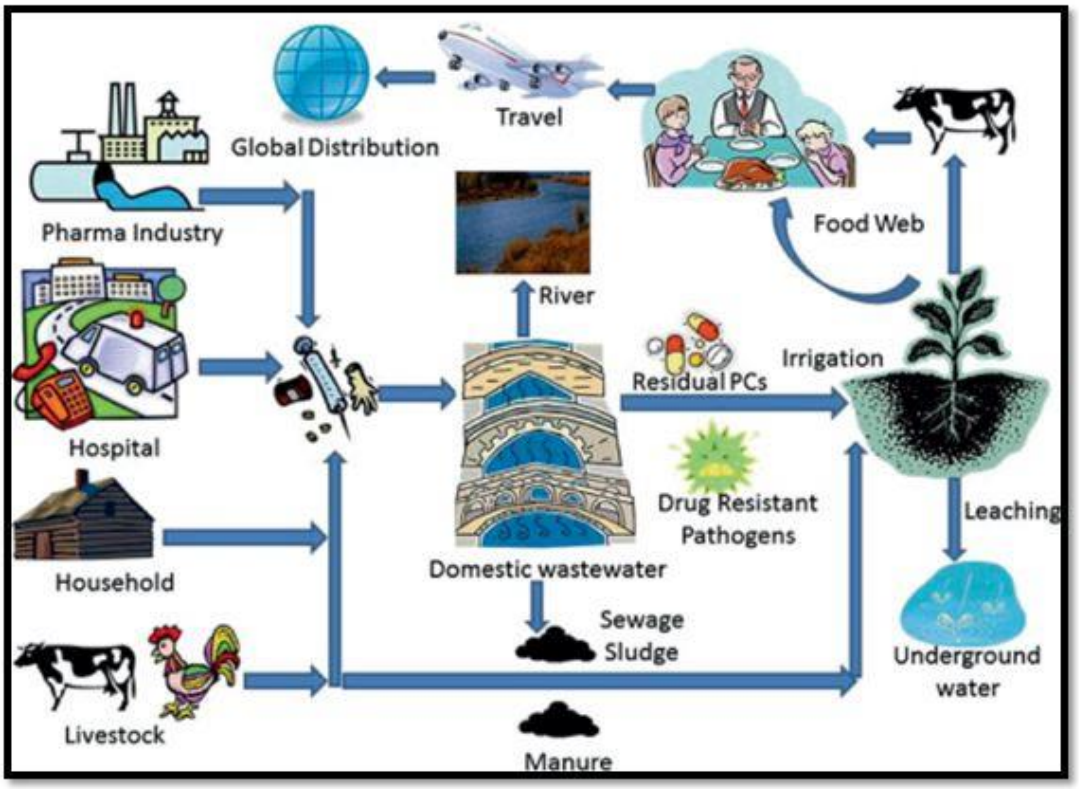

Figure 1.2 medicines' movement through an ecosystem's life cycle, from sources to receptors.

The committees have the power to create programs and plans that govern how different wastes are disposed of in the air, land, and sea. They can also pass laws that require chemical factories to subject their products to numerous tests to determine how quickly they degrade in nature, how concentrated they are in food chains, how much influence they have on genes, and how frequently they cause cancerous diseases[33].

Adsorption, which is regarded as the most successful technique utilized in the separation and purification processes, is one of the most effective approaches that complies with the international committee's recommendations. The adsorption technique was widely utilized for

eliminating pharmaceutical compounds and industrial dyes in varied waste water, according to a recent literature review of waste treatment and green chemistry techniques Figure (1.3). [34].

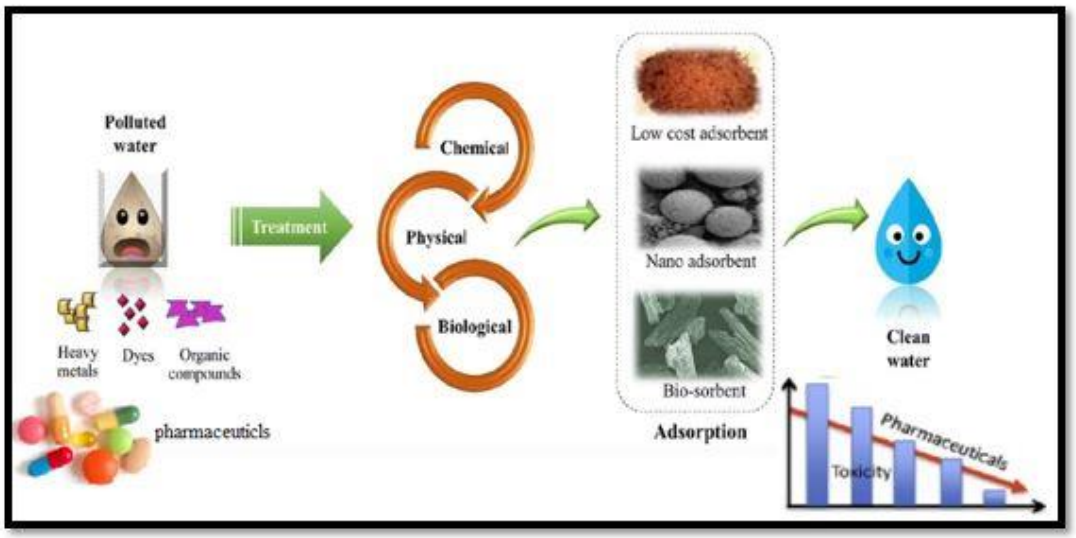

Figure 1.3 Contribution of adsorption process in the treatment of polluted water.

Furthermore, the researchers created a highly efficient absorbent for waste water treatment and are constantly developing new materials with high adsorption efficiency. Among these materials:

1.3.1 Factor Influencing Adsorption Process

1.3.1.1 Concentration of Adsorbent:

Adsorbent dose is an important element that must be carefully regulated during wastewater treatment. Initially, the quick rise in adsorption with increased adsorbent dosage was attributed to the availability of more adsorption sites [35] The amount of adsorption capacity would decrease as the adsorbent dose is increased further; the decrease in adsorption was caused by the concentration gradient between adsorbent and adsorptive. [36] .

1.3.1.2 Concentration of Adsorbate:

The initial concentration acts as a powerful motivator to overcome all mass transfer resistances of all molecules between the aqueous and solid phases [37]. The percentage of dye removal dropped as the starting dye concentration increased, while the actual amount of dye adsorbed per unit mass of adsorbent increased. This rise is attributed to a decrease in barrier to solute uptake from dye solution. Because the initial concentration is a significant driving force in overcoming dye mass transfer resistance between the aqueous and solid phases,[38,39] .However, in some cases, adsorption may be limited to a single layer of adsorbed molecules. Adsorption cannot be increased further because the surface of the adsorbent's crystal lattice is covered [40].

1.3.1.3 Surface Area and pore size of Adsorbent:

The specific surface area and pore volume are the most important adsorption factors for substances [41] . As a result, when the surface area grows, it relates to high active sites, which create an increase in adsorption capacity [42]. The pore structure of the adsorbents impacts dye adsorption in two ways : (1) Adsorption of adsorbates of a particular size and shape is limited by size exclusion (sieve effect), and (2) The adsorption capacity may rise as the particular pore volume increases [43].

1.3.1.4. Temperature:

It is generally known that temperature affects the adsorption process significantly [44]. The effective layer thickness for adsorption reduces as grows. That refers to the adsorption procedure in general. This can be explained by the exothermic spontaneity of the adsorption process and by the weakening of interactions between dye molecules and the active sites of adsorbents at high temperatures [39] .

1.3.1.5 Effect of pH:

The ability of adsorption may grow, decrease, or remain unchanged as a result of changing pH because within a range of pH values, the structure of dyes will vary, and the adsorption process will be affected by this shift as well [45]. The degree of ionization and speciation of various contaminants, as well as the surface charge of the adsorbents, are all influenced by the pH of the solution. Changes in pH have an impact on the adsorptive process by causing the functional groups of the active sites on the adsorbent's surface to dissociate [46] .

1.3.1.6. Ionic Strength:

One of the variables that affects the electrostatic and non-electrostatic interactions between the adsorbate and the adsorbent surface is the ionic strength of the solution [38] .

The solubility of ionic salts affects the adsorption process since it can either increase or decrease adsorption depending on how well the ionic salts can dissolve in comparison to the adsorbent substances [47].

Ionic salts' solubility has an impact on the adsorption process since it can either increase or decrease adsorption depending on how well they dissolve in comparison to adsorbent substances [48].

1.4 Nanomaterials

Ionic salts' solubility has an impact on the adsorption process since it can either increase or decrease adsorption depending on how well they dissolve in comparison to adsorbent substances [48]. Nanotechnology is described as science, engineering, and technology associated to how to understand, control, and use materials whose dimensions are between 1-100 nanometers. Nanotechnology is a huge project aimed at reducing substances, instruments and tools. This technique not only reduced of the

size of nanomaterials produced, but also greatly sought to enhance the properties of nanomaterials and the invention of new nanomaterials with unique properties [49]. It is noteworthy that chemistry plays a main role in the development of nanotechnology by controlling the stages of formation and breakdown of links between atoms in chemical reactions. They have gained control over chemical processes, the capability to synthesize materials as nanoparticles of different shapes and sizes, such as nanosuspention, nanocomposite, metal oxide nanoparticles, etc. [50]. Many nanomaterials have been used for water and wastewater treatment as adsorbents, in membrane filters, photo catalysis, microbial control and sensing [51].

The word "nanomaterial" refers to a wide range of substances with particles that have 1 or 2 dimensions and a nanometer size range of 1–100 nanometers. where the nanoscale is roughly a thousand times smaller than the micrometer [52]. Atoms and microstructures are connected via nanomaterials. Nanomaterials are far closer to atomic-scale dimensions. For comparison, the distance between regular carbon atoms in a molecule, or their length bond, is between 0.15 and 0.12 nm. The shape, size, and chemical makeup of nanoparticles, for example, which might change depending on how they are created, have an impact on the attributes of nanomaterials. Because nanomaterials have excellent properties and can be used in novel applications, there is a difference. [51]. The characteristics of the identical materials' nanostructures, including their chemical, electrical, spectral, magnetic, and many other properties, varied greatly from their microstructures. . Gold nanoparticles, for example, can change color from yellow to red or blue as they shrink to the nanoscale, while semiconductors like titanium dioxide can connect as they get smaller to the nanoscale. [53].

1.4.1. Properties of Nanomaterials

Due to the existence of two significant variables, specifically the expansion of the specific surface area and the quantum effects, nanomaterials differ from other materials in their properties. Additionally, we observe that many nanomaterials have increased surface-to-volume ratios that give rise to novel quantum mechanical effects. For instance, the "quantum size effect" causes solids' electrical properties to alter as they are shrunk to nanometers. When the material is at the nanoscale, an effect that cannot be produced when it is in the macro dimension or microstructure occurs. By demonstrating how some physical characteristics can change when a tiny system is involved. The unique characteristics of nanomaterials have increased researchers' interest in the field [54-56].

1.4.1.1. Electrical Properties

These characteristics vary between metallic and semiconducting materials in the nanoscale range. It depends on the nanoparticles' diameter. Because of the structure's few defects, nanomaterials have good electrical conductivity.

1.4.1.2. Thermal Conductivity

The high heat conductivity of nanomaterials is caused by the shaking of the covalent bonds. Ten times higher than the mineral, it has a high heat conductivity. Due to the structure's few distortions, nanomaterials have strong heat conductivity.

1.4.1.3. Mechanical Properties

Nanomaterials are incredibly resilient and can withstand great pressure. In contrast to nanoparticles, which have few structural deformities, many materials degrade as a result of structural flaws.

1.4.2 Classification of Nanomaterials

Depending on whether they are manufactured or natural, nanomaterials can be categorized. For instance, while fuel fire smoke is regarded as an industrial source of production, volcanic ash is a naturally occurring product. [57]. According to the diameters of their X, Y, and Z particles, which are subjected to this nanoscale as shown in Figure (1-4), nanomaterials can be divided into the following four primary categories:

1.4.2.1 Zero-Dimensional Nanostructures

Are the nanostructures with Lx, Y, and Z all-external dimensions less than 100 nm. This category contains spherical nanoparticles and quantum dots. [58].

1.4.2.2 One-dimensional Nanostructures

A scale of less than 100 nm corresponds to two exterior dimensions in nanomaterials. The micrometer (Lz>100nm) is the last dimension. Nanowires, nanotubes, and nanofibers fall under this group. [59] .

1.4.2.3 Two-dimensional Nanostructures

Are nanomaterials such as nanosheets and monolayers, whose second dimension is larger than 100 nm and whose first dimension is the nanometer [60] .

1.4.2.4 Three-dimensional Nanostructures

The structures in this latter category, such as nanocomposite, which consists of multiple phases provided one of the solid phases is subjected to nanoscale transformation, exhibit nanoscale properties as a result of their internal nanoscale dimensions but lack an outer nanoscale dimension. [61] .

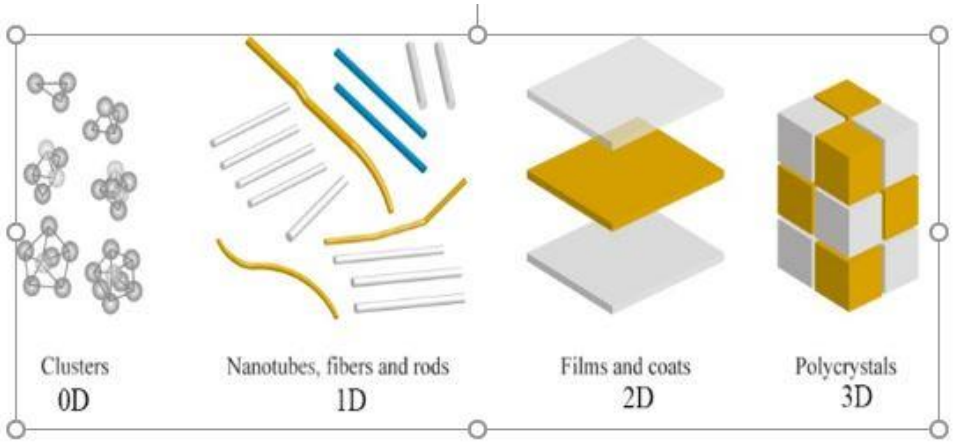

Figure (1-4): A system for classifying nanoparticles based on their dimensions.

1.5 Synthesis Methods of Nanomaterials

1.5.1 The Top-down Approach

This idea demonstrates how large-scale materials can be converted into nanoparticles. These structures are gradually disintegrating as a result of unique modifications that cause particles to become nanoscale. To create nanomaterials, a variety of methods are used, including grinding and mechanical milling. [62] either dry etching or wet etching techniques [63] .

1.5.2. The Bottom-up Approach

The foundation of this approach is the exact opposite of the preparatory strategies mentioned above. Through the homogenous or heterogeneous nucleation of molecules or atoms of liquid or gaseous material, nanomaterials are created. Since chemical processes make up the majority of the techniques used in this field, the work is based on the precise control of chemical reactions that result in the collection of partial or atomic components for nanoparticles. Sol-gel, sedimentation, chemical vapor deposition, ultrasound synthesis, solvothermal process, electro deposition, reverse micelle, and microwave synthesis are just a few of the numerous techniques used in this methodology [64].

1.5.3 The Bottom-bottom Approach

Using high-precision equipment, such as scanning tunneling microscopy, an atomic force microscope, or photolithography, these techniques require moving the atom by another atom or nanoparticle by another nanoparticle to its stated place [65].

1-6 Hydrothermal Process for Synthesis of Nanomaterials

These techniques entail moving the atom one atom at a time or a nanoparticle one nanoparticle at a nanoparticle to where it is thought to be using high-precision tools like scanning tunneling microscopy, an atomic force microscope, or photolithography. It is possible to define hydrothermal synthesis as a process for creating single crystals that relies on a metal's solubility in hot, aqueous solution under high pressure [66].Where the process of growth of the crystals in a steel pressure vessel called an autoclave ,in which a nutrient is provided along with water. The process is also excellent for growing massive, high-quality crystals while maintaining compositional control [67] as shown in Figure (1-5).

Figure (1-5): Hydrothermal synthesis frequently performed in an autoclave

1.7 Multiwall carbon Nanotubes (MWCNT)

It is a nanostructure with a cylindrical shape made of a fused and coil-like carbon skeleton composed of six-member rings. The constructed tube comprises more tubes inside of it that were also created in the same way *Figure (1.6)*

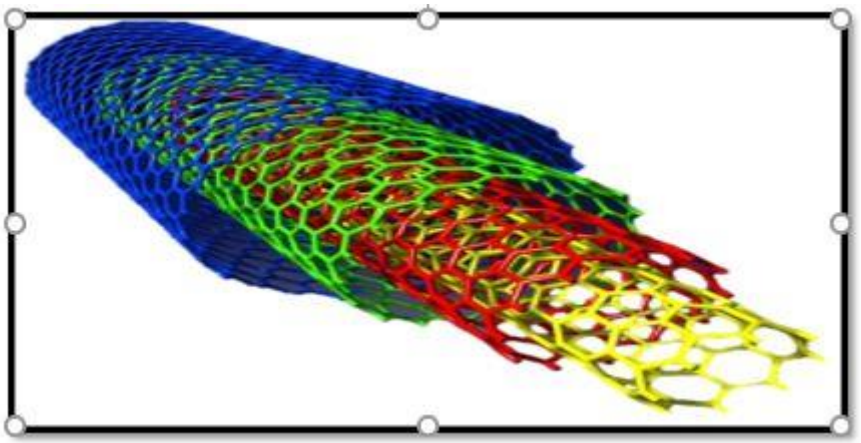

Figure 1.6 Carbon nanotubes with many walls and their geometric structure.

The most effective adsorbent materials are multi-walled carbon nanotubes because of their small size, huge surface area, and hollow layered structure [68]. Recently, the researchers have paid great attention to MWCNT as it has high efficiency for removing heavy metals, pesticides, oil, industrial dyes, and pharmaceutical substances from waste water[69-72]. Table (1.1) illustrates some of the new synthesized MWCNT-based material as an efficient adsorbent for pharmaceutical products.

Table 1.1 The most common recently synthesized MWCNT-based adsorbent for pharmaceuticals removal.

Nanoadsorbent	pharmaceutical removed	Adsorption capacity	Ref.
polyaniline/MWCNT composite	Meloxicam	221.2 mg g^{-1}	[73]

MWCNT	Tetracycline	135 mg g^{-1}	[74]
MWCNT-Composite	Ethynilestradiol	2.5–4.5 mg m^{-2}	[75]
Fe_3C@NCNTs	sulfamethoxazole	----	[76]
Co@CoO/NC	Tetracycline	385.60 mg. g^{-1}	[77]
MWCNs-C/$CoFe_2O_4$ composites	sulfamethoxazole	354 mg. g^{-1}	[78]
	17β-estradiol	30 mg. g^{-1}	
MWCNTs-N/$CoFe_2O_4$ composites	sulfamethoxazole	17826 mg. g^{-1}	
	17β-estradiol	31.8 mg. g^{-1}	
MIL-100(Fe)-CNTs Composite	Oxytetracycline	429 mg·g^{-1}	[79]
MWCNT/NH_2-MIL-53(Fe) Composite	Tetracycline.HCl	368.49 mg g^{-1}	[80]
	Chlortetracycline.HCl	254.04 mg g^{-1}	
$MnFe_2O_4$/ MWCNTs Composite	Tetracycline	494.91 mg g^{-1}	[81]
CNTs/L-cys@GO/SA hydrogels	Ciprofloxacin	200 mg g^{-1}	[82]

1-8 Zinc oxide–based hydrogels

Zinc oxide (ZnO) can be found in nature as a zincite mineral; however the majority of it is prepared synthetically. Its crystal structure can be found in a hexagonal wurtzite form or cubic zinc blende .The form that is most stable and commonly found at ambient temperature is the wurtzite structure. ZnO is commonly used for treating skin-related problems such as nappy rash, dandruff and incorporation in ointments used in wound dressing [83, 84].where adsorbent hydrogel incorporated with ZnO nanoparticles was used for removing pollutant from water. The group reported that incorporating ZnO nanoparticles improved the recovery of the adsorbent from the aqueous solution after the removal of

pollutant . Also , hydrogel was modified with ZnO for antimicrobial activity, Therefore, looking at these properties, the ZnO would be ideal for preparing hydrogels for adsorbing pollutant [85, 86].

1.9 Hydrogel

Hydrogels are a three-dimensional network that belong to the family of water-insoluble cross-link polymers with hydrophilic properties, which make these polymers swell seven to ten orders of magnitude larger than their original size as a result of absorbing a large amount of water *Figure* (1.7) [87-90]. These polymers are affected by pH, Temperature, ionic strength, and existence of some compounds [91]. The cross-link structure of these polymers is held together as water-swollen gels by: (1) polymer crystallites; (2) hydrophobic interactions; (3) bio-recognition interactions or affinity; (4) hydrogen bonds; (5) ionic forces; and (6) primary covalent cross-links [92].

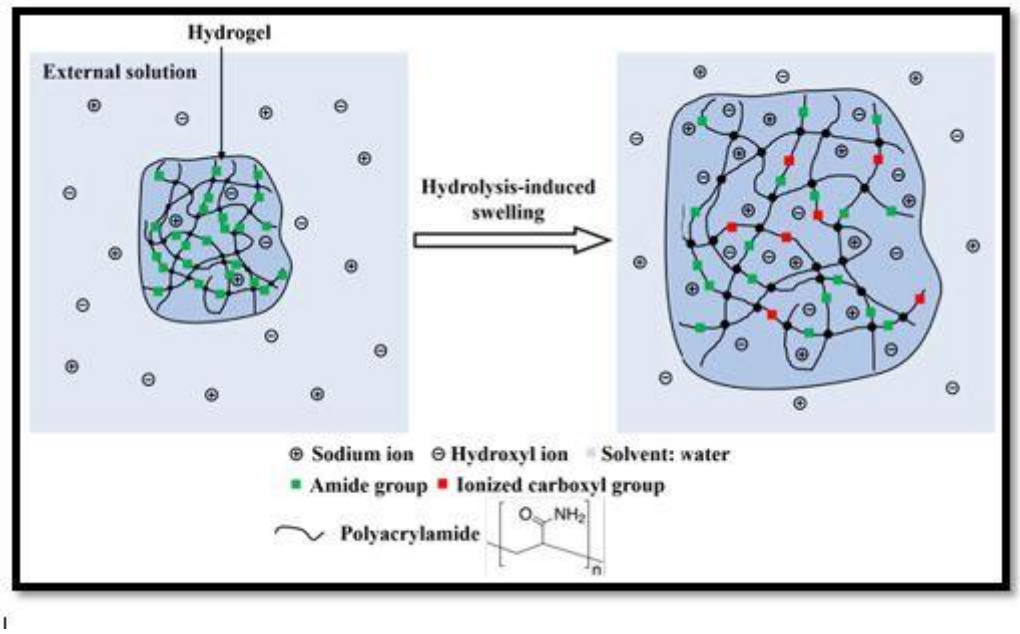

Figure 1.7. Polyacrylamide-derived hydrogel with its swelling process in water.

Hydrogels have several applications in numerous fields of ecosystem. In medicine, it is used as a salve to promote healing of the injured or burned skin, as well as in aesthetic medicine [93]. Moreover, due to the high tendency of these polymers to absorb large amounts of water, they have been used in the preconcentration technique for a decade [94].

Recently, it has attracted great attention in the purification and water treatment fields as they have a high tendency to extract heavy metals, pesticides, oil, industrial dyes, and pharmaceutical substances from waste water [95] **Table (1.2).**

Table 1.2 The most common recently synthesized Hydrogel-based adsorbent for pollutants removal.

Hydrogel	Pollutant removed	Adsorption capacity mg g^{-1}	Ref.
Agar-graphene oxide hydrogel	Chloroquine diphosphate	63	[96]
	Safranin-O	100	
Tripeptide hydrogel	Rhodamine B	-------	[97]
	Reactive blue 4		
	Direct red 80		
NFe_3O_4@Zn(GA)/Starch-Hydrogel	Fluvastatin statin	782.05	[98]
3D graphene oxide hydrogels	Naproxen	360	[99]
	Ibuprofen	466	
	Diclofenac	489	
N-PSPB/starch hydrogel	Chromium (VI)	420.13	[100]
	Naproxen	309.82	
HIPS/SA hydrogel	Cu(II)	25.81	[101]

graphite oxide hydrogel	Ofloxacin	134	[102]
sodium alginate/polyethyleneimine hydrogel	Methyl blue	400	[103]
Peptide hydrogel	Diclofenac sodium	-----	[104]
Peptide hydrogel	Pb^{2+} and Cd^{2+}	-----	[105]

1-10 Adsorption Isotherms:

Adsorption isotherms the amount that is adsorbed on the surface in terms of pressure (if gas) or concentration (if liquid) at a constant temperature [106]. The most important of these isotherms in the application are:

1-10-1 Langmuir Isotherm:

Assumes that the molecules are adsorbed on a fixed number of adsorption sites on the surface of the adsorbate material. These sites are equally energy-efficient, and each site can be occupied by only one molecule. These particles are not interfering with each other or with other molecules in the solutions. Thus, one layer of adsorbed particles will form on the surface of the adsorbate material. Langmuir isotherm can be expressed mathematically as follows[107]:

$$q_e = \frac{q_m K_a C_e}{1 + K_a C_e} \qquad (1\text{-}1)$$

Where Ce the residual concentration, qe ,qm is the adsorption capacity at equilibrium and the maximum adsorption capacity respectively, Ka Langmuir constant. The linear form of the equation of Langmuir isotherm is according to the following equation [108]:

$$\frac{C_e}{q_e} = \frac{C_e}{q_m} + \frac{1}{K_a q_m} \qquad (1\text{-}2)$$

1-10-2 Freundlich Isotherm:

The Freundlich equation is one of the most important used isotherms in the case of adsorption of solution. This model assumes that the surface of the adsorbate material is heterogeneous because of the different energy levels for adsorption sites, and adsorption does not reach saturation. The mathematical relationship of the Freundlich isotherm can be expressed as follows[109]:

$$q_e = K_f C_e^{\frac{1}{n}} \qquad (1\text{-}3)$$

K_f is a Freundlich constant and their values depend on the nature of the absorbent material, the surface, and the temperature. The linear form of Freundlich isotherm can be expressed as follows:

$$\log q_e = \log k_f + \frac{1}{n} \log C_e \qquad (1\text{-}4)$$

1.11 Spectrophotometry

Spectrophotometry is a one branch of electromagnetic spectroscopy which deals with the measurement of the interaction of light with materials. It considers a global and inexpensive technique in which the incident light passed through the sample solution undergoes absorption or transmission by the chemicals inside the solution. spectrophotometry is most commonly applied to ultraviolet, visible, and infrared radiation[113-115].

The device used to produce and measure the light intensity transmitted through the sample solution is called a spectrophotometer which

comprise from two instruments – a photometer and spectrometer. The spectrometer provides the initial incident light from deuterium or tungsten lamp with a given wavelength. However, the photometer measures the transmitted light intensity passed through the sample solution[116].

Spectrophotometers **Figure (1.8)** also consist of a source of light in the UV-Visible range, wavelength selector, sample cell holder, detector, and computer with data processing software program[117].

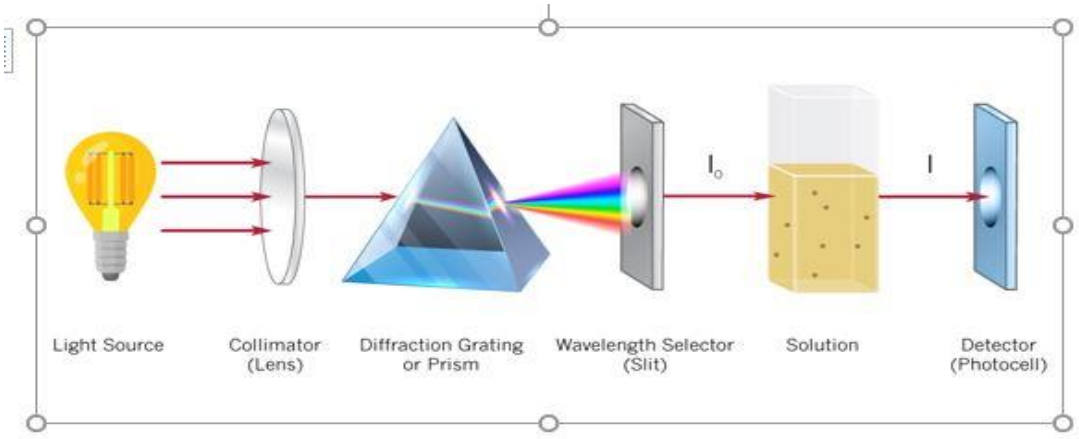

Figure 1.8 The main apparatus of a typical single beam spectrophotometer

In spectrophotometry, a beam of light produced from tungsten or deuterium lamp with a certain wavelength within the range of (180 to 800 nm) passes through the cuvette that contained a sample solution. The sample then absorb a part of incident light and transmit the other. According to Beer's law (*equation 1.4*) The analyte concentration is directly proportional to the absorbed light[118].

$$A = \varepsilon bc \qquad (1-5)$$

Where A = absorbance of light at a specific wavelength

Ɛ = molar Absorptivity (if solution concentration in mole/L), or a = Absorptivity (if the solution concentration in mg/L)

C = sample concentration

b = The optical path length of sample solution

if the solution concentration in 1 w/v % or (1mg/100mL) in 1 cm optical path length, the molar absorptivity then called specific absorbance ($A_1^1\ dL\ g^{-1}cm^{-1}$) where dL: Decaliter = 10 Liters. Therefore, Beer's law will give as shown in equation (1-5):

$$A_{1CM}^{1\%} = abC_{100g/0.1L} \qquad (1-6)$$

The relation between molar absorptivity (ε), absorptivity (a), and specific absorbance (A_1^1) are shown in *(equation 1-6)*.

$$a = \frac{A_{1cm}^{1\%}}{10} = \frac{\varepsilon}{MW} \ \ldots\ldots\ \varepsilon = a.MW = \left(\frac{A_{1cm}^{1\%}}{10}\right).MW \qquad (1-7)$$

Where M represent molecular weight of the analyte.

Specific absorbance is very important constant in the analysis of pharmaceutical product especially when the molar mass of the analyte is unknown or those with higher molecular weight like proteins. Moreover, specific absorbance is also used in the analysis of multicomponent existed in the same mixture[119].

1.12.1 Spectrophotometric quantification Methods

The Direct spectrophotometric quantification of several pharmaceutical products suffers from either excipient interferences existed with the drug of interest (active material) or from interferences caused by the presence of secondary drug with the drug of interest (as in combination drugs). These problems can be overcome by using one of the

analytical correction methods[120] . These methods were also used in the quantification of substance in the multicomponent sample of these methods:

1.12.2 Simultaneous equations method (vierdott's method)

This method was the most commonly used in the analysis of two drugs existed in a single dosage form (combination drugs). The method was applied when the two drugs (x and y) absorb at the λ_{max} of each other *Figure (1.9*) .This method was applied for quantification of levosulpiride and rabeprazole sodium in pharmaceutical formulation[121].

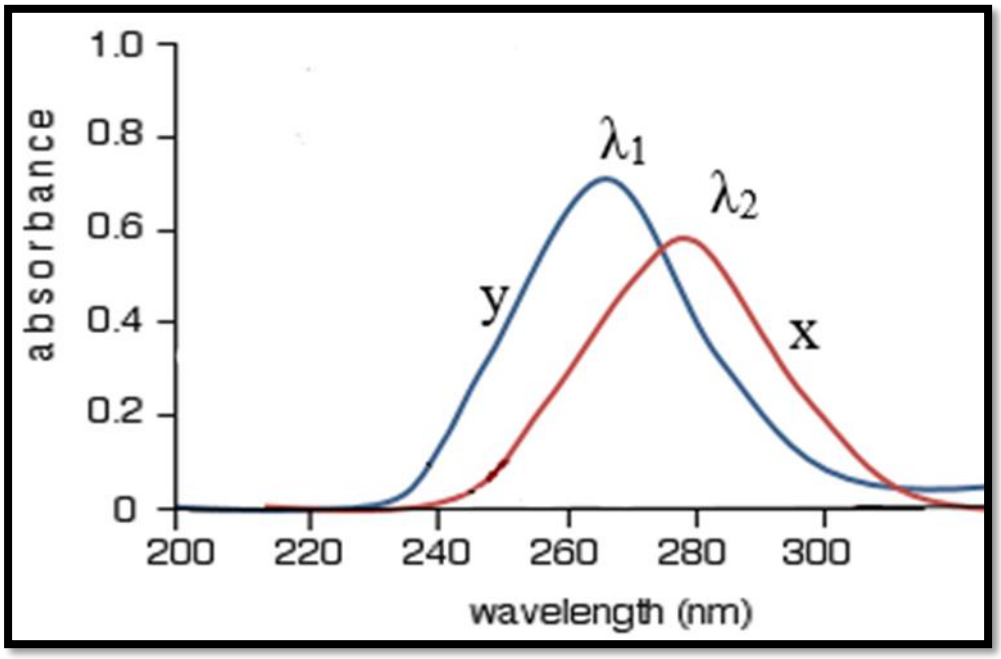

Figure 1.9 Absorption spectra of x and y drugs

1.12.3 Q-Absorbance method

Vierdott's method was modified to produce a new procedure known as absorbance ratio or Q-Absorbance method. It based on a principle that for a material that follow beer's law at all wavelengths, the absorbance ratio is a constant value at any two wavelengths independent on path length or concentration. For example, the absorbance ratio is the same

when two different dilutions of the same chemical are used as shown (equation (1-4 and 1-5)) and *Figure (1.10)[122]*.

$$Q = \frac{A_1}{A_2} = \frac{0.9}{0.58} = 1.55 \dots\dots (1-8)$$

$$Q = \frac{A_1^{\backslash}}{A_2^{\backslash}} = \frac{0.59}{0.38} = 1.55 \dots\dots (1-9)$$

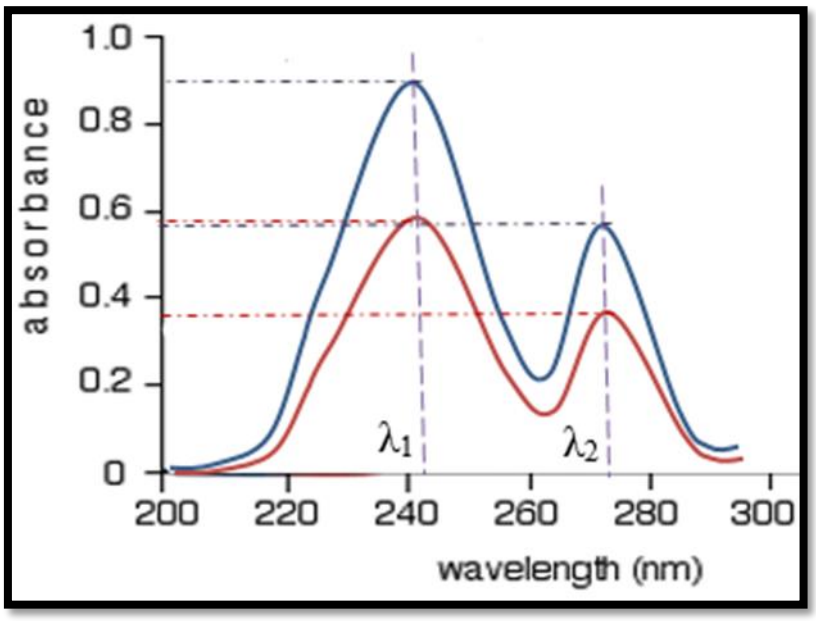

Figure 1.10 Absorption spectra of x material before and after dilution.

In the spectrophotometric quantification of two drugs in admixture using Q-absorbance method, the absorbance is taken at two wavelengths, the first one represents the λ_{max} of one drug and the other at iso-sbestic point, the wavelength at which the absorptivity of the two drugs are equal Figure (1.11)[123]. The method was used for quantification of Hydrochlorothiazide and Carvedilol in combined dosage form with high accuracy and recovery value[124].

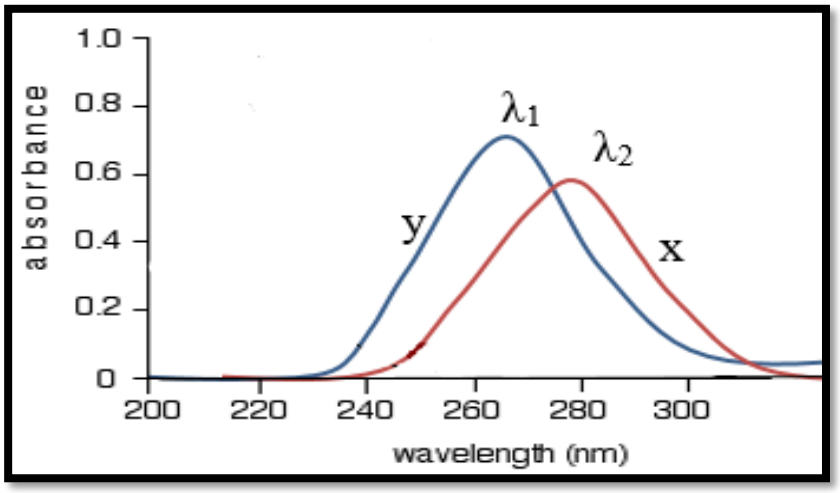

Figure 1.11 Absorption spectra of x and y drugs with iso-sbestic point .

1.12.4 Geometric correction method

Several mathematical correction procedures can be used to eliminate or reduce the background undesirable absorption that is present in the quantification of substances in biological sample. When the unfavorable absorption at three wavelengths is linear, the three-point geometric correction method is the simplest and most widely used. Figure (1.12)[125].

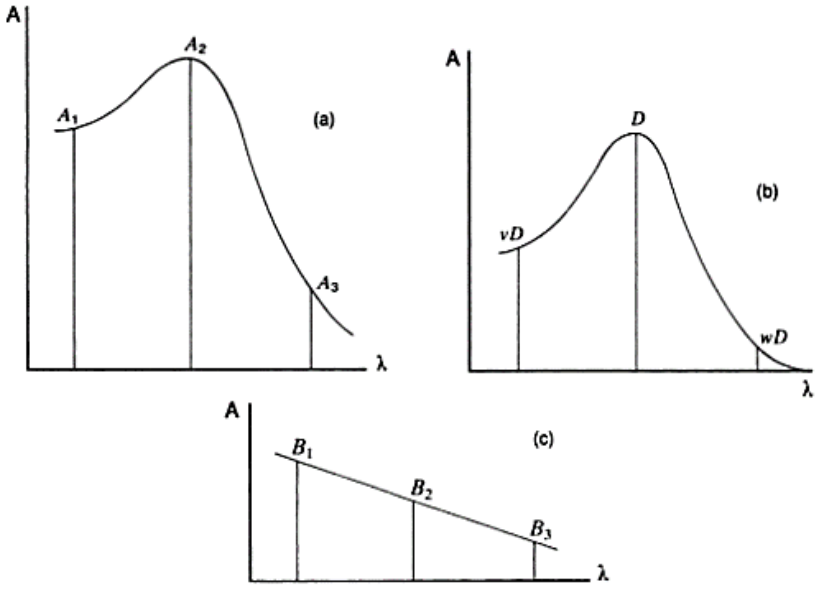

Figure 1.12 shows the drug solution's absorption spectrum in the presence of linear unpleasant absorption, in the absence of undesirable absorption, and in the individual spectra of the undesirable linear absorption.

Numerous compounds in multicomponent systems, including amlodipine besylate and azilsartan medoxomil in biological samples, were quantified using the geometric method. [126].

1.13 Derivative spectrophotometry

It is a potent analytical method used to extract quantitative and qualitative information from unresolved spectral regions. Additionally, the method used to cancel out baseline tilts and shifts. The approach is based on transforming the fundamental spectrum into one of its first, second, or higher derivatives, as shown in Figure (1.6). The resulting spectrum data is thus presented in a possibly more beneficial manner, offering a practical resolution to a number of analytical issues such matrix background correction, sample turbidity reduction, increasing spectral features, and resolving spectra associated with multi-component systems. Modern microcomputerized UV-Vis spectrophotometry is now considering derivative techniques as valuable instruments.[127-129]. Nabumetone and paracetamol concentrations were determined using the first derivative method. [130], along with letrozole, the determination of which was made using the first and second derivative techniques. [131].

1.14 Dual wavelength method

When there is an interfering component present, dual wavelength analysis is an effective way to analyze the component. In order to analyze the other medication, the approach involves choosing two wavelengths for each analyte (drug) such that the difference in absorbance for one drug is zero. Therefore, regardless of the interfering component, the drug concentration is directly proportional to the difference in absorbance between two points on the mixture spectra. Prednisolone acetate and Gatifloxacin sesquihydrate were measured using

a dual wavelength technique in a combination dose form as show in figure (1.13) [132].

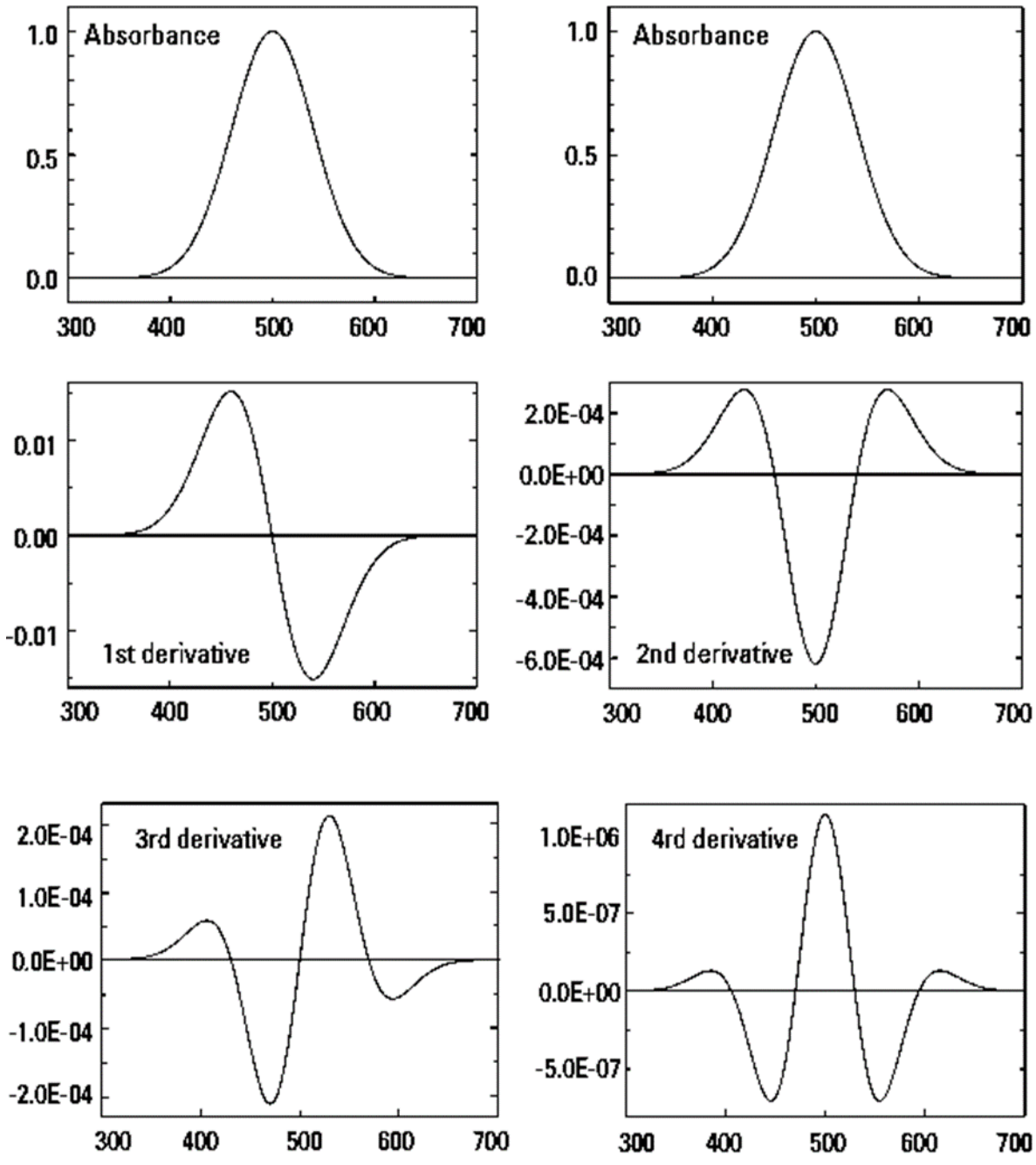

Figure 1.13 The most common mathematical derivatives of absorption spectra used in spectrophotometry.

1.15 H-point standard addition method (HPSAM)

H-point takes into account a hybrid approach that is created by combining the dual wavelength method and the traditional addition method. It relies on transforming the irreparable error brought on by the presence of a direct interferent into a persistent systematic fault that may be identified and fixed.[133].

For the direct correction of constant and proportional errors brought on by the sample matrix, H-point is regarded as a highly powerful and effective technique. It is the method of choice for resolving badly overlapped spectra. HPSAM only needed two wavelengths, and the analytical signal arising from the interferent component had to remain constant while that of the analyte had to differ as little as feasible.[134, 135]. The procedure was used to identify the amounts of caffeine and phenazone in pharmaceutical formulations. Figure (1.14) .Additionally, the H-point method was used in pharmaceutical formulations to determine the amounts of Hydrochlorothiazide, Irbesartan, and Telmisartan. [136].

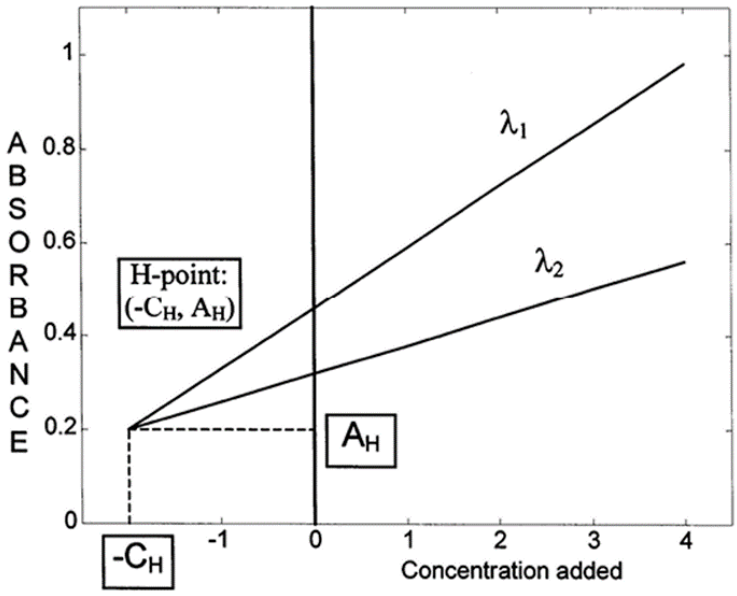

Figure 1.14 H-point standard addition lines determination of Caffeine and Phenazone in pharmaceutical formulations

1.16 Derivatization methods

Derivatization methods have recently gained a widespread because they have solved many problems with regard to analytical quantification in several analytical technique such as Spectrophotometric, HPLC, GC, LC, and electrophoresis. Thus, analytical chemists during last decade period have adapted well-known reaction from the organic and organometallic fields to carry out derivatization reactions in order to improve some necessary parameters of the analyte such as spectral properties, thermal stability, sensitivity, volatility, selectivity, and peak shape. Therefore, derivatization methods are very important for quantifying compounds that do not in general reveal the desired characteristics required for the analytical technique and those that are more prone to decomposition throughout the analysis[137].

Analysis of colorless material in the UV range of spectrum using spectrophotometric method suffer from poor sensitivity and selectivity and more prone to matrix interferences. For these reasons, the derivatization technique is highly used in spectrophotometric method, in which the colorless analyte reacts with a suitable chromogenic reagent to produce a stable and colored product that can be quantified spectrophotometrically with high accuracy and selectivity. Generally, Derivatization method consider indirect method where the analytical signal is directly proportional to the concentration of colored product [138].

1.17 Color-forming reactions used in Pharmaceutical Analysis

The reaction to be used in the spectrophotometric method should be carried out rapidly under simple conditions to produce a single, stable, and highly colored product in high yield. There are several chemical reactions used in analytical chemistry to quantify numerous pharmaceutical products [139], including:

1.17.1 Azo dyes formation [140-146]

This reaction is considered one of the most important types of color-generating reactions used in pharmaceutical analysis and is characterized by its relatively high speed, stable, and produce highly colored product. Azo dyes were prepared by azo coupling reaction, in which a diazonium salts undergoes an electrophilic substitution reaction with electron-rich compound like arenes (especially, aromatic amine and phenols) *Figure (1.15)*. However, Diazonium salts were synthesized by reacting aromatic amine compounds with nitrous acid, which spontaneously formed inside the reaction solution after reacting mineral acids (HCl or H_2SO_4) with sodium nitrite. Diazonium salts synthesis are performed under cooled conditions (0-5 ^oC) because the low temperature increases the stability of most diazonium salts, which are unstable at room temperature.

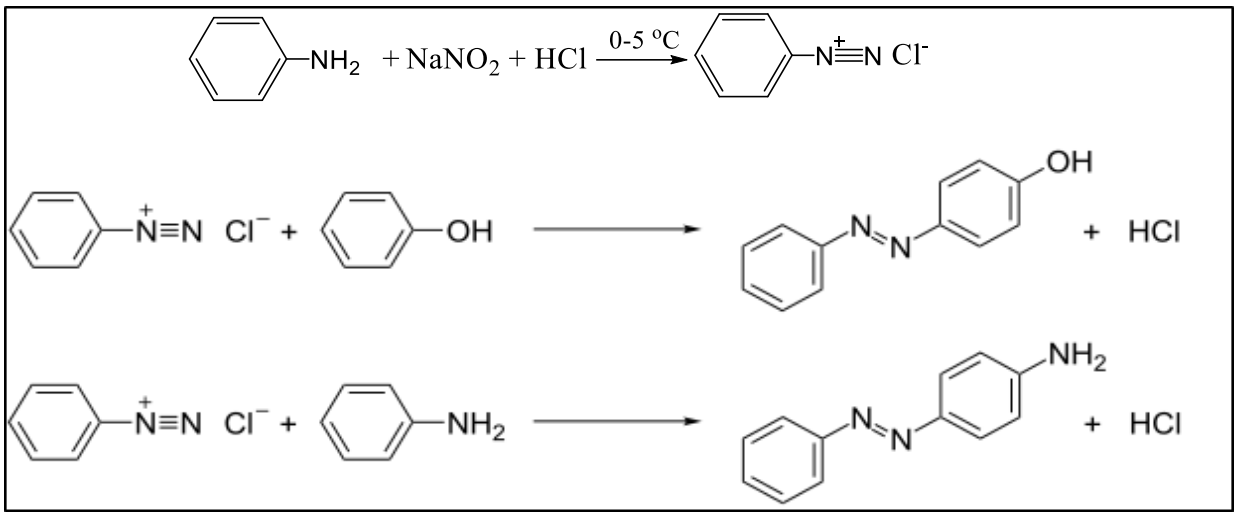

Figure 1.15 Diazonium salt formation and coupling with arenes compounds

1.17.2 Charge-transfer complex

Also termed as electron donor-acceptor (EDA) complexes is a kind of supramolecular assembly made up of two or more ions or molecules held together by electrostatic forces. Charge-transfer complex formed when the electron transferred from electron-donor substance (Lewis base) to electron-acceptor reagent (Lewis acid). The electron transition energy occurs in the visible region of spectrum and, therefore these complexes have intense color which in turn giving higher absorptivity value. Most of pharmaceutical products are electron-donor substances and the quantification methods depend on the finding of a suitable electron-acceptor reagent. The formation of charge-transfer complexes is characterized by rapidity and is dependent on solvent polarity[147].

A typical examples that gives rise of this method are the quantification of Amitriptyline, ganciclovir, trazodone, metamizole, cinnarizine, lisinopril, rifampicin, terfenadine, ciprofloxacin, sodium flucloxacillin, norfloxacin, analgin, cinnarine, amineptine and Trazodone using 7,7,8,8-tetracyanoquinodimethane (TCNQ) as electron-acceptor reagent as well as quantification of tetracyclines, ganciclovir, levofloxacin, prochlorperazine, thioridiazine, promethazine, chlorpromazine, pyrimethamine-sulfadoxine combination drug, moclobemide, Fifteen cephalosporins using Chloranilic acid as electron-acceptor reagent in acetonitrile [148].

1.17.3 Schiff base formation

Schiff bases are the compounds that contain an azo methene group (-C=N-) and are produced from a condensation reaction between an aldehyde reagent and primary amino group-containing compounds in an ethanol solvent with the addition of one drops of glacial acetic acid as a

catalyst [149]. The reaction was utilized for the quantification of several pharmaceutical products like tinidazole, olanzapine, and metronidazole using p-dimethylaminobenzaldehyde as a chromogenic analytical reagent [150].

1.17.4 Metal complexation reaction

It is a reaction that occur between metal ion (Lewis acid) with a certain reagent (Lewis base) to produce a coordination complex. The reagent known as ligand or chelating agent. The most preferred chelating agent in analytical chemistry must meet a set of basic requirements[151, 152]:

A. Contain at least two or more donor atoms sited in such a way as to lead to the formation of a five- or six-membered chelating ring with a metal ion through covalent or coordinate bond formation.

B. React with only one metal ion (high selectivity).

C. water-soluble and rapidly produce a stable, intensely colored complex with a higher absorptivity value.

Metal complexation is considered the most simple, convenient, and popular quantification method because it is utilized for the determination of both metal ions and drugs in pharmaceutical formulations. For example, quantification of zinc and metoprolol tartrate in pharmaceutical preparations [153, 154].

1.17.5 Ion pair formation

Ion pair is a type of supramolecular assembly that formed when two or more ions with opposite charge attractive to each other by electrostatic force. This phenomenon was used for analysis of various pharmaceutical

active material using ion pair extraction at which the ion of interest in the solution is neutralized by adding counterion (electron-donor reagent like dyes), the product then extracted in polar solvent and analyzed[155-159]. Diclofenac, Itopride, sumatriptan, midodrine, fluoroquinolones and mesalamine were quantified in pharmaceutical preparations via formation of ion-pair complex with bromothymol blue in an acidic media. The yellow ion-pair complex formed were quantitatively extracted into chloroform

Moreover, chlorpromazine hydrochloride was also analyzed in pharmaceutical tablets via formation of ion-pair complex with methyl orange dye. The yellow ion-pair complex formed were quantitatively extracted into ethyl acetate [160].

1.17.6 Oxidation-reduction reactions

In a redox reaction, an electron or electrons are transferred from one species to another, causing the responding species to transition from an oxidized to an oxidized state. Due to electron loss, the oxidation process results in an increase in the oxidation number. However, because of the electron gain during the reduction process, the number of oxidations is reduced. Figure (1.16) [161]. The reduced species is known as an oxidizing agent, whereas the oxidized species is known as a reducing agent. Ranitidine hydrochloride was quantified by the redox method utilizing N-bromosuccinimide (NBS) or Ce (IV) as oxidizing agents in pharmaceutical formulations. [162]. Metronidazole was also measured in pharmaceutical formulations that used sodium hydroxide solution and potassium permanganate as an oxidizing agent. [163]. Utilizing Ce (IV) as an oxidizing agent in an acidic medium, the pharmaceutical

formulations of timolol maleate, captopril, diltiazem hydrochloride, and atenolol were all identified. [164].

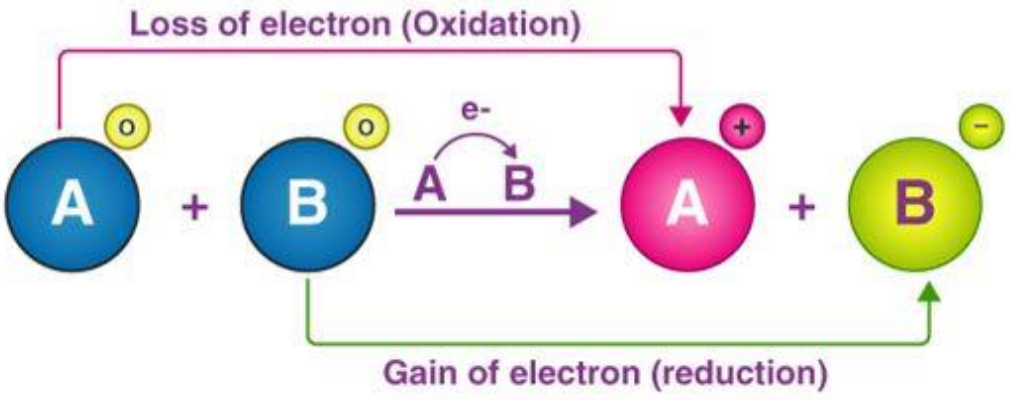

Figure 1.16 .Schematic diagram of electron transfer in the redox process.

Spectrophotometric methods are typically regarded as the most well-liked, straightforward, quick, adaptable, affordable, and highly effective way for measuring an analyte in a real sample. Due to their capabilities in the analysis of large samples in a variety of applicable fields, such as foodstuffs, spectrophotometric methods have found increased use in the most routine analysis, scientific research, and chemical process monitoring. This was revealed by a recent review of the chemical literature industrial products medical products pharmaceuticals , contaminants trace analysis criminal investigations , environmental and agricultural products [165-167].

1.18 Chloramphenicol

Chemically known as D-threo-(1R,2R)-1-p-Nitrophenyl-2-dichloroacetamido-1,3-propanediol (Figure 1.17), chloramphenicol is a semi-synthetic antibiotic that is a member of the nitrobenzene derivative drug class. It has a broad spectrum of activity against both gram-negative

and gram-positive bacteria [168]. The condition most frequently treated with it is bacterial conjunctivitis, an infection of the eye's mucous membrane [169]. It is utilized as the medicine of choice to treat a variety of infectious disorders in food-producing animals (such as honeybees) because of its good pharmacokinetic properties, high penetration into the tissues, and low manufacturing cost [170].

In the pharmaceutical dose form of the medicine, chloramphenicol contains a number of contaminants and related chemicals that might coexist with the active ingredient. These contaminants have the ability to alter a drug's activity and exacerbate its negative effects [222]. Numerous negative effects have been connected to chloramphenicol and related substances. Leukemia, gastrointestinal issues, deadly aplastic anemia, bone marrow depression, and allergic reactions are only a few of the human side effects that have been reported . For this reason, it is strongly advised to regulate the use of chloramphenicol in animals used for food [225]. Chloramphenicol has been measured using a number of verified methods, which are listed and summarized in Table (1.3).

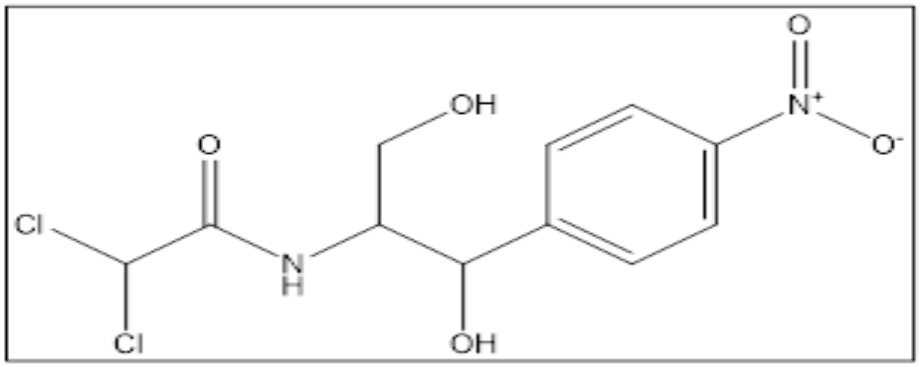

Figure 1.17 Chemical structure of Chloramphenicol

Table 1.3 Some of analytical approachs used for quantification of Chloramphenicol in real samples.

Method	Linearity range ng mL^{-1}or g^{-1}	LOD (LOQ) ng mL^{-1}or g^{-1}	Sample	Ref.
Colorimetric	0.5–5.0	----	Pharmaceutical formulation	[171]
Colorimetric	0.400-12000	----	Pharmaceutical formulation	[172]
LC-MS	----	0.04 (0.15)	Fish and mice	[173]
GC-MS	----	(0.05)	urine, shrimps and meat	[174]
HPLC	5–50	(0.25)	Aquatic Products	[175]
HPLC	------	800	Spiked plasma	[176]
HPLC	0.1-100	0.10	Tilapia fish	[177]
LC-MS	0.1-20.0	(0.05-0.09)	Animals-derived food	[178]
	0.50 -10.0	0.08 (0.3)	Shrimp	[179]
	0.1-5.0	0.015 (0.5)	Milk sample	[180]
	0.01-0.1	---	Meat	[181]
	0.1–2.0	0.1	Milk samples	[182]
	0.10–2.00	0.06 (0.10)	Shrimp	[183]
	0.6-28	0.15(0.3)	Royal jelly	[184]
	0.5-5.0	(0.15)	Honey	[185]
	---	0.01(0.04)	Animals-derived food	[186]
	0.01–0.6	0.01	Honey	[187]
	0.025–0.15	0.5	Animals-derived food	[188]
	0.2-20	0.002 (0.007)	Drinking Water	[189]
LC-MS	0.2 - 5 ng g^{-1}	----	Animals-derived food	[190]
LC-MS	0-5 ng g^{-1}	0.29 (32) ng g^{-1}	Poultry Meal	[191]

1.19 Clonazepam

Chemically speaking, clonazepam (1,3-Dihydro-7-nitro-5-(2-chlorophenyl)-2H-1,4.benzodiazepin-2-one) is used to treat anxiety, panic, and seizure disorders. owing to its extraordinary effects on the

brain and central nervous system It is used as a muscle relaxant, particularly to manage infantile spasms caused by epilepsy[247-251]. There are numerous quantification methods for clonazepam, as shown by the current literature review of analytical publications, which is described in Table (1.4).

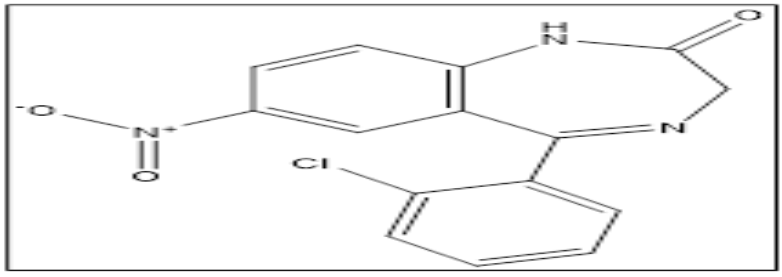

Figure 1.18 Chemical structure of Clonazepam

Table 1.4 Some of analytical approaches used for quantification of Clonazepam in real samples.

Method	Linearity range ng mL^{-1}	LOD (LOQ) ng mL^{-1}	Sample	Ref.
HPLC	16000-24000	29 (50)	Pharmaceutical formulation	[192]
Spectrophotometric	320 - 4100	240	Pharmaceutical formulation	[193]
LC-MS	2-1000	0.5 (2)	Human Serum	[194]
HPLC	600-1500	(5-10)	Human Plasma	[195]
LC	3–500	1.44	Human Plasma	[196]
HPLC	2400-5600	0.03 (0.09)	Pharmaceutical formulation	[197]
Spectrophotometric	5000-40000	3240 (10800)	Pharmaceutical formulation	[198]
LC-MS	10-160	0.8 (10)	Human Serum	[199]

LC-MS	----	5 (10)	Surface Water	[200]
HPLC	20000-300000	----	Human Serum	[201]
HPLC	0.5–50	0.5	Human Plasma	[202]
LC-MS	0.25-128	0.25	Rate Plasma	[203]
Spectrophotometric	2000-35000	570	Pharmaceutical formulation	[204]
HPLC	0.1–600	0.062 (0.21)	Biological fluids and wastewaters	[205]
Potentiometric	1.0×10^{-7} - 1.0×10^{-1} M	7.3×10^{-7} M	Biological fluid	[206]
Gas-Liquid chromatography	5-900 nM	3 nM	Biological fluid	[207]
Spectrophotometric	316–3160	130	pharmaceutical and urine	[208]
Spectrofluorometric	1000-5000	0.055 (0.169)	Pharmaceutical formulation	[209]
HPLC	1000-14000	60 (180)	Pharmaceutical formulation	[210]

1.20 Aim of the study

The aim of this work is to investigate of the following:

1- Establishing a rapid, accurate, and precise spectrophotometric methods for the determination of Chloramphenicol ,and Clonazepam in aqueous solution .
2- - To synthesize new adsorbent surface by the free-radical-induced graft co-polymerization of acrylic acid in the presence of alginate bio-polymer and ZnO NPs for the uptake of two pollutants
3- To characterize the adsorbent surface by using different techniques X-ray diffraction(XRD), Field Emission Scanning Electron Microscopes (FE-SEM), Energy Dispersive X-Ray (EDX) Thermo-gravimetric analysis (TGA) ,Fourier–transform-infrared-spectroscopy(FTIR), and Transmission Electron Microscopy (TEM).
4- Investigate the effectiveness of the hydrogel composite to adsorb selected two pollutants through batch treatment processes. And investigate the effects of contact time, adsorbent dosage, pH, temperature, during batch treatment methods.
5- Determine the applicability of Freundlich, and Langmuir approach to estimate design parameters characterizing the performance of the adsorption batch tests, and determine the adsorption constants of two pollutants onto hydrogel surfaces.
6- Estimate the thermodynamic parameters for two pollutants on the hydrogel surfaces.
7- -Study the effect of adsorbent Regeneration , and In vitro drug release on the adsorption capacity.

Chapter Two
Experimental Part

Experimental Part

2.1. Chemical materials

The Table 2.1 displays the molecular weight, purity, and supplier of the chemical substance used in this study. The MSDS provided the warning instructions for these hazardous compounds.

Table 2.1. Chemical material used in this study.

Seq.	Name	Molecular Formula	Purity%	Supplier
1	1,4-dioxan	$C_4H_8O_2$	99.8	Merck
2	Acetone	C_3H_6O	≥ 99.5	Merck
3	Acetonitrile	CH_3CN	≥ 99.9	Merck
4	Aluminum chloride	$AlCl_3$	99.9	BDH
5	Ammonia	NH_3	98.5	Merck
6	Butanol	$C_4H_{10}O$	≥ 99.5	Merck
7	Chloramphenicol	$C_{11}H_{12}Cl_2N_2O_5$	99.9	SDI
8	Clonazepam	$C_{15}H_{10}ClN_3O_3$	99.9	SDI
9	DMF	C_3H_7NO	≥ 99.5	Merck

2.2 Instruments

Several methods were employed in the current study, the majority of which are listed in table (2.2).

Table (2.2): Instruments used in this research

No.	Instrument	Model	Company supplied	Location of current measurement
1	UV-Visible spectrophotometer, Double beam	PC 1650	Shimadzu, Japan	University of Babylon / College of science for women-Chemistry Department
2	UV-Visible spectrophotometer, Single beam	UV mini-1240	Shimadzu, Japan	University of Babylon / College of science for women-Chemistry Department
3	Field-Emission Scanning electron microscope (FE-SEM)	MIRA3	TESCAN ,Czechia Republic	University of Tehran
4	Transmission electron microscope (TEM)	912AB	Leo, Germany	University of Tehran
5	X-Ray diffraction (XRD)	D2 Phaser	Bruker AXS Gmbh, Germany	University of Tehran
6	Thermogravimetric analysis (TGA)	DTG-60	Shimadzu, Japan	University of Babylon / College of science for women-Chemistry Department
7	Energy Dispersion X-ray (EDX)	MIRA3	TESCAN ,Czechia Republic	University of Tehran
8	Shaker water bath	CL002	K&K Scientific, Korea	University of Babylon / College of science for women-Chemistry Department

9	Centrifuge	CL008	JANETZI - T5, Belgium	University of Babylon / College of science for women-Chemistry Department
10	Ultrasound bath	405 power sonic	Hwashin, Korea	University of Babylon / College of science for women-Chemistry Department
11	Oven	LDO-060e	Labtech, Korea	University of Babylon / College of science for women-Chemistry Department
12	pH meter	HI 83141	Hanna, Romania	University of Babylon / College of science for women-Chemistry Department
13	Autoclave and Stainless steel device	Binder	Germany	University of Babylon / College of science for women-Chemistry Department

2.3 Preparation of standard solutions

2.3.1 Vitamin B6 reagent 0.01 M

In a 100 mL volumetric flask, 170 mg of the reagent was dissolved with a small amount of distilled water, and the solution was then diluted to the proper concentration with the same solvent.

2.3.2 Reduced form of Clonazepam or Chloramphenicol 100 µg mL^{-1}

In a 100 mL beaker, 100 mg of the medication was dissolved with a tiny amount of methanol and distilled water to create a stock solution of chloramphenicol or clonazepam. Then, 0.3 g of zinc metal powder and 0.5 mL of concentrated HCl were added. The reaction mixture was heated to 50 °C for 5 minutes while being vigorously shaken to quicken the reduction process. The mixture was filtered after 15 minutes of standing time. To make sure the drug's nitro group was converted to an amino group, the addition and heating stages were done again. In a 100 ml volumetric flask filled with distilled water, the final filtered solution was diluted to the proper concentration. Further dilution was used to create the working standard solution.

2.3.3 Sodium hydroxide 1.0 M

4.0000 g of NaOH was dissolved in a tiny amount of distilled water in a 100 ml calibrated flask to create a stock solution, which was then diluted to the desired concentration with the same solvent.

2.3.4 Hydrochloric acid 1.0 M

Pipetting 8.36 ml of 37% HCl into a 100 mL calibrated flask and diluting it to the proper concentration with distilled water produced a working solution of 1.0 M HCl.

2.3.5 Ammonium hydroxide (NH_4OH) 1.0 M

The solution was prepared by transferring 29 ml of ammonia (NH_3 con. 17.3 M) to 50 ml volumetric flask and diluted to the mark by distilled water.

2.3.6 Sodium nitrite solution 0.5 M

The solution was prepared by dissolving 4.2500 g sodium nitrite in 100 ml distilled water.

2.3.7 Sulfamic acid solution 0.2 M

The solution was prepared by dissolving 1.9420 g sulfamic acid in 100 ml distilled water.

2.4. Procedures for pharmaceutical formulations

2.4.1. Procedure for Chloramphenicol Eye ointment

Ten grams of Chloramphenicol 1% w/w eye ointment (HAYAPHENICOL 1%, 4g) equivalent to 100 mg Chloramphenicol were dissolved in 50 mL petroleum ether in 100 ml volumetric flask and diluted to the mark with distilled water. The mixture underwent quintuple extraction with distilled water. The solution was filtered, treated with 2 ml ethanol and diluted to mark with distilled water. Ten milliliters of the resulting solution were transferred into a 100 ml beaker and submitted to the reduction process, whose steps were described in Section (2.3.2).

2.4.2. Procedure for Chloramphenicol eye drops

The contents of three eye drops (0.5 w/v, 10 mL) were mixed to produce a solution labeled to contain 150 mg of chloramphenicol. Ten milliliters of the resulting solution, equivalent to 50 mg of

chloramphenicol, were transferred into a 100-mL beaker and submitted to the reduction process, whose steps were described in Section (2.3.2).

2.4.3. Procedure for Chloramphenicol capsules

The contents of 10 capsules were mixed and accurately weighed. An accurate amount of the powder equivalent to 100 mg of chloramphenicol was weighed, dissolved in a small amount of ethanol in a 100 mL volumetric flask, and diluted to the mark with distilled water. The solution was submitted to the reduction process, whose steps were described in Section (2.3.2).

2.4.4. Procedure for Clonazepam tablets

Using a stoneware mortar and pestle, fifty Rivotril® 2 mg tablets were precisely weighed and ground into a fine powder. Weighed precisely, the amount corresponding to 10 mg of clonazepam was dissolved in 3 mL of ethanol. The reduction method, whose steps were laid out in Section (2.3.2), was applied to the solution.

2.4.5. Procedure for Clonazepam eye drops

Five eye drops (2.5 mg/mL, 10 mL each) were combined to create a solution with the label "125 mg of Clonazepam." A 100 ml beaker was used to transfer 20 milliliters of the resulting solution, which contained 50 mg of Clonazepam, and subject it to the reduction procedure, the steps of which were outlined in Section (2.3.2).

2.5 Synthesis of Nanocomposite :

2.5.1 Synthesis of Carbon decorated / ZnO Nanocomposite:

Nanocomposite (Carbon decorated/ ZnO) was synthesized using the hydrothermal process Scheme (2-1). Ten grams of zinc acetate together with 5 g of oxalic acid and 1.0 g of CNT was mixed with 100 mL distilled water in Erlenmeyer flask and shacked for 30 min. The obtained mixture was transferred into the stainless steel or Teflon-lined autoclave and heated at 160 °C for 24 h under autogenous pressure. The obtained mixture was filtered, washed with distilled water several times, sonicated for 10 minutes, and dried at 80°C for 24 hr. to produce a dark-brown fine powder.

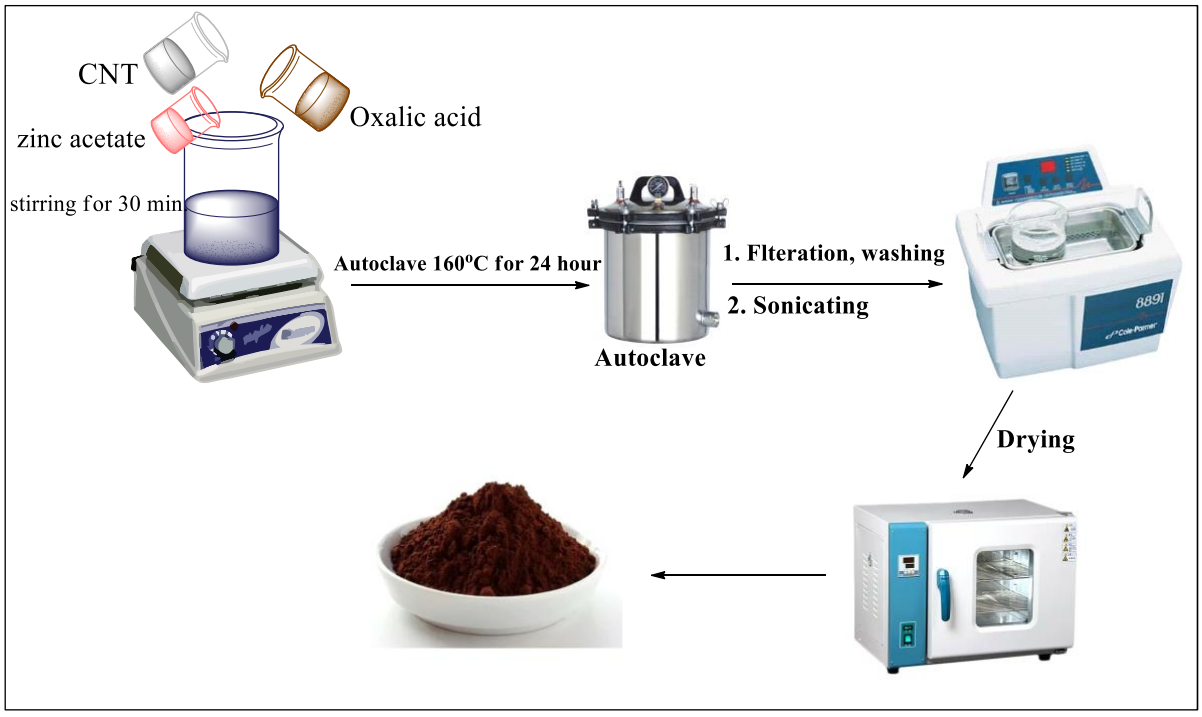

Scheme () : preparation of CNT / ZnO Nanocomposite

2.5.2 Synthesis of Sodium alginate poly (acrylic acid-co-acrylamide)/ZnO-CNT hydrogel nanocomposite

N, N-Methylenebisacrylamide was used as a cross-linking agent during the free radical polymerization process to create the hydrogel nanocomposite. 20 mL of distilled water was used to shatter a (0.2 g) of ZnO/CNT for five hours, followed by two hours of sonication. 40 mL of 5% sodium alginate was progressively added to the mixture while swirling it for three hours at 25 oC.. Addition of 0.5 g of acrylamide and 3 mL of acrylic acid transformed the reaction mixture into a consistent, pasty-like gelatinous solution after stirring. N,N-Methylenebisacrylamide and potassium persulfate were added as a free-radical initiator for polymerization and a cross-linking agent for acrylamide, respectively, in the following step.. The poly(acrylic acid)-based nanocomposite hydrogel (SA-g-P(Ac-co-AM)/ZnO-CNT) was then created by heating the reaction mixture at 75 oC in a thermostatically controlled water bath. The dried hydrogel was then ground into a fine powder and Photo (2-2) Real image of hydrogel nanocomposite was included. Scheme (2-3) Synthesis of Sodium alginate poly (acrylic acid-co-acrylamide)/ZnO-CNT hydrogel nanocomposite was also added.

Photo (2-2): Real image of hydrogel nanocomposite preparation in real image.

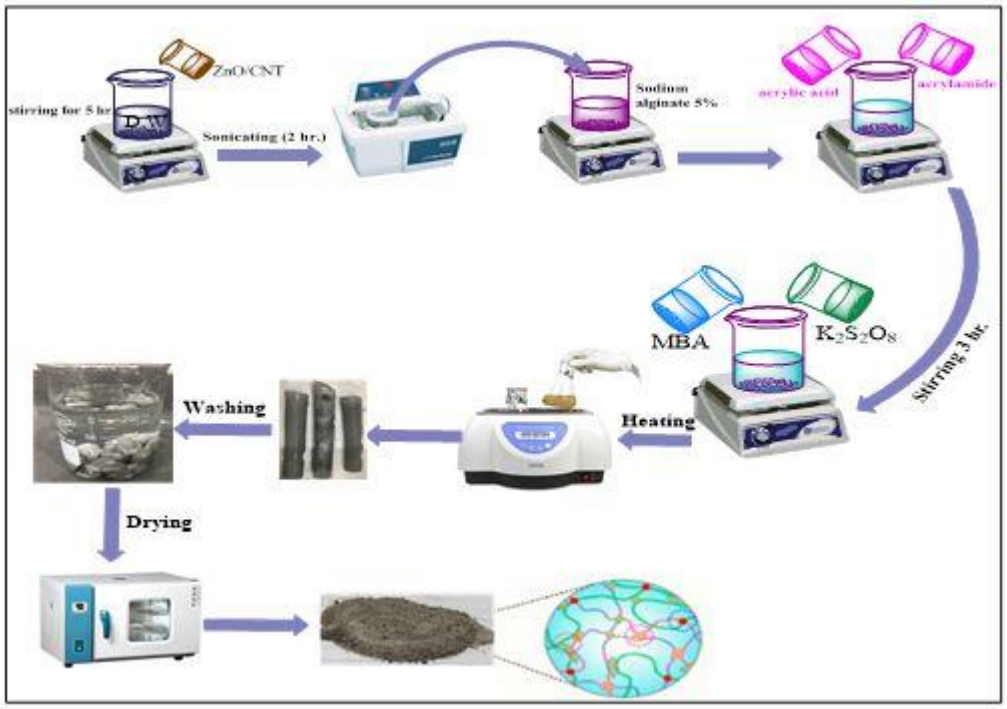

Scheme (2-3): Preparation of (SA-g-P(Ac-co-AM)/ZnO-CNT) hydrogel nanocomposite.

2-6 Characterization of the Prepared hydrogel Nanocomposites:

Transmission electron microscopy (TEM), Field emission scanning electron microscopy (FE-SEM), X-ray diffraction spectroscopy (XRD), Surface area analyzer (BET), Thermogravimetric analysis (TGA), Fourier Transform Infrared (FT-IR) Analysis, pH and absorbance values by spectrophotometer, separated advice (centrifuge), shaker, and other devices for measurements were used in this study to examine the samples.

2-6-1 Fourier Transform Infrared (FT-IR) Analysis:

The chemically bound components of matter vibrate at frequencies in the infrared spectrum. When the frequencies are in resonance, the oscillations caused by specific vibrational modes give the matter a way to couple with an impinging beam of infrared electromagnetic radiation and exchange energy with it. As a result, infrared frequency will excite molecular vibration, increasing molecular vibration energy. As the photon

energy is transferred to excite molecular vibrations, the electromagnetic radiation with a particular frequency will be absorbed by the molecule in the interim. Shimadzu's 8400S FTIR equipment was used to record FTIR spectra in the 4000-400 cm-1 frequency band. In an agate mortar, dried nanocomposite (1 mg) and KBr powder (10 mg) were combined. The combination was formed into a pellet and compressed for 2-4 minutes under a weight of 10 tons, and the spectrum was instantly recorded as shown in figure (2-4) [268].

Figure (2-4): **Fourier Transform Infrared (FT-IR) Analysis**

2-6-2 Ultraviolet-Visible Spectroscopy (UV–Vis):

An important method used to assess medication solution transfer and absorption. Where 0.1 mg.mL-1 of the composite are dissolved in the medication solution, and then the quartz cells are filled for measurements as shown in Figure (2-5) [211].

Figure (2-5) : A photo of ultraviolet-visible spectroscopy

2-6-3 Field Emission Scanning Electron Microscopy (FE-SEM) :

In order to characterize sample morphology, such as grain size, particle size, particle dispersion, crystal flaws, and surface structure, FE-SEM is a potent tool. Due to the fact that it also uses electrons as the probe, FE-SEM provides a number of advantages such a large depth of field, higher resolution, and more control over the degree of amplification, as shown in Figure (2-6) [212].

Figure (2-6): A photo of Scanning Electron Microscopy

2.6.4 Transmission Electron Microscopy (TEM) :

A beam of electrons is passed through an incredibly thin material using the TEM microscopy technique, where the electrons are converted to light and produce an image. Figure (2-7) illustrates how TEM can provide information on phase composition, structure, and lattice defects. [213].

Figure (2-7): A photo of Transmission electron microscopy

2.6.5 X-ray Diffraction Spectroscopy (XRD) :

A potent nondestructive method for characterizing crystalline materials is X-ray diffraction. Measures the size, shape, and internal stress of small crystalline regions and provides information on the average distance between layers or rows of atoms, the orientation of a single crystal or grain, and the crystal structure of an unknown material. Utilizing nickel as a filter, a single wavelength of light (1.5104 nm) from a CuK source was used to examine the crystalline characteristics of materials created using an X-ray deflection technique. As shown in Figures (2–8), the measurement's range (5–80 degrees) is derived from deviation angles (2). [214].

Figure (2-8): A photo of X-ray diffraction spectroscopy

2-6-6 Thermogravimetric analysis (TGA) :

The thermodynamic analysis is performed to determine the thermal stability of prepared nanomaterials and to determine the purity of these particles. The sample was heated from 10 °C to 600 °C and at a heating speed of 10 °C/min. as show in Figure (2-9).

Figure (2-9): A photo Thermo gravimetric analysis

2-6-7 Brunauer–Emmett–Teller (BET):

The Brunauer-Emmett-Teller (BET) hypothesis, which forms the cornerstone of a crucial analysis method for calculating the specific surface area of materials, tries to explain the physical adsorption of gas molecules on a solid surface. In order to measure a given surface area, BET theory typically uses probing gases—gases that do not chemically react with the surfaces of the materials—as adsorbates. As shown in Figure (2-10) nitrogen is the most widely used gaseous adsorbate when using BET techniques for surface probing. [215](Hameed Mahmood, Riadi et al. 2022)(Hameed Mahmood, Riadi et al. 2022)[215]

Figure (2-10):A photo Brunauer–Emmett–Teller (BET)

2.7 Removal of Pharmacetical polutant by using hydrogel nanocomposite:

2.7.1 Determination of optimum wavelengths (λ_{max}) and Calibration curves of two drugs:

2.7.1.1 Chloramphenicol

Chloramphenicol (CHL) is a widely used antibiotic with the chemical formula C11H12Cl2N2O5 and the molecular weight (323.132 g/mol). It comes in the form of a white, colorless powder and is used for a variety of purposes. By dissolving (1.0 g) of the medication in (1000 mL) D.W., a stock solution (1000 mg L-1) was created. The UV-Visible absorption spectra of the chloramphenicol medication solution were acquired between wavelengths of 200-800 nm in order to identify the maximum wavelength of the drug. The solution's highest absorption in the UV-Vis spectrum, which was discovered at the wavelength max CHZ= 278 nm in Figure (2-11), was used to determine its maximum wavelength.

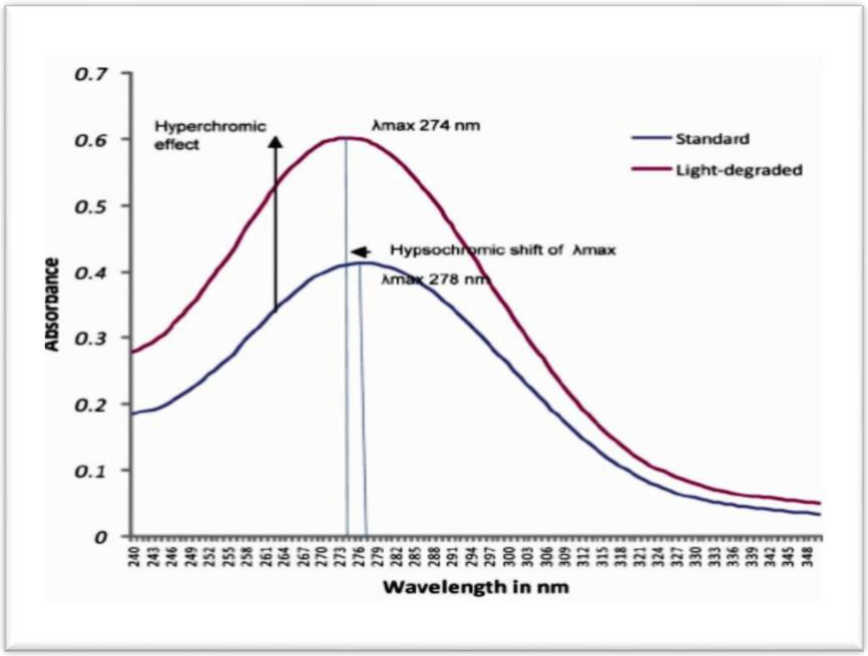

Figure(2-11): UV-Visible absorption spectra of Chloramphenicol drug .

In a series of dilutions ranging from 2 to 100 mg/L, the calibration curve for various chloramphenicol concentrations was created. Absorbance was calculated at the maximum drug concentration and

displayed versus drug concentration data in (Figure 2-12).

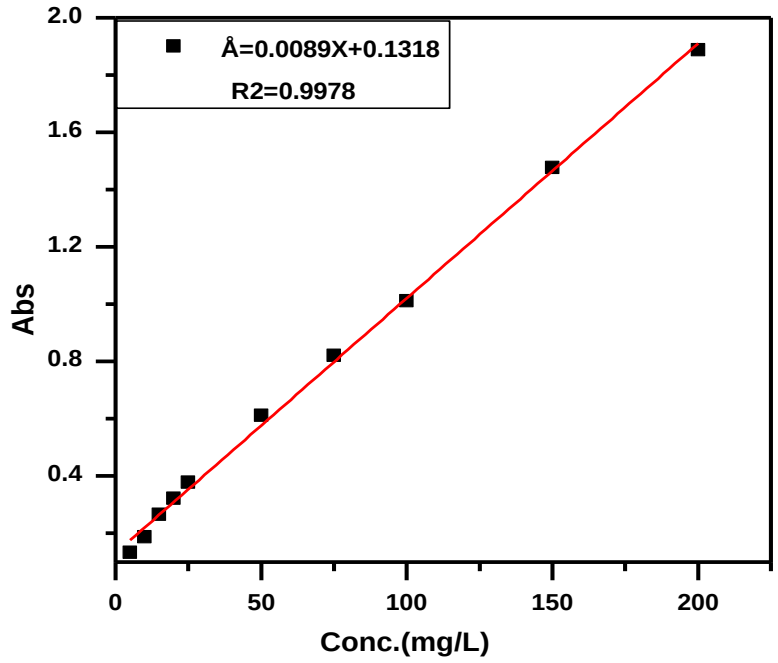

Figure (2-12): Calibration curve for Chloramphenicol drug .

Table (2-3): Statistics data of calibration for different concentrations of Chloramphenicol drug

Parameters	Proposed Method CHZ drug
λ_{max} (nm)	278
Beer's law limit (mg.L^{-1})	1-200
Regression equation	(Y = m X + C) y=0.0089x- 0.1318
Slope (m)	0.0089
Intercept (C)	0.1318
Correlation coefficient (R^2)	0.9978
Color	Colorless

2.7.1.2 Clonazepam

The antibiotic Clonazepam (CLZ), which has the chemical formula C15H10ClN3O3 and the molecular weight 315.715 g/mol, is highly well-known and is used for a variety of things.Amoxicillin was dissolved in 1000 mL of D.W. to create a stock solution (1000 mg L-1). The UV-Visible absorption spectra of the clonazepam (CLZ) medication solution were obtained between wavelengths of 200-800 nm in order to determine the drug's maximum wavelength. In Figure (2-13), the solution's peak absorption in the UV-Vis spectrum was observed at a wavelength of 243 nm, which was used to calculate the solution's maximum wavelength.

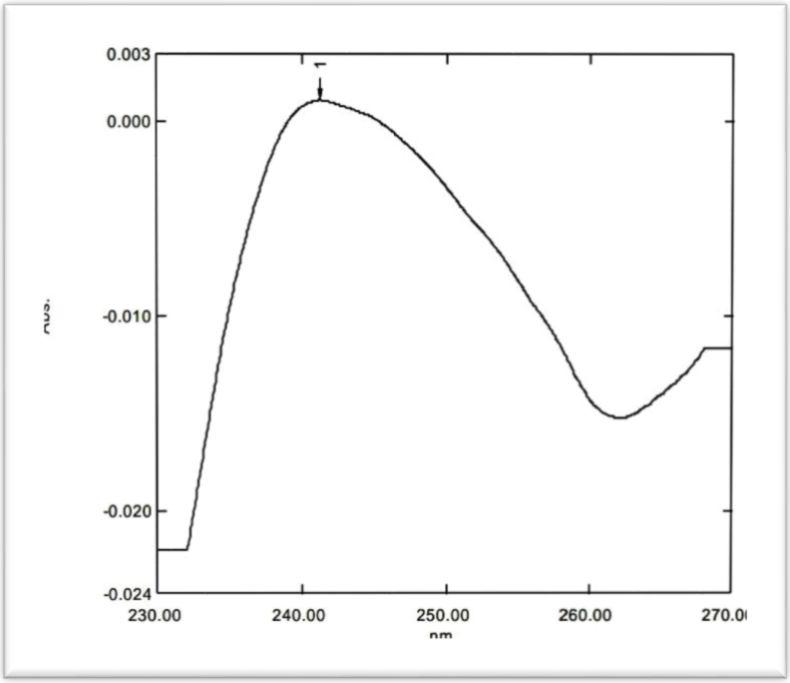

Figure(2-13): UV-Visible absorption spectra of Clonazepam (CLZ) .

The calibration curve of various Clonazepam (CLZ) medication concentrations was created by a series of dilutions (2–100 mg/L). In (Figure 2-14), the absorbance was calculated at the maximum drug

concentration and plotted versus drug concentration values.

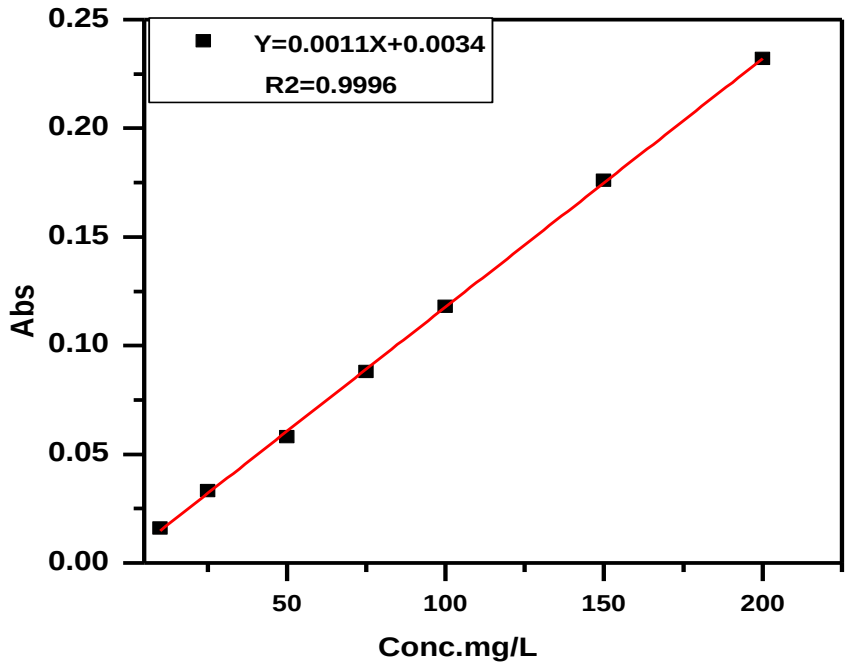

Figure (2-14): Calibration curve for Clonazepam (CLZ) drug.

Table (2-4): Statistics data of calibration for different concentrations of Clonazepam (CLZ) drug.

Parameters	Proposed Method CLZ drug
λ_{max} (nm)	243
Beer's law limit ($mg.L^{-1}$)	1-200
Regression equation	(Y = m X + C) y=0.0011x- 0.0034
Slope (m)	0.0011
Intercept (C)	0.0034
Correlation coefficient (R^2)	0.9996
Color	Colorless

2.8 Effect of different parameters on the adsorption process:

2.8.1 Effect of contact time:

100 mL of dye solution (100 mg.L-1) is made and placed in a conical flask together with 0.1 g of hydroel nanocomposite as an adsorbent concentration, pH (6.1), 25°C, and 220 rpm. The temperature of the water bath was regulated, as well as the shaking speed and separation. A single beam UV-Visible spectrophotometer will be used to spectrophotometric ally measure the drug concentration at the wavelength that corresponds to the maximum absorbance, or max. The centrifugation procedure separates the samples taken at various intervals. The solution's absorbance is then measured, and the medication concentration is to be checked every 5 to 120 minutes, or whenever equilibrium has been attained. Equation (2-1) was used to compute the adsorption capacity. [216]

$$qe = \frac{(C_0 - C_e) * V_L}{m_{gm}} \qquad (2-1)$$

Where: q_e = Amount of dye adsorbed per unit mass of adsorbent (mg/g).

C_o= Initial dye concentration ($mg.L^{-1}$). , C_e= Equilibrium drug concentration ($mg.L^{-1}$).

m = Dose of adsorbent (g). , V_L= is the volume of solution (L).

The percentage removal (E%) of the drug was calculated based on the reduction in absorbance at λ_{max} value of the drug as follows: [217]

$$E\ \% = \frac{C_{0-}C_e}{C_0} * 100 \qquad (2-2)$$

Where: C_0 and C_e are initial and equilibrium dye concentrations, respectively.

2.8.2 Effect of Initial Concentration of drugs :

In this investigation, two medicines at various concentrations of 100 mL (ranging from 25 to 200 mg) were employed.At 25°C and 220 rpm, L-1 was introduced to an Erlenmeyer conical flask containing (0.1g/100 mL) of hydrogel nanocomposite. The remaining concentration of the two medicines in the aqueous phase is measured spectrophotometrically for the selected wavelength after the supernatant was separated from the series and shaken for one hour.

2.8.3 Effect of dose of adsorbent:

For the hydrogel nanocomposite, different doses (ranging from 0.005 to 0.13) were used in the study. The samples' concentrations were (100) mg.L-1. The solutions were maintained in a water bath shaker at (220 rpm) for approximately one hour at a constant temperature (25 0C) and pH 6.1; the concentration of the remaining two medicines in the aqueous phase was then determined spectrophotometrically for the selected wavelength.

2.8.4 Effect of solution pH:

By adjusting the initial pH solutions (2-11) in conical flasks (100 mL) with container concentrations (100 mg.L-1) in 100 mL, the impact of solution pH on pollutant removal is investigated.A pH meter was used to monitor the pH and to modify it using (0.1N) HCl and/or (0.1N) sodium hydroxide (NaOH). The hydrogel nanocomposite adsorbent surface concentration was then established on the conical flask at 0.1 g/100 mL.

The flasks were placed inside a shaker water bath that was kept at 25 oC and fixed at 220 rpm during the investigation. The final drug concentration was determined using a single beam UV-Vis

spectrophotometer, and the calibration plot of the drug was created after 1 hour.

2.8.5 Effect of Temperature:

The adsorption studies are carried out in a thermostated water bath with a shaker at various temperatures (15-35°C). With (0.1g) dose of adsorbent hydrogel nanocomposite mixed with (100mL) aqueous solution of drugs concentration (25-200) mg/L, the effect of temperature was examined. The sample was shaken at a period for one hour, and the remaining two drug concentrations in the aqueous phase were then measured using spectrophotometry at the selected wavelength.

2.9 Adsorbent regeneration experiments:

Evaluation of the adsorbent's reusability, which is assessed in the desorption trials, is required to optimize the adsorption process. Three distinct solutions (pH 4.0, 7.0, and 10.0) containing distilled water were made, and varying concentrations of the saturated adsorbent (0.1 g) were added to the solutions.[218]. The regenerated adsorbent particles were separated after a 1-hour contact period and dried at 45°C for 3-hours. The effectiveness of the regenerated adsorbent is compared to that of fresh adsorbent in the treatment of 100 mg L-1 two drug solutions at an adsorbent dose of 0.1 g.L-1, pH 6.1, and contact period of 1 hour in order to evaluate the reusability. [219].

2.10 A Comparative adsorption between different surfaces to removal Two drugs:

The study uses a sample of 100 mL of two drugs at a concentration of 100 mg.L-1, which is added to an Erlenmeyer conical flask along with 0.1g of prepared hydrogel and carbon nanotubes, and shaken in a water bath for one hour. The supernatant is then separated by centrifugation,

and the remaining concentration is determined by using a UV-Visible spectrophotometer to measure the two drugs' maximum nm.

2.11 Removal of Pollutants (pharmaceutical) by Using hydrogel nanocomposite

Tow pharmaceutical pollutants used in this study. They were added to a conical flask (Erlenmeyer) along with 0.1g of the prepared hydrogel nanocomposite, then the mixture was placed in a shaker water bath for 1 hour.

Chapter Three
Result and discussion

3.1 Quantification of Clonazepam and Chloramphenicol in pharmaceutical formulations

3.1.1 Absorption spectra

A reddish-pink complex is created when vitamin B6 and chloramphenicol interact through an azo coupling process. The solutions containing the medication chloramphenicol and the azo complex produced were compared to their blank solutions using a spectral scan in the 190–800 nm range to explore the creation of the azo complex.. At a wavelength of 453 nm, figure (3-1a) shows the red-pink complex's maximum absorption intensity. figure (3-1b) shows the red-pink complex's maximum absorption intensity for CLZ .

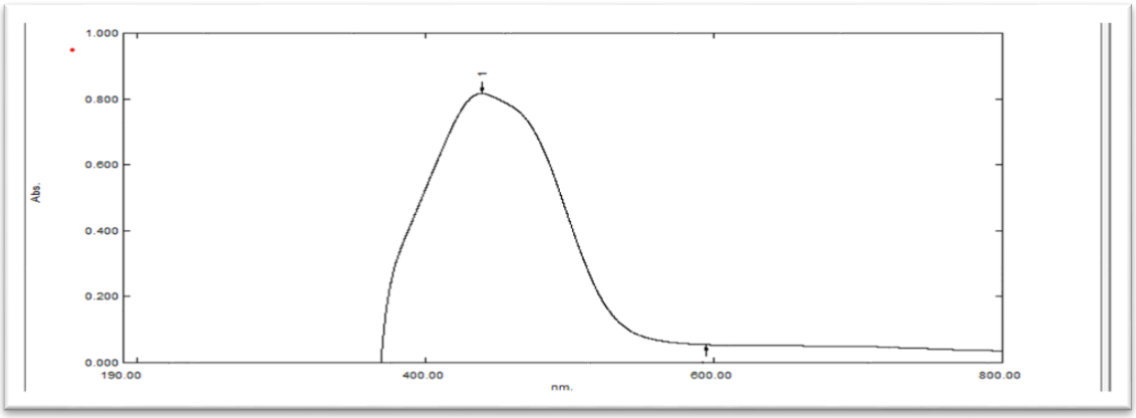

Figure 3-1a-. **spectrum of CHL against suitable blank and. The λ max of reddish-pink complex product = 453nm.**

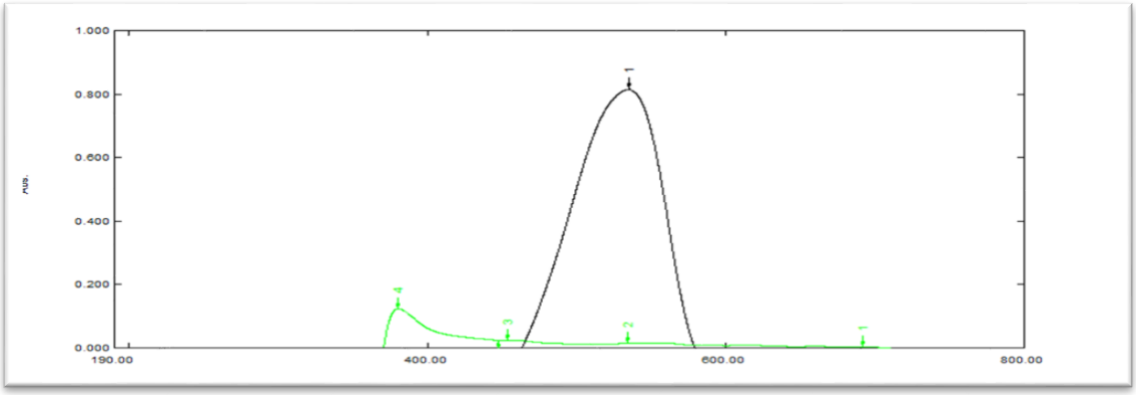

Figure 3-1b-. **spectrum of CLZ against suitable blank and. The λ max of reddish-pink complex product = 532nm.**

The results show that chloramphenicol and clonazepam, which are most sensitive to the technique at 453 nm and 532 nm of the complex, respectively.

3.1.2 Optimization of experimental conditions [26-30].

The suggested method's experimental parameters that influence the stability and absorbance of the colored product were meticulously calculated and refined. While the other values remained fixed, each parameter was examined separately.

3.1.2.1 Effect of reagent volume (Vitamin B_6)

Different amounts of Vitamin B6 (0.01 M; 0.25–2.5 mL) were used. Figure 3-2 illustrates how the absorbance rose in relation to the reagent volume until it reached a steady state point (1.25 mL), after which there was no further rise in absorbance. Therefore, 1.25 mL of Vitamin B_6 was selected for the absorbance of the colored product for both CLZ and CHL.

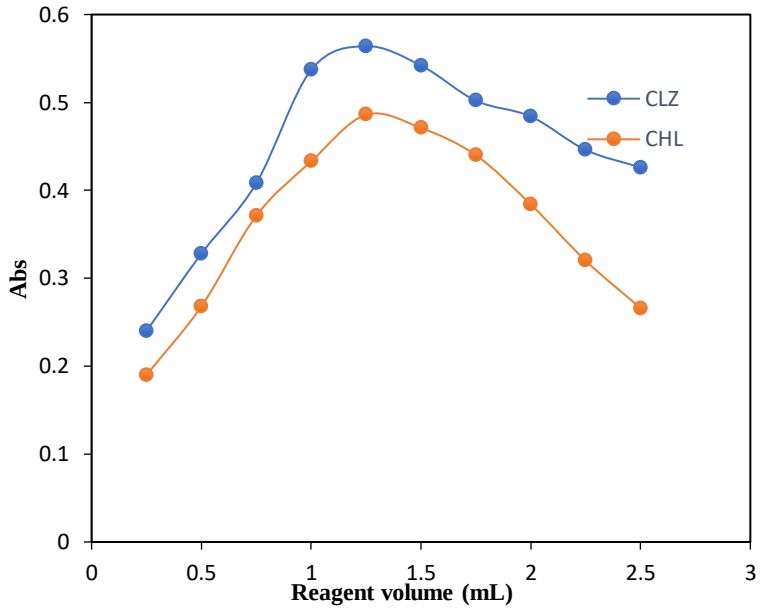

Figure 3-2- Effect of VB_6 volume on the absorbance of the colored product

3.1.2.2 Effect of NaOH volume

Various concentrations of 1.0 mol.L^{-1} sodium hydroxide, ranging from 0.25 to 2.0 mL, were employed. 1.25 mL was chosen as the ideal NaOH volume since this volume produced the highest absorbance, as shown in Figure 3-3

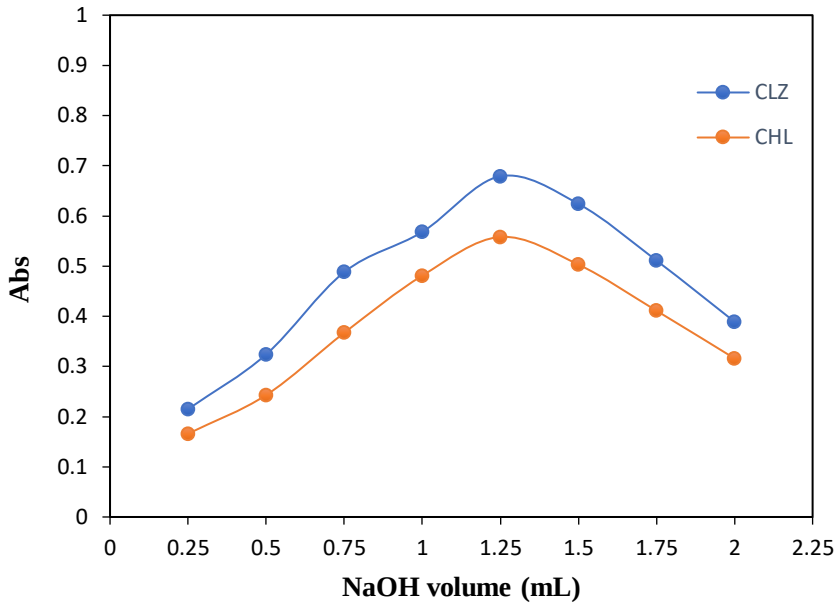

Figure 3-3- Effect of NaOH volume on the absorbance of the colored product

3.1.2.3 Effect of HCl volume

According to reports, aromatic amine reacts with either sodium nitrate or just nitrous acid in the presence of a strong metallic acid to produce diazonium salt. The second method for making diazonium salt is strongly advised due to the toxicity and gaseous nature of nitrous acid. Various volumes of 1.0 mol.L^{-1} HCl ranging from 0.25 to 2.0 mL were employed. Various volumes of 1.0 mol.L^{-1} HCl ranging from 0.25 to 2.0 mL were employed. As shown in Figure 3-4, the tangible HCl volume was chosen since the highest absorbance was reached at 1.0 mL.

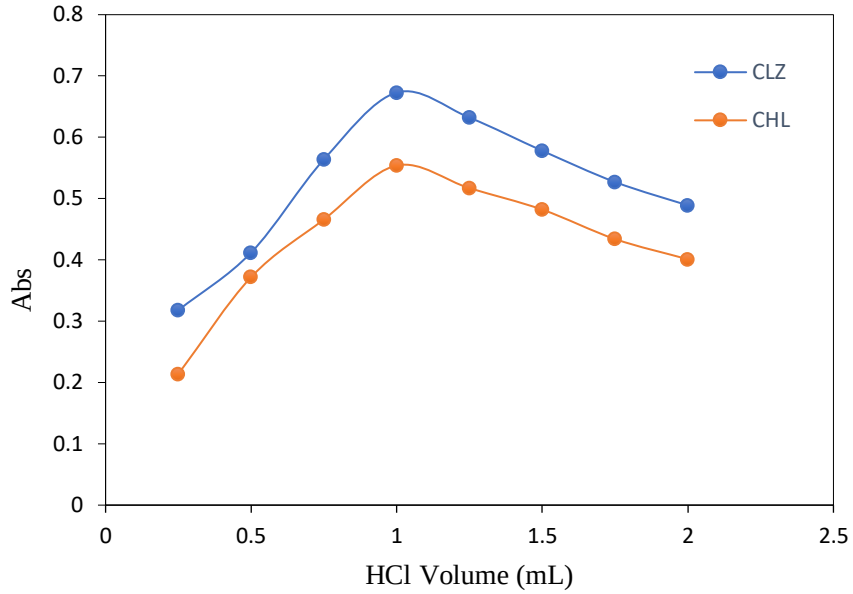

Figure 3-4- Effect of HCl volume on the absorbance of the colored product

3.1.2.4 Effect of sodium nitrite volume

The range (0.25-2.0 mL) was covered by several volumes of 0.5 M $NaNO_2$. Figure 3-5 illustrates the relationship between the absorbance of the formed azo complex and the $NaNO_2$ volume. The absorbance increased with respect to the $NaNO_2$ volume until it reached a point at 0.75 mL for CLZ and 1.0 mL for CHL, after which the absorbance gradually decreased, so these points were chosen as the optimum volume of $NaNO_2$ volume.

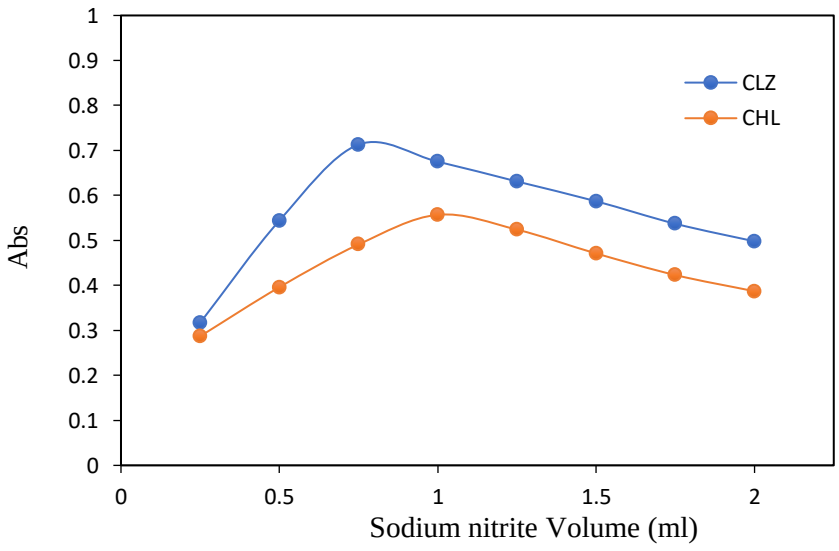

***Figure 3-5.*-Effect of $NaNO_2$ volume on the absorbance of the colored product**

3.1.2.5 Effect of sulfamic acid volume

It has been suggested that adding a specific quantity of sulfamic acid will remove the excess nitrite produced by the azo coupling reaction. This is why several concentrations of 0.2 M sulfamic acid in the range of (0.25-2 mL) were utilized. Figure 3-6 shows that for CLZ and CHL, respectively, 0.75 mL and 1 mL of sulfamic acid were found to be the ideal volumes.

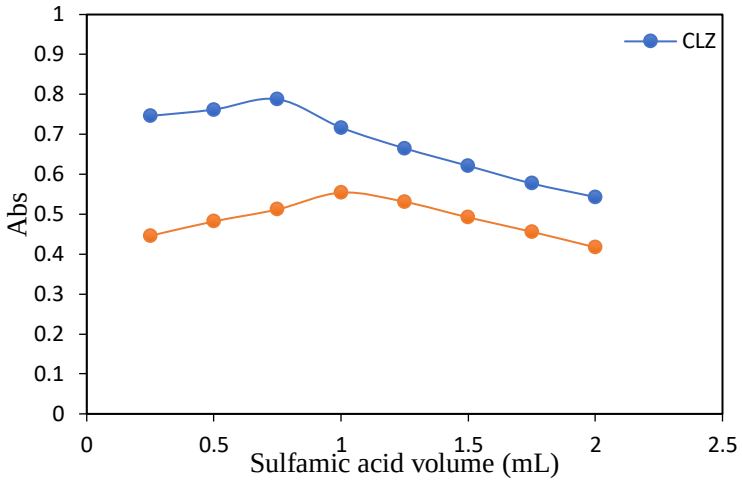

***Figure 3-6*- Effect of sulfamic acid volume on the absorbance of the colored product**

3.1.2.6 Effect of the time required for diazonium salt formation

The range of (2.0-16.0 min) was evaluated as the adequate time interval necessary to finish the synthesis of diazonium salt. Figure 3-7 shows that for CLZ and CHL, respectively, 8 and 12 minutes were found to be the

ideal times to finish the synthesis of diazonium salt .

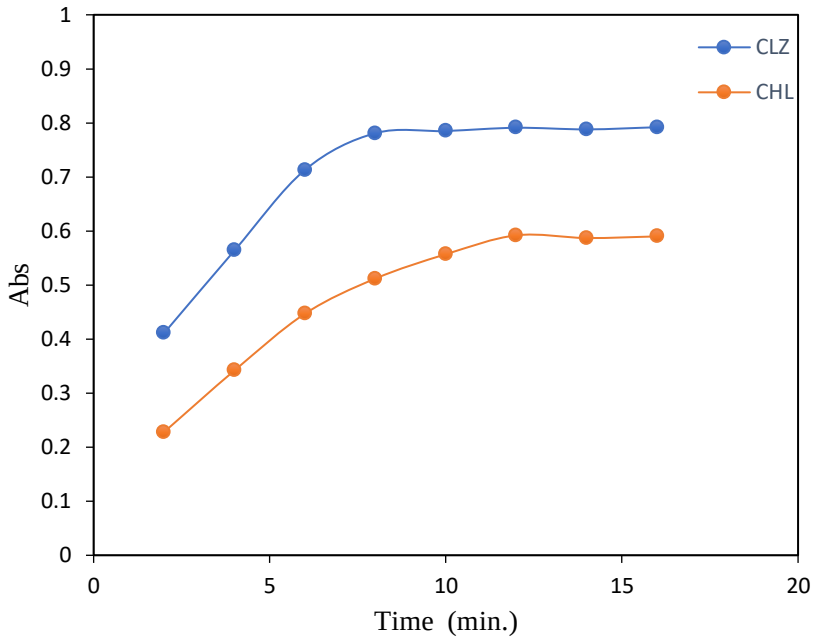

Figure 3-7. **Effect of diazonium time on the absorbance of the colored product**

3.1.2.7 Effect of the stability time

Different time intervals between (1.0-30.0 min.) were employed to assess how much time was needed to fully generate the azo product. Figure 3-8 shows that for CLZ and CHL, respectively, 3 and 4 minutes were found to be the optimum times needed to complete the azo coupling reaction.

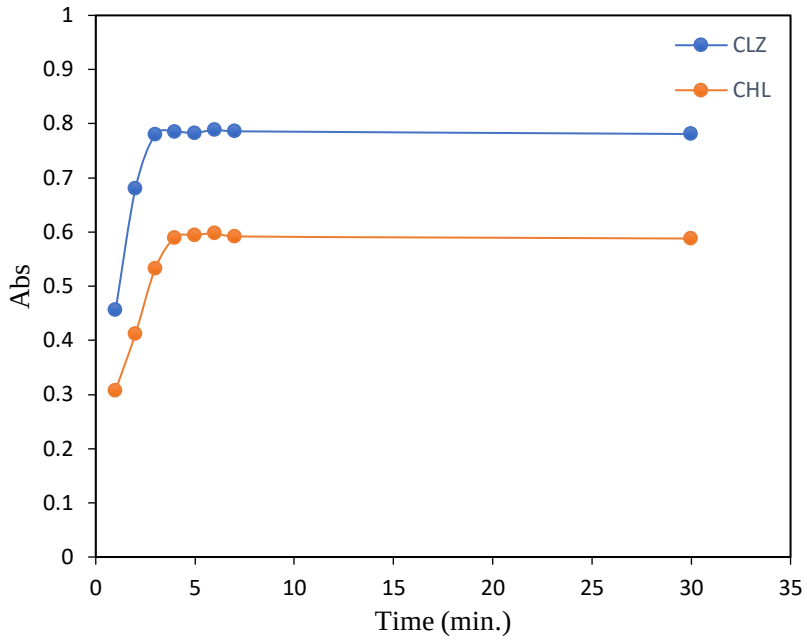

Figure 3-8- Effect of stability time on the absorbance of the colored product

*3.1.2.*8 Diluting solvents Effect

Different diluting solvents, including acetonitrile, 1,4-dioxan acetone, methanol, butanol, ethyl acetate, dimethylfloride, dimethylsulfoxide, ethanol, and distelwater, have been examined in order to determine which solvent give the maximum absorbance of the produced azo product. It was discovered that diluting the produced azo product with ethanol produced the highest absorbance (Figure 3-9).

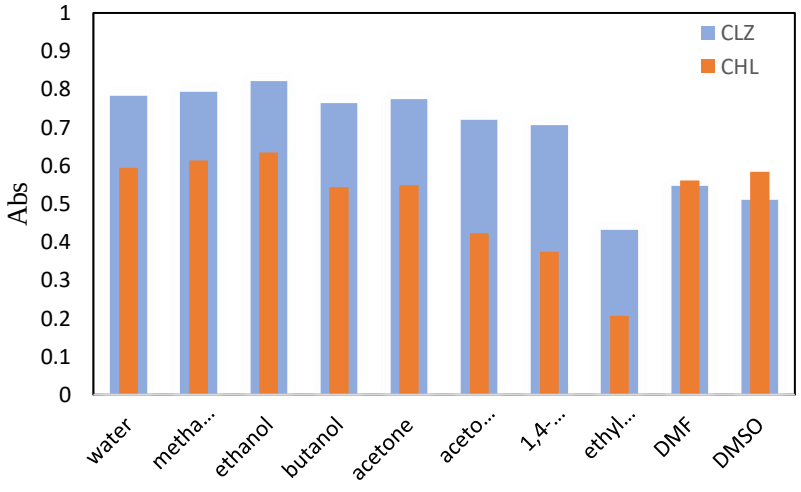

Figure 3-9- **Effect of diluting solvent on the absorbance of the colored product**

3.1.3 Validation of method for determination of clonazepam

In accordance with the recommendations of the International Conference on Harmonization (ICH), the created approach has been validated.

3.1.3.1 Calibration curve (Recommended procedure)

In order to create solutions with CLZ concentrations ranging from (0.5-17.0 g mL^{-1}), appropriate aliquots of the working standard solution (50 g mL^{-1}) were accurately transferred using a micropipette to a set of 10 mL volumetric flasks. Next, 1.0 mL of 1.0 M HCl was added. The sodium nitrite solution was gradually added to the flask contents while gently mixing, and the mixture was allowed to cool in an ice bath (0-5 °C). The cooled mixture was then left to stand for an additional 8 minutes. Once cooled, a solution made by combining 1.25 mL of 0.01 M reagent with 1.25 mL of 1.0 M NaOH was added gradually to the resulting combination. Then 0.75 mL of sulfamic acid, concentration 2, was added. Next, ethanol was used to dilute the flask's contents to the proper level. After 3 minutes, the absorbance of the resulting pinkish azo product was measured at 532 nm in comparison to a blank solution made in a similar manner. Figure 3-10 The absorbance of the colored product at 532 nm as a function of clonazepam concentration was plotted to create a calibration curve. The calibration graph's associated regression equations were constructed.

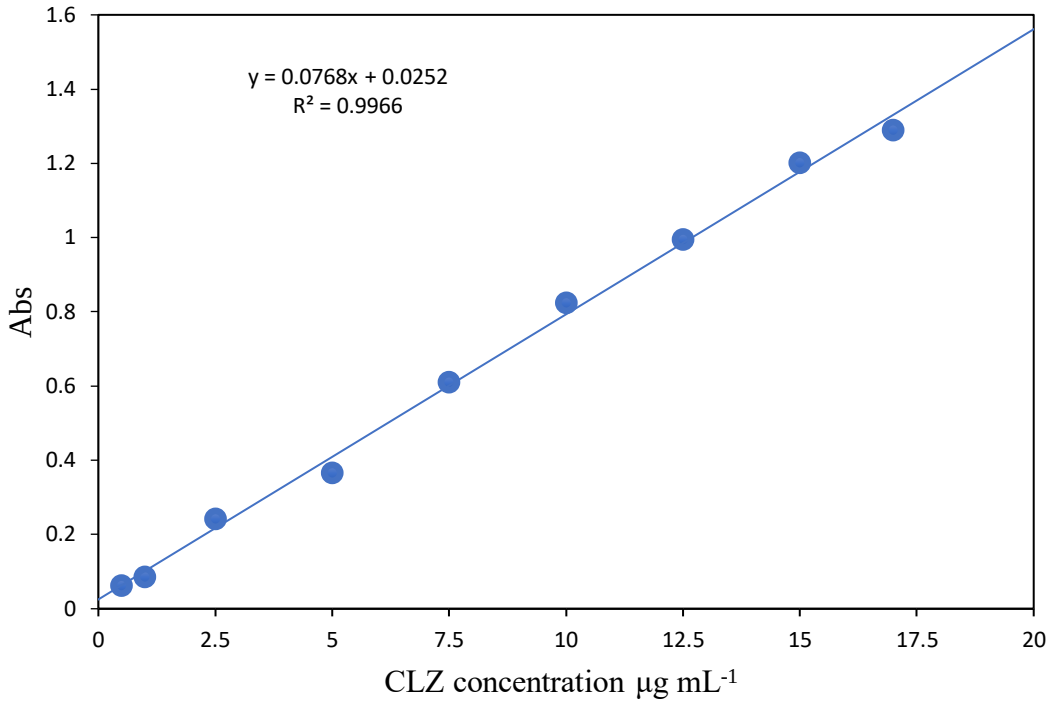

Figure 3-10-Calibration curve of clonazepam.

3.1.3.2 Linearity and range

The following is how the linear regression equation represented the calibration curve:

$y = ax + b$

In which y is the analytical response, an is the slope, x is the concentration, and b is the intercept.

The analysis of the data using the suggested method produced the following linear regression equation:

A = 0.0768 C + 0.0252

Where A represent Absorbance,C represent CLZ concentration in µgmL^{-1}

The linear concentration of the calibration graph ranged from 0.5-17 µg mL^{-1} of CLZ. The resulted data were summarized in *Table 3-1*.

Table 3-1 Analytical parameters of the suggested approach.

Parameter	suggested method
λ_{max} (nm)	532
Concentration range (µg mL^{-1})	0.5-17
Slope	0.0768
SD of Slope	0.0017
Determination coefficient (r^2)	0.9966
Correlation coefficient (r)	0.9982
Intercept	0.0252
SD of intercept	0.0166
Sandell's sensitivity (µg cm^{-2})	0.013
Molar absorptivity (L $mol^{-1}cm^{-1}$)	$3.57*10^4$
LOD* (µg mL^{-1})	0.117
LOQ** (µg mL^{-1})	0.355

****LOQ:** Limit of quantitation. ***LOD:** Limit of detection

3.1.3.3 Limit of detection (LOD) and Limit of quantitation (LOQ)

The lowest analyte concentration at which a signal can be consistently identified or separated from background or blank signal at a sufficient level of confidence is known as the limit of detection. The lowest value of an analyte concentration that can be detected with a 95% confidence level with respectable accuracy and precision is known as the limit of quantification (LOQ). The suggested approach's LOD and LOQ were calculated by dividing the standard deviation (S.D.) of ten blank solutions. The derived S.D value was inserted in the ICH Q2 (R1) guidelines' equations, where

$$LOD = \frac{3.3\,S}{b}$$

$$LOQ = \frac{10\,S}{b}$$

where S stands for standard deviation and b for the slope of the regression line on the calibration graph. The modest LOD and LOQ values, as shown in Table 3-1, show that the suggested technique is highly sensitive.

3.1.3.4 Sensitivity and Molar absorptivity

Sandell's sensitivity (g/cm^2/0.001 Abs unit), which is the lowest analyte concentration in g mL-1 that produces absorbance equal to 0.001, was calculated to estimate the sensitivity of the suggested spectrophotometric approach. Using the following equation, Sandell's sensitivity and Molar absorptivity were derived.:

$$Molar\ absorptivity\ (\varepsilon) = Slope \times Molecular\ weight \times 10^3$$

$$\varepsilon = 0.0768 \times 465.89 \times 1000$$

$$\varepsilon = 3.57 \times 10^4\ L\ mol^{-1}cm^{-1}$$

$$Sandell's\ sensitivity = \frac{Molecular\ weight}{Molar\ absorptivity}$$

$$Sandell's\ sensitivity = \frac{465.89}{35700} = 0.013\ \mu g\ cm^{-2}$$

3.1.3.5 Accuracy

Three parameters were used to show the precision and accuracy of any analytical method: relative error (E%), percent recovery (Rec%), and relative standard deviation (RSD%). Relative error (E%) represents the uncertainty of the analytical method, which in turn indicates how large the analytical error could be. mathematically, It is a ratio of the absolute error to the true or theoretical $\text{Absolute error} = \text{measured value} - \text{theoretical value}$

$$E\% = \frac{absolute\ error}{theoretical\ value} \times 100$$

The percentage of the original drug that was present in the sample that has been recovered is expressed as a percentage (Rec%). The following equation was used to calculate the percentage of recovery (Rec%):

$$Re\% = 100 \mp E\%$$

The relative standard deviation (RSD%) illustrates how closely the data are scattered around the mean and how far away they are from it. The following equation was used to compute RSD%:

$$RSD\% = \frac{SD}{Mean} \times 100$$

The accuracy of the proposed method was evaluated by measuring the absorbance of the colored product at three concentration levels (5, 10, and 15 g mL^{-1}) in the calibration graph and carrying out five replications of each concentration. The findings were evaluated to determine percent recovery (Re%) and RSD%, which data show that the suggested approach is very accurate, as shown in Table 3-2.

Table 3-2 Accuracy data of the suggested approach

Sample	**Concentrations µg mL^{-1}**	**Recovery%* ± SD**	**RSD%**	**E%**
1	5	96.04 ± 0.0029	0.74	-3.95
2	10	103.28 ± 0.0033	0.41	3.28
3	15	101.99 ± 0.0138	1.15	1.99

* Mean of five determinations

3.1.3.6 Precision

Inter-day precision (Reproducibility) and intra-day precision (Repeatability) have been used to describe the precision of the suggested approach. Three CLZ concentrations (8, 12, and 16 g mL-1) were chosen to evaluate the accuracy of the proposed method. To ensure repeatability, each concentration was examined at the same time every day, and to ensure reproducibility, it was examined on various days. As shown in Table 3-3, the low relative standard deviation value (RSD% less than 2) indicates the high precision of the suggested strategy.

Table 3-3 Intra- and inter-day precisions of the suggested approach.

Concentration µg mL^{-1}	**Intra-day precision**		**Inter-day precision**	
	Recovery %*	**R.S.D.%**	**Recovery%***	**R.S.D.%**
8	100.78	1.14	100.61	1.29
12	99.65	1.01	100.15	1.44
16	99.20	0.52	99.10	1.04

* Mean of five determinations

3.1.3.7 Continues method (job) and Molar ratio method

using the molar ratio method and continues method (job), the Stoichiometry and reaction mechanism were known. Both ways have proven that the ratio between CAP and Vitamin B6 reagent about 1:1 (Drug1: 1 Reagent) as show in Figures (3-11 and 3-12) .

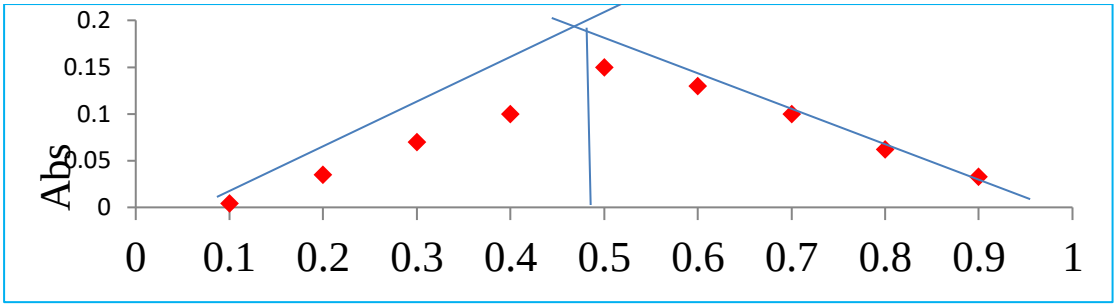

mol R/mol D

Figure (3-11)-Molar ratio method using in the Spectrophotometric determination for CLZ

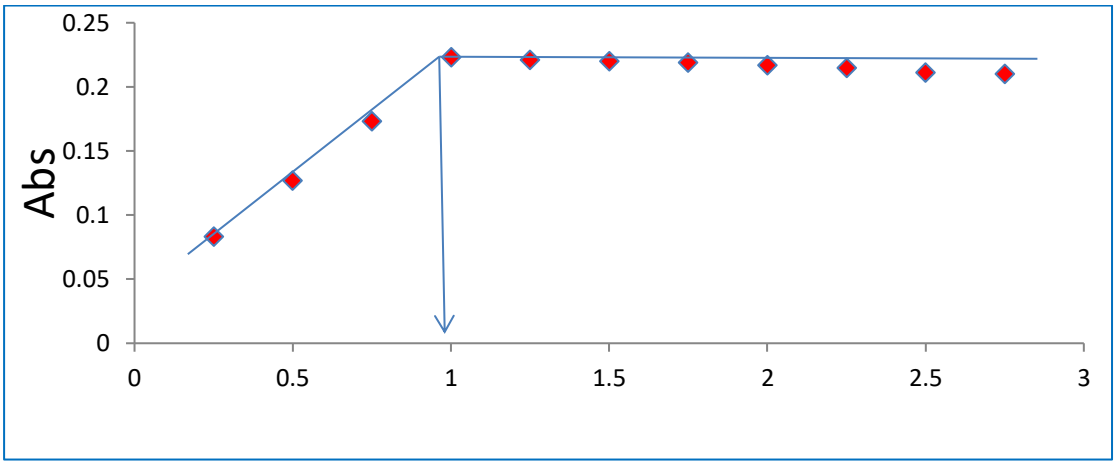

$$\frac{V_{CLZ}}{V_{B6}}$$

Figure (3-12) Job's method using in the Spectrophotometric determination for CLZ

3.1.3.8Reactionmechanism:

According to the FTIR chart

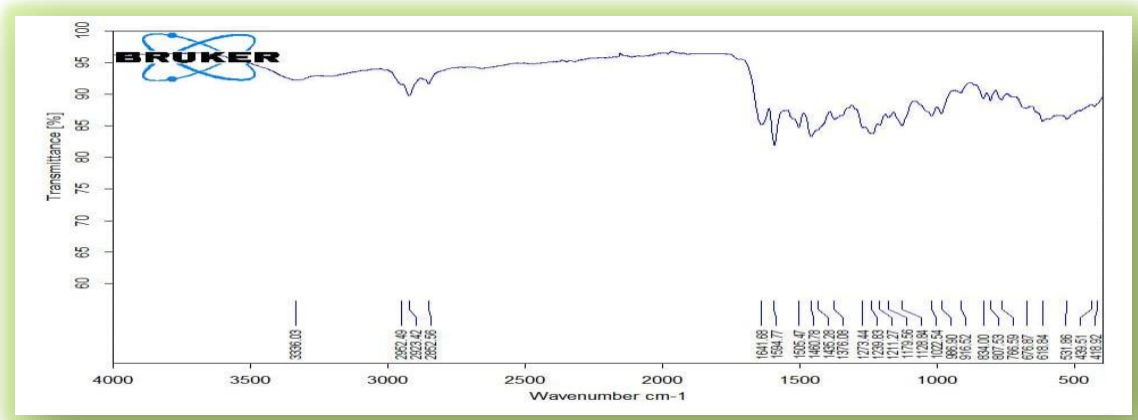

Figure (3-13)- FTIR chart of CLZ-VB_6 azo colord compound

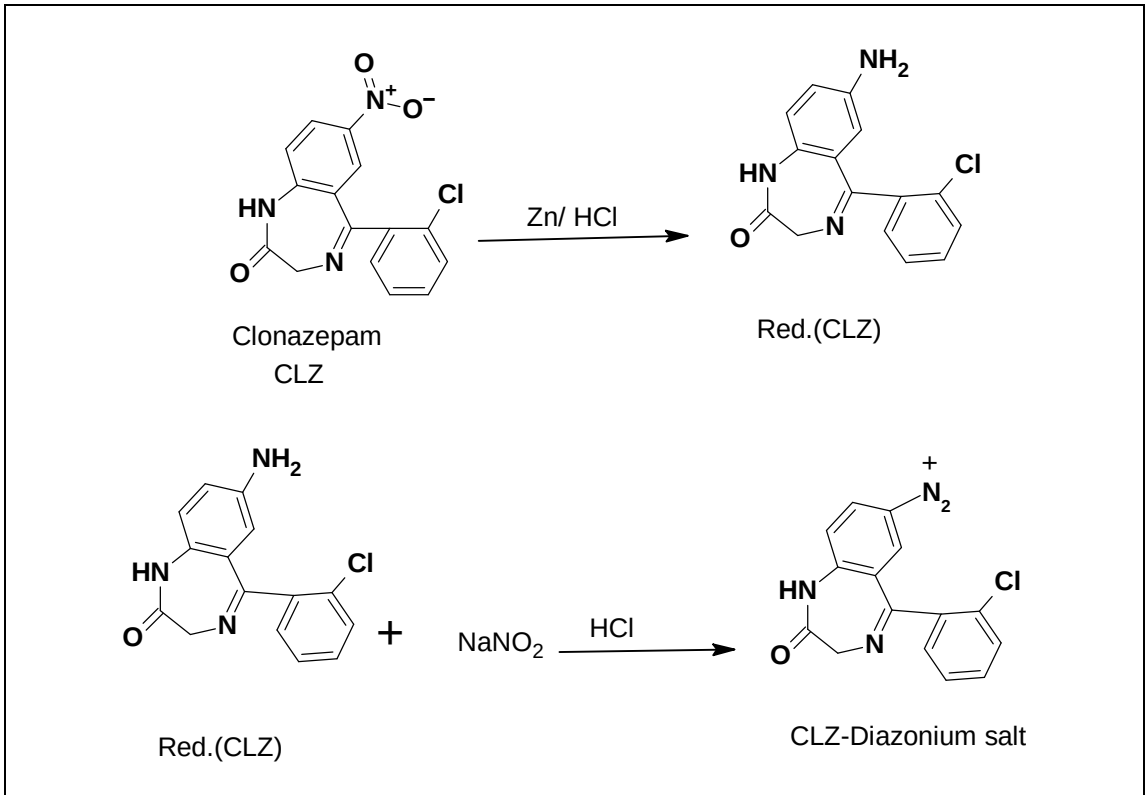

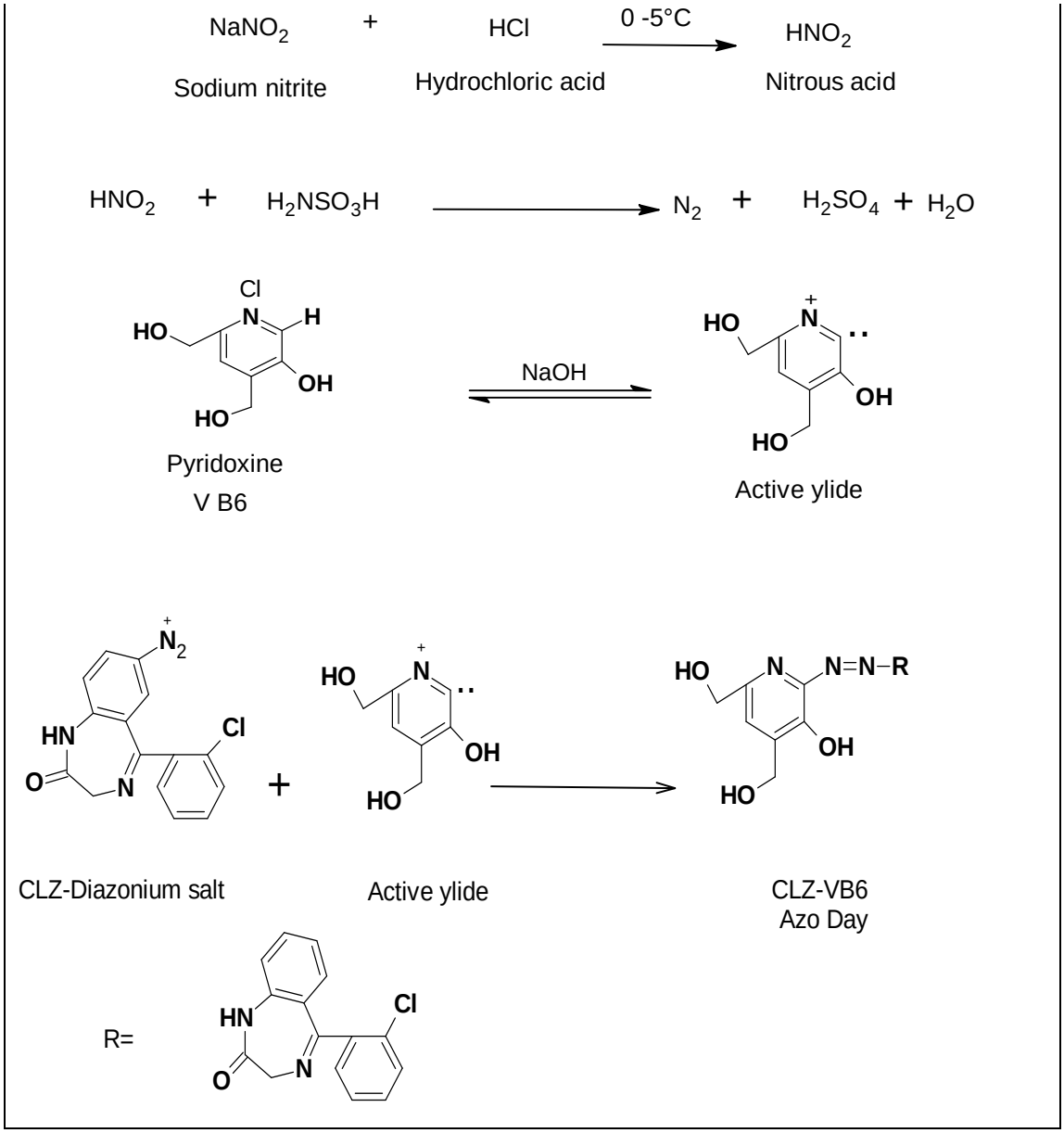

Scheme 3-1-1 : Mechanism proposed for the reaction between CLZ and VB_6.

t – test and F- test

The method was compare with the reference method by using t test and F test and the result was shown the method has high precision where the values of the t test and F test are less than the tableted values

Table 3. comparison between Standard method and Proposed method.

Standard method						
A	A Mean		(A-A Mean)	(A-A Mean)^2		sum (A-A Mean)^2
30.7	30.047		0.65	$4.27*10^{-1}$		3.29
30.87			0.82	$6.78*10^{-1}$		
28.57			-1.48	2.18		
Proposed method						
A	A Mean		(x-A Mean)	(A-A Mean)^2		sum (A-A Mean)^2
29.27	29.947		-0.68	$4.58*10^{-1}$		5.28
28.77			-1.18	1.38		
31.8			1.85	3.43		
Parameters						
S1-2	t	S1	S2	s_1^2	s_2^2	F
1.46	0.17	1.28	1.62	1.64	2.64	0.62

3.1.4 Validation of method for determination of chloramphenicol

The suggested approach has been validated in accordance with (ICH) recommendations.

3.1.4.1 Calibration curve (recommended procedure)

To create solutions with final CHL concentrations spanning the range (1.2-26 g mL^{-1}), a suitable portion of the working standard solution (50 g mL-1) was carefully transferred to a succession of 10 mL calibrated flasks. 1 mL of 1 M HCl is added after that, It was thoroughly combined before the contents of the flask were allowed to cool in an ice bath (0 to 5 °C). After that, 1.0 mL of the chilled sodium nitrite solution was progressively added while being gently mixed. The cooled liquid was then left to stand for a further 12 minutes. Once cooled, a solution made by combining 1.25 mL of 0.01 M reagent with 1.25 mL of 1.0 M NaOH was added gradually to the resulting combination. After that, 1.0 mL of sulfamic acid at 0.2 M was added. The flask contents were then diluted with ethanol to the proper concentration. At a wavelength of 453 nm, the colored product's absorbance was measured. To obtain blank solution, the

same method was carried out without CHL, Figure 3-11 shows the calibration curve that was created by charting the increasing absorbance of colored products with respect to CHL concentration. The calibration curve regression equation was simultaneously derived.

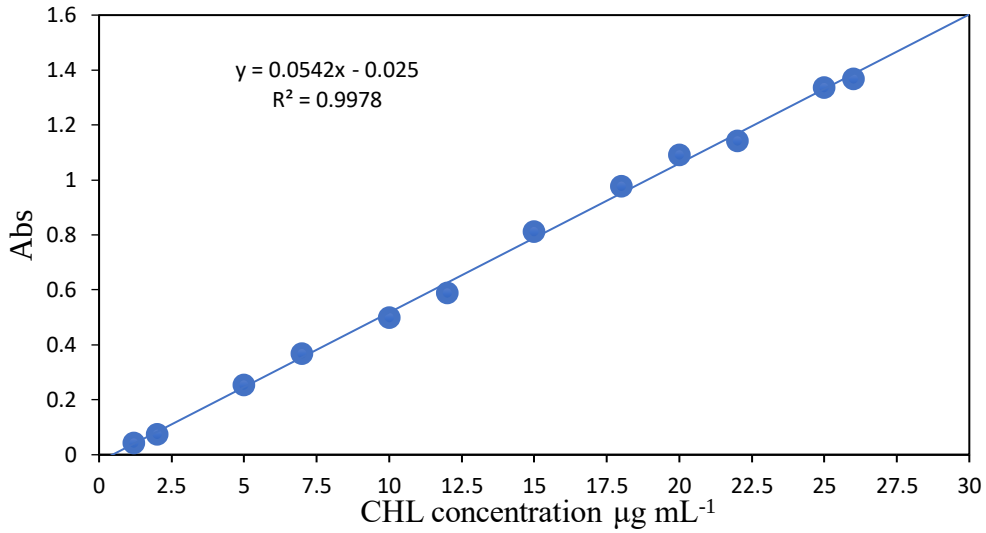

Figure 3-11. Calibration curve of Chloramphenicol .

3.1.4.2 Linearity and range

The following is how the linear regression equation represented the calibration curve:

$y = ax + b$

In which y is the analytical response, an is the slope, x is the concentration, and b is the intercept, The data from the suggested method's analysis were given the following linear regression equation:

A = 0.0542 C + 0.025Where A stands for absorbance and C for the amount of CHL in g per milliliter. From 1.2 to 26 g mL-1 of CHL, the

calibration graph's linear concentration was measured. Table 3-4 provides an overview of the collected data.

Table 3-4 Analytical parameters of the suggested approach.

Parameter	suggested method
λ_{max} (nm)	453
Concentration range (µg mL^{-1})	1.2-26
Slope	0.0542
SD of Slope	0.0008
Determination coefficient (r^2)	0.9978
Correlation coefficient (r)	0.9989
Intercept	0.0250
SD of intercept	0.0127
Sandell's sensitivity (µg cm^{-2})	0.0184
Molar absorptivity (L $mol^{-1}cm^{-1}$)	$2.56*10^4$
LOD* (µg mL^{-1})	0.299
LOQ** (µg mL^{-1})	0.908

****LOQ:** Limit of quantitation. ***LOD:** Limit of detection

3.1.4.3 Limit of detection (LOD) and Limit of quantitation (LOQ)

The suggested approach's LOD and LOQ were calculated by dividing the standard deviation (S.D.) of ten blank solutions. The derived S.D value was inserted in the ICH Q2 (R1) guidelines' equations, where

$$LOD = \frac{3.3\,S}{b}, \qquad LOQ = \frac{10\,S}{b}$$

where S stands for standard deviation and b for the slope of the regression line on the calibration graph. The modest LOD and LOQ values, as shown in Table 3-4, show that the suggested technique is highly sensitive.

3.1.4.4 Sensitivity and Molar absorptivity

Sandell's sensitivity (g/cm2/0.001 Abs unit) was used to calculate the spectrophotometric method's sensitivity. Using the following equation, Sandell's sensitivity and Molar absorptivity were determined:

$$Molar\ absorptivity\ (\varepsilon) = Slope \times Molecular\ weight \times 10^3$$

$$\varepsilon = 0.0542 \times 473.31 \times 1000$$

$$\varepsilon = 2.56 \times 10^4\ L\ mol^{-1}cm^{-1}$$

$$Sandell's\ sensitivity = \frac{Molecular\ weight}{Molar\ absorptivity}$$

$$Sandell's\ sensitivity = \frac{473.31}{25600} = 0.0184\ \mu g\ cm^{-2}$$

3.1.4.5 Accuracy

The accuracy of the proposed method was evaluated by measuring the absorbance of the colored product at three concentration levels (5, 10, and 20 g mL^{-1}) on the calibration graph, with five replications of each concentration. As shown in Table 3-5, the examined findings were used to calculate percent recovery (Re%), whose values show that the proposed strategy is very accurate.

Table 3-5 Accuracy data of the suggested approach

Sample	Concentrations µg mL^{-1}	Recovery%* ± SD	RSD%	E%
1	5	98.89 ± 0.0031	1.30	-1.11
2	10	98.74 ± 0.0054	1.05	-1.26
3	20	97.95 ± 0.0126	1.22	-2.05

* Mean of five determinations

3.1.4.6 Precision

The suggested approach's precision has been expressed as intra-day precision (Repeatability) and inter-day precision (Reproducibility). To evaluate the accuracy of the proposed method, three CHL concentrations (4, 12, and 22 g mL-1) were used. For repeatability and reproducibility purposes, each concentration was examined at regular intervals throughout the day. The low relative standard deviation number (RSD% less than 2), as shown in Table 3-6, indicates the great precision of the suggested approach.

Table 3-6 Intra- and inter-day precisions of the suggested approach.

Concentration µg mL^{-1}	**Intra-day precision**		**Inter-day precision**	
	Recovery%*	**R.S.D.%**	**Recovery%***	**R.S.D.%**
4	98.89	1.21	99.07	1.64
12	97.66	0.78	97.04	1.58
22	99.17	0.20	99.26	0.68

* Mean of five determinations

3.1.4.7 Analytical applications

The assay solutions (eye drop, ointment, and capsule) were prepared, and the amount of CHL in each type of assay was calculated based on the absorbance of the amount taken from the reducing solution. Additionally, calculated were Relative Error E% and Recovery percentage (Rec%). The outcomes are shown in Table (3-6-1) below.

Table (3-6-1) .Application of the method for determination of CHL in pharmaceutical preparations.

Type of assay		Drug taken from solution ppm	Drug found in solution ppm		E%	Rec %
Eye ointment		**10**	**9.910**		**3.1**	**101.5**
		8	**7.886**			
		6	**5.989**			
		4	**3.786**			
Eye drop		**10**	**10.077**		**-3.6**	**97.1**
		8	**8.089**			
		6	**6.138**			
		4	**4.107**			
Capsule		**10**	**9.895**		**2.8**	**102.4**
		8	**7.819**			
		6	**6.113**			
		4	**4.097**			

The proposed method was successfully in determination CHL in pharmaceutical preparations with good values of recovery presents (97.1%-102.4%).

Preparation solutions of pharmaceuticals containing CLZ drugs at a concentration of (100) g.ml-1, the ensuing steps were carried out in the preparation of the calibration curve, and the results are shown in Table (3-6-2). These results show that the suggested method may be very useful for pharmaceutical preparations. [220, 221].

Table (3.6.2). Application of the method for estimation of CLZ in pharmaceutical preparations.

Pharmaceutical formulations	Drug taken in PPM from 50mg	Drug found in mg	Drug found in PPM	Average	E%	Rec%
Tablet(50 mg)	8	50.208	8.033	50.208	0.417	100.417
	8	50.067	8.011			
	8	50.350	8.056			
Via oral drop (50mg)	8	50.208	8.033	50.080	0.039	100.039
	8	49.966	7.965			
	8	50.067	8.011			

3-2 Characterization of The Preparation Hydrogel Nanocomposites

3-2-1 X-Ray Diffraction (XRD)

To investigate the crystal phases and purity components of nanomaterials, X-ray diffraction measurements were made. It provides comprehensive details on the lattice parameter, lattice defects, lattice strain, crystallite size (in the case of nanoparticles), and the kind of molecular bond present in the crystalline phase. Therefore, the Sheerer equation can be used to estimate the average particle size [222].

$$D = \frac{k\lambda}{\beta \cos\theta} \qquad (3\text{-}1)$$

D stands for average particle size, K for form factor (0.9), W for wavelength (0.15418 nm for Cu-K), FWHM for the diffraction peak at 2 (which is wide because of the crystallite dimensions), and A for angle at maximum diffraction curve intensity.

The X-ray diffraction patterns of the ZnO NPs, the hydrogel, and the hydrogel nanocomposite are displayed in Figures 3-12, respectively. The existence of ZnO NPs is confirmed by the crystalline peaks that occur at 32o, 34o, and 36o. The broadness demonstrates that sodium alginate (SA) was grafted with poly(acrylic acid) chains.[223]. After adding CNT-ZnO NPs to hydrogel, the crystalline peaks were shown to vanish. The diffusion of ZnO NPs into the micro- and macro-pores of the hydrogel nanocomposite may be the cause of the change from crystalline to amorphous. The integration of CNT-ZnO NPs in the hydrogel matrix is confirmed by the hydrogel nanocomposite's XRD patterns, which show very little peaking in the case of ZnO [224].

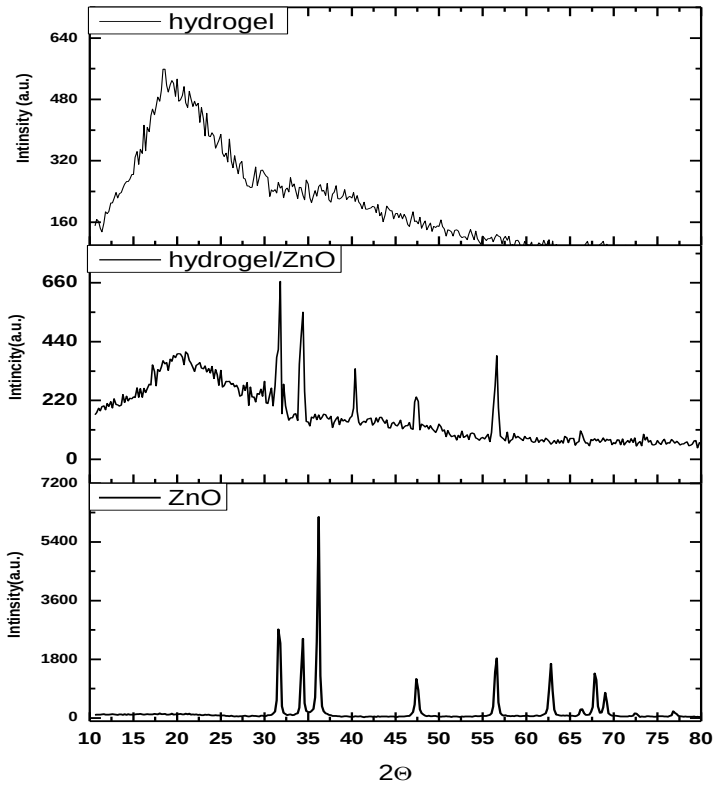

Figure (3-12):X-ray diffraction patterns for (a) ZnO NPs, (b) hydrogel,(d) hydrogel nanocomposite

3-2-2 FTIR characterization for adsorbent/adsorbate

The surface functional groups responsible for two medicines' (CLZ and CHL) adsorption were examined using the FTIR method. After adsorption, samples of hydrogel nanocomposite adsorbent surfaces and adsorbents loaded with drugs were heated to 65 °C for four hours. On an infrared spectrophotometer, FTIR, 8000, Shimadzu-Japan, the infrared spectra of three pollutants, including the drugs CLZ and CHL, on adsorbents were recorded before and after the adsorption process. Figures (3-13) and (3-14) present the findings.

Figures (3-13 and 3-14) show a large peak in the spectra of alginate that is due to the COOH groups and is seen at 3000 to 3500 cm^{-1};

minimal change in peak intensity was seen when alginate was modified with ZnO NPs. A novel distinctive adsorption band 1718 cm^{-1}, assigned to the C=O stretching of poly(acrylic amide), in the spectrum of hydrogel nanocomposite, supports the grafting of (acrylamide AM) on (Sodium alginate SA) [225].

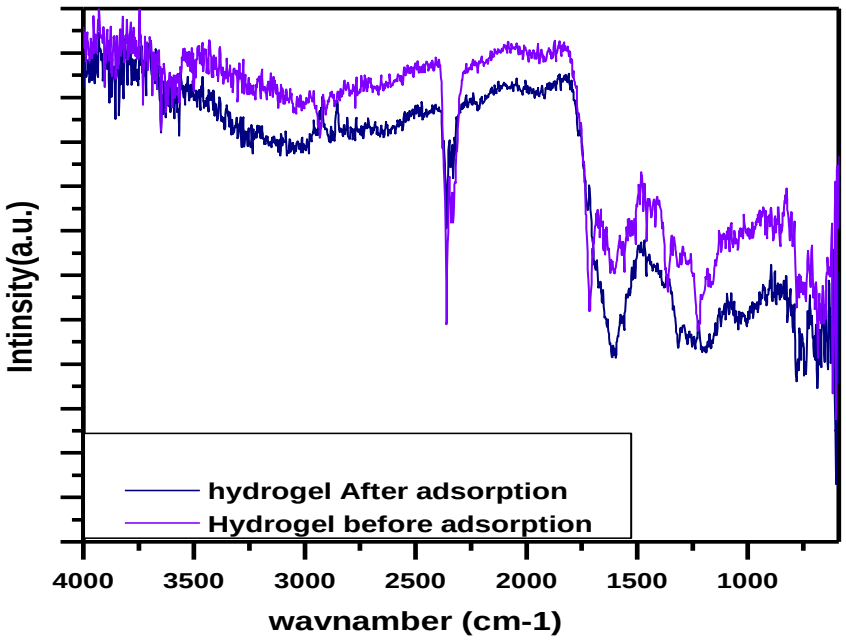

Figure (3-13) FT-IR spectra of hydrogel nanocomposite surface before, and after adsorption of CLZ drug.

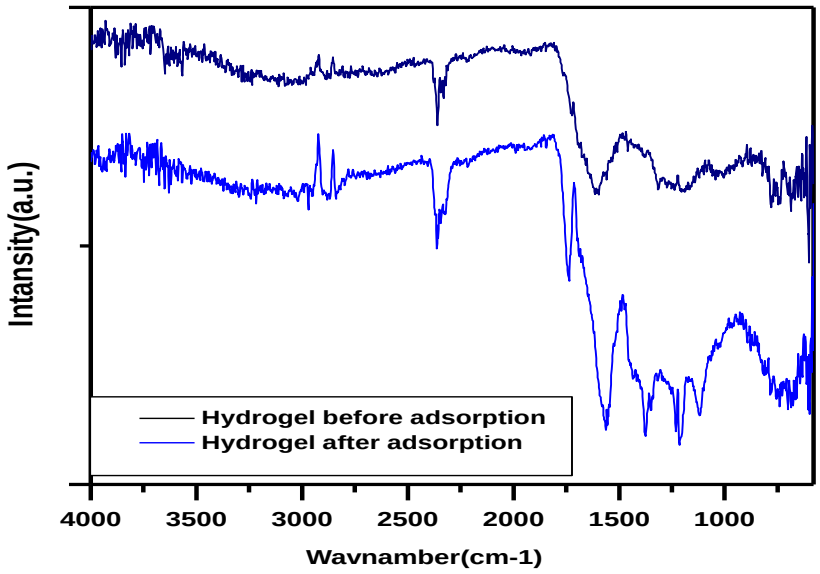

Figure (3-14) FT-IR spectra of hydrogel nanocomposite surface before, and after adsorption of CHL.

3.2.3 FE-SEM characterization for adsorbent/adsorbate:

Domain Emission The principal method for describing the surface appearance and essential physical characteristics of the adsorbent is scanning electron microscopy (FE-SEM). Figure 3-15 (a) shows ZnO NPs organized in a pattern resembling a flower. ZnO NPs have a good opportunity to become entangled in these pores [226]. Figure 3-15(b) of the CNT/ZnO micrographs depicts changes in the phase's morphology caused by the appearance of new, irregular bulky particles on the surface. This causes the surface texture's protuberance and coarseness to increase. By increasing the absorbents' surface area, water can more easily diffuse into the absorbent[227]. The hydrogel nanocomposite smooth porous surface and new irregular bulky particle presence on the hydrogel nanocomposite surface were both visible in the hydrogel's micrographs as rough porous surfaces (Figure 3-15(c and d)). Figure 3-15 (e and f) hows

a FE-SEM of an adsorbent material before and after the adsorption of two medicines onto the surface of a hydrogel nanocomposite [227, 228].

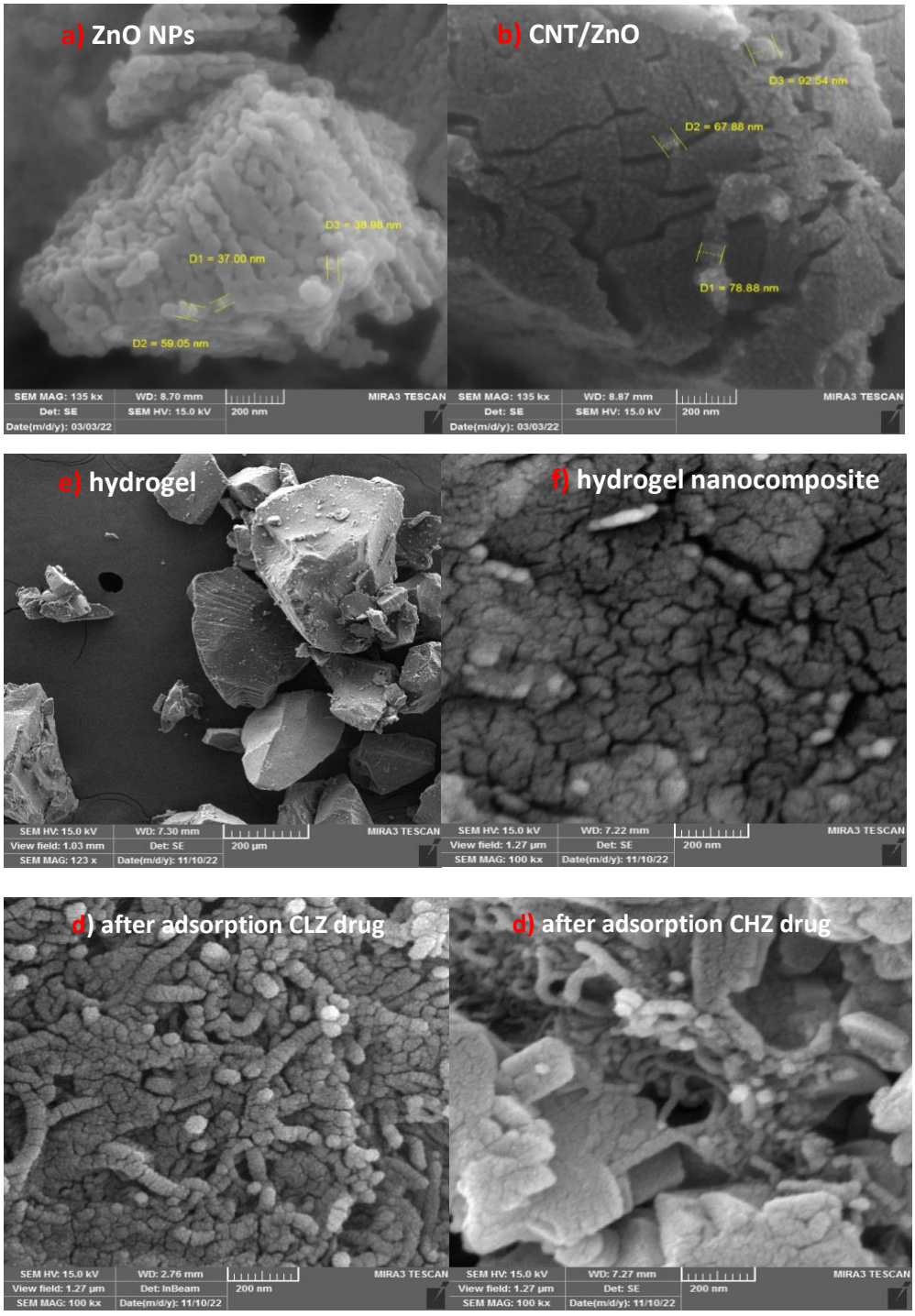

Figure (3-15) FE-SEM image of (a) ZnO NPs, (b)CNT/ZnO, (c) hydrogel, (d) hydrogel nanocomposite (e, f) for hydrogel nanocomposite before and after adsorption of two pharmaceutical CLZ & CHL

3.2.4 Transmittance Electron Microscopy (TEM) and Energy Dispersive X-Ray (EDX):

It was evident from Figure (3-16) that the cloud was more available and new geometry was created after decorated the CNT-ZnO on the hydrogel surface; this may be attributed to the role of amount of CNT-ZnO on the hydrogel surface. The morphology of the surface of ZnO; CNT, CNT/ZnO, and hydrogel nanocomposites were also investigated. The geometrical makeup of hydrogel nanocomposite materials as they are created is made clearer by TEM data. As can be observed in (Figure 3-16 (a-c)), the architecture-like nanostructure is made up of several single-crystal nameplates [229]. Figure 3-16 (d) illustrates how a single-crystal nameplate structure takes the form of a single cylinder stacked on top of another when CNT-ZnO is loaded.The results of the TEM experiments and the XRD and FESEM analyses were in good agreement. [230, 231]. The presence of CNT-ZnO on the hydrogel is indicated by the elements C, O, and Zn in the produced hydrogel nano-composite. the modified hydrogel nanocomposite's values of the greatest and lowest elements by 75.7 weight percent and 8.4 weight percent, respectively[232].

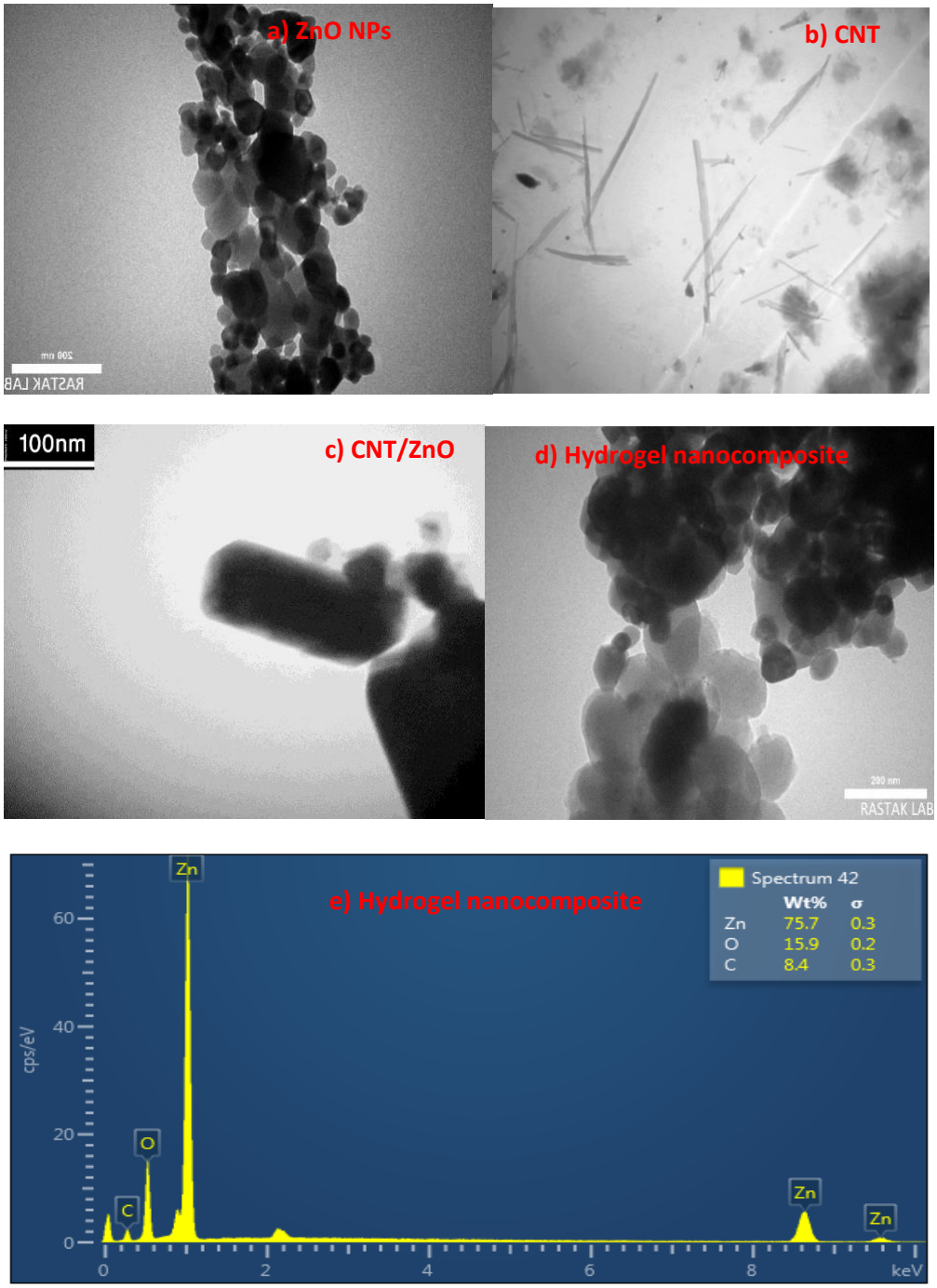

Figure (3-16): TEM images of (a)ZnO NPs, b) CNT, (c) CNT/ZnO, (d) hydrogel nanocomposite and (e) EDX of hydrogel nanocomposite.

3.2.5 Thermogravimetric analysis (TGA):

The mass change of a sample can be examined under predetermined conditions, which is the fundamental idea behind thermogravimetric analysis (TGA). TGA is therefore mostly used to comprehend certain thermal events as absorption, adsorption, desorption, oxidation, reduction,

sublimation, decomposition, and vaporization. TGA can also be used to assess volatile or gaseous compounds that are lost during chemical processes involving samples including nanomaterials, polymers, polymer nanocomposites, fibers, paints, coatings, and films. Using TGA, it is also able to forecast the thermal stability of samples and analyze the kinetics of chemical reactions under various conditions [233]

The hydrogel nanocomposite's thermal gravimetric study was looked at. One can see that the degradation process differs from that achieved at a heating rate of 5 °C/min up to 600 °C under a dry nitrogen flow in (Figure 3-17). It is well recognized that any weight loss below 200 degrees' Celsius results from the loss of unbound water, while weight loss between 200 and 800 degrees Celsius is mostly caused by the breakdown of organic matter [234].

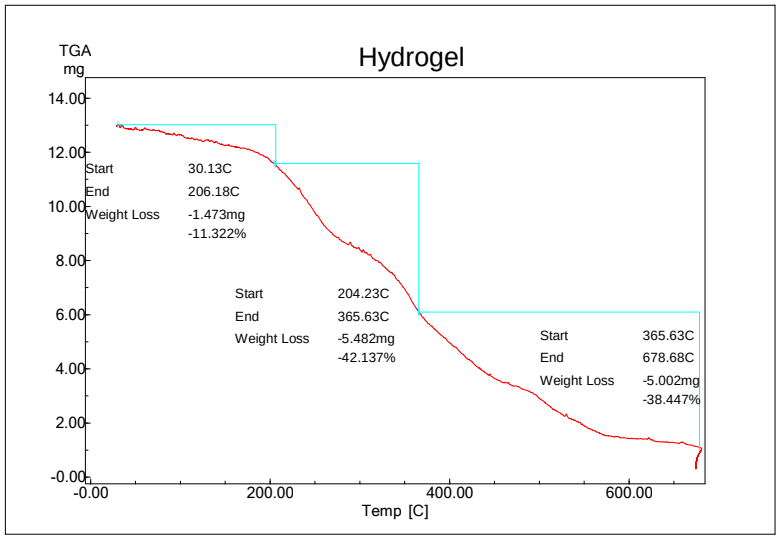

Figure (3-17): Thermal gravimetric analysis curve of the hydrogel nanocomposite

3.2.6 Surface Area Analyzer:

The nitrogen isothermal adsorption technique is used to determine the surface area and pore structure of hydrogel and hydrogel nanocomposite. Figures 3-18 and 3-19 show the pore size distributions

and nitrogen adsorption-desorption isotherms of hydrogel and hydrogel nanocomposite, respectively. A type IV hysteresis loop is visible in the nanocomposite's isotherm profile and is rather tiny. After adding carbon to the CNT-ZnO grafted onto hydrogel, the surface area, average pore diameter, and total pore volume increased (Tables 3-7 and 3-8). This work shows that the material's pore structure is significantly influenced by the interfacial interactions between CNT and ZnO [235, 236].

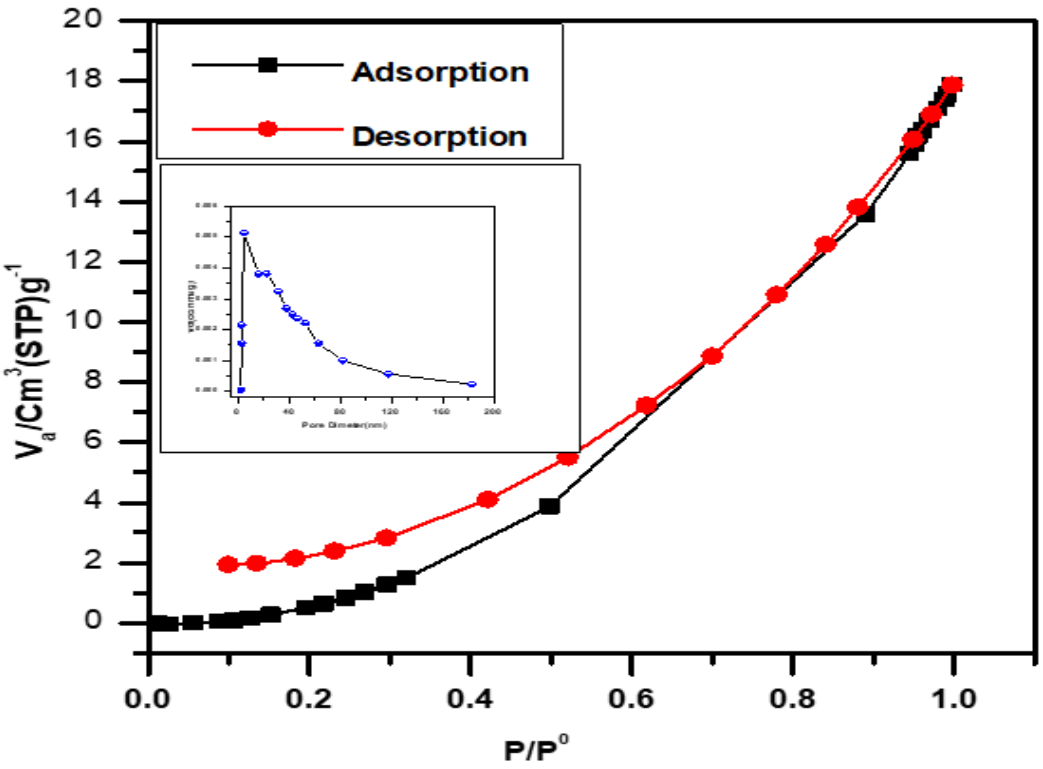

Figure (3-18): Nitrogen adsorption-desorption isotherms and the corresponding pore size distribution curve of hydrogel.

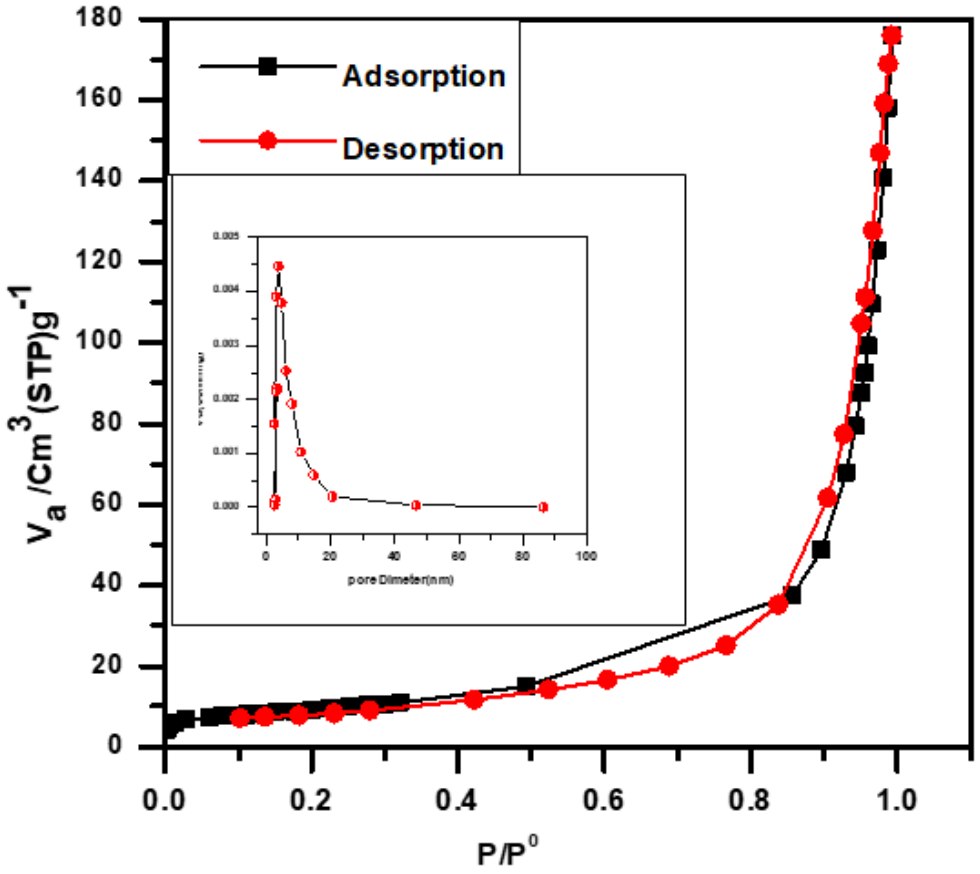

Figure (3-19): Nitrogen adsorption-desorption isotherms and the corresponding pore size distribution curve of hydrogel nanocomposite.

Table (3-7): Surface physical characteristics of hydrogel

Surface physical parameters	Value
BET surface area (m^2 g^{-1})	3.898
Langmuir surface area (m^2 g^{-1})	4.879
Micro pore surface area (m^2 g^{-1})	1.288
Cumulative pore volume (cm^3 g^{-1})	0.0149
Micro pore volume (cm^3 g^{-1})	0.0044

Table (3-8) :Surface physical characteristics of hydrogel nanocomposite

Surface physical parameters	Value
BET surface area ($m^2 g^{-1}$)	33.193
Langmuir surface area ($m^2 g^{-1}$)	96.23
Micro pore surface area ($m^2 g^{-1}$)	4.423
Cumulative pore volume ($cm^3 g^{-1}$)	0.012
Micro pore volume ($cm^3 g^{-1}$)	0.0344

3.3 Effect of different parameters on the adsorption process:

3.3.1 Effects of equilibrium time on the adsorption process:

One of the crucial considerations when evaluating the practical applicability of the adsorption process is the equilibrium time. [237] . The experimental outcomes of the adsorption of two medicines at initial concentrations of 100 mg. L^{-1} with contact time on the adsorbent surfaces of the hydrogel nanocomposite. Figures (3-20 and 3-21) depict the equilibrium result and indicate that the adsorption grew significantly in the first 20 minutes before increasing gradually till the equilibrium. Adsorption capacity rises as contact duration increases because as adsorption time grows, the active sites of absorbent surfaces saturate, suggesting that an apparent equilibrium has been established [238] .

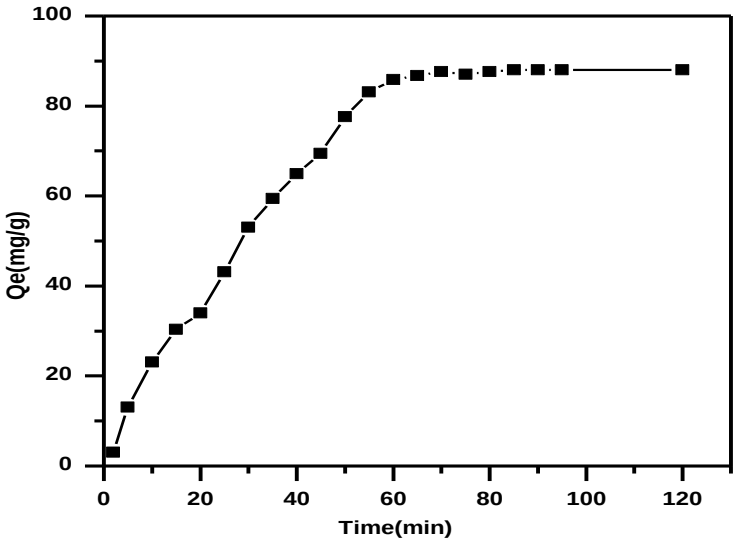

Figure (3-20) Effect of contact time on adsorption capacity for removal of CLZ drug by hydrogel nanocomposite at pH 6.6, Temp. 25 ºC and mass adsorbent 0.1 g.

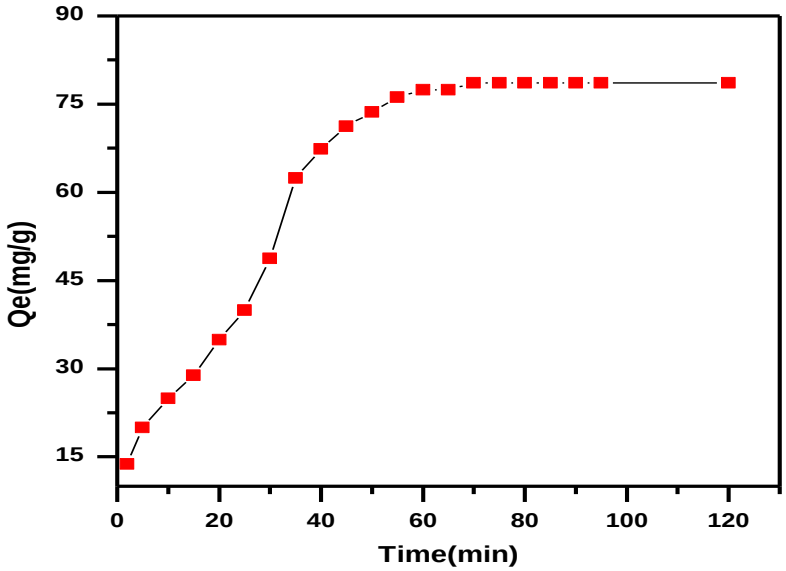

Figure (3-21): Effect of contact time on adsorption capacity for removal of CHZ drug by hydrogel nanocomposite at pH 6.6, Temp. 25 ºC and mass adsorbent 0.1 g.

3.3.2 Adsorbent Dose:

To notice the smallest amount that demonstrates the highest adsorption stoichiometric, the weight of the adsorbents has to be taken into consideration. From 0.05 to 0.13 g/100 mL of hydrogel nanocomposite were used as adsorbents. Table 3-9 to Table 3-10 and Figures 3-22 and 3-23 present the results.

Table (3-9): Effect of adsorbent dose on the removal percentage of CLZ drug on to hydrogel nanocomposite

$Co(mg.L^{-1})$	W(g)	$Ce(mg.L^{-1})$	E%	Qe mg/g
100	**0.05**	36.90909	63.09091	126.1818
100	**0.08**	22.36364	77.63636	97.04545
100	**0.1**	12	88	88
100	**0.12**	10	90	75
100	**0.13**	6.909091	93.09091	71.60839

Table (3-10): Effect of adsorbent dose on the removal percentage of CHZ drug on to hydrogel nanocomposite

$Co(mg.L^{-1})$	W(g)	$Ce(mg.L^{-1})$	E%	Qe mg/g
100	**0.05**	43.8427	56.1573	112.3146
100	**0.08**	31.37079	68.62921	85.78652
100	**0.1**	21.37079	78.62921	78.62921
100	**0.12**	17.4382	82.5618	68.8015
100	**0.13**	13.73034	86.26966	66.36128

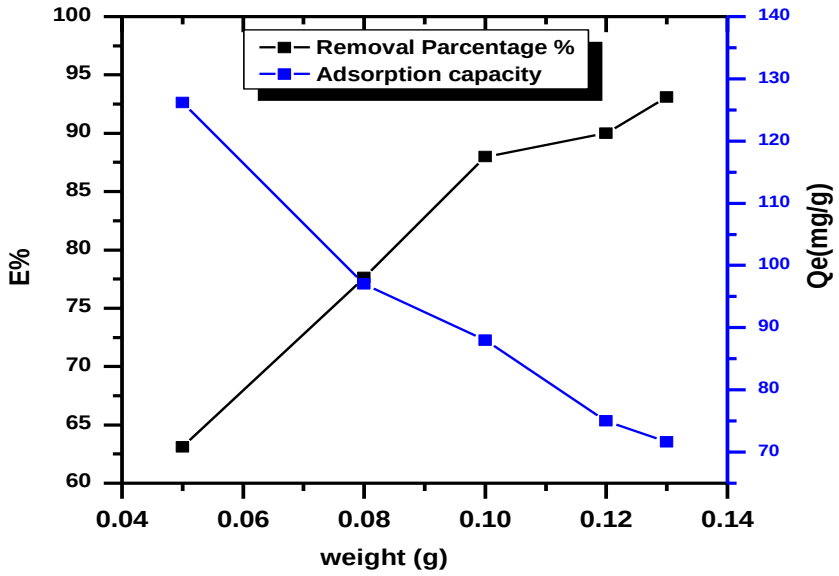

Figure (3-22): Effect of the weight amount of adsorbent hydrogel nanocomposite on the percent removal and amount of adsorbed CLZ drug, initial concentration = 100 mg.L^{-1}, Temp. = 25°C, contact time 1hr., pH=6.1.

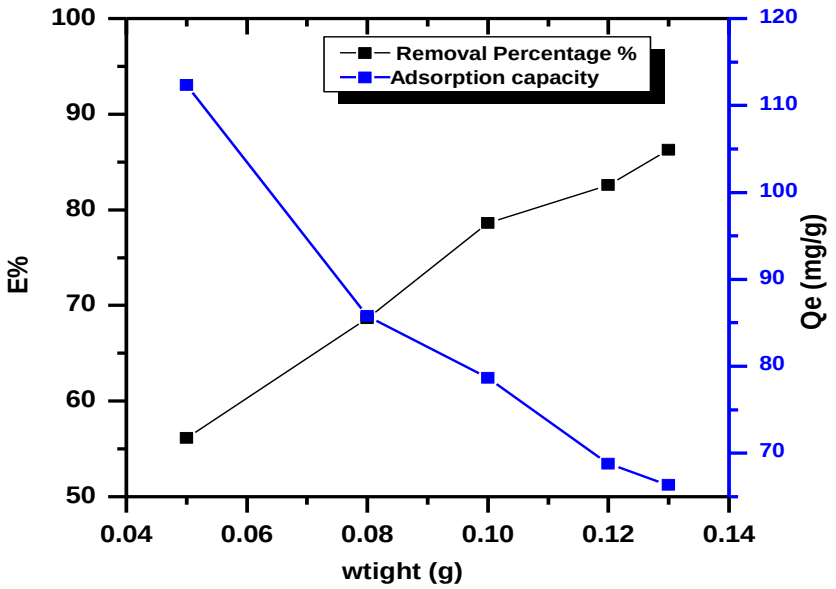

Figure (3-23): Effect of the weight amount of adsorbent hydrogel nanocomposite on the percent removal and amount of adsorbed CHZ drug, initial concentration = 100 mg.L^{-1}, Temp. = 25°C, contact time 1hr., pH=6.1.

3.3.3 Effect of Initial Pharmacetical Concentration

Surfaces hydrogel nanocomposite was used in this work to eliminate the initial concentrations of the (CLZ, CHL) medicines. The amount of adsorption required to remove two medicines relies on their initial concentration and the number of sites available on the adsorbent surface. Table (3-11) to (3-12) illustrates the influence of starting drug concentration on the removal of drug by hydrogel nanocomposite, and Figures (3-24 to 3-25) displays the removal efficiency versus initial drug concentration. The reduction in adsorption caused by a shortage of accessible active sites causes the drug clearance percentage to decline as drug concentration rises. As drug uptake resistance reduces as drug concentration rises, the adsorption capacity ((Qe) mg/g) is proportional to initial drug concentration. Due to an increase in driving force, the adsorption rate likewise rises as the drug's starting concentration does [239-242] **.**

Table (3-11): Effect of Initial CLZ drug on the removal percentage drug by hydrogel nanocomposite.

Co(mg.L^{-1})	Ce(mg.L^{-1})	E%	Qe mg/g
25	11.81818	52.72727	13.18182
50	16.36364	67.27273	33.63636
75	17.27273	76.9697	57.72727
100	19.09091	80.90909	80.90909
150	22.72727	84.84848	127.2727
200	28.18182	85.90909	171.8182

Table (3-12): Effect of Initial CHL on the removal percentage drug by hydrogel nanocomposite.

Co(mg.L^{-1})	Ce(mg.L^{-1})	E%	Qe mg/g
25	11.81818	52.72727	13.18182
50	16.36364	67.27273	33.63636
75	17.27273	76.9697	57.72727
100	19.09091	80.90909	80.90909
150	22.72727	84.84848	127.2727
200	28.18182	85.90909	171.8182

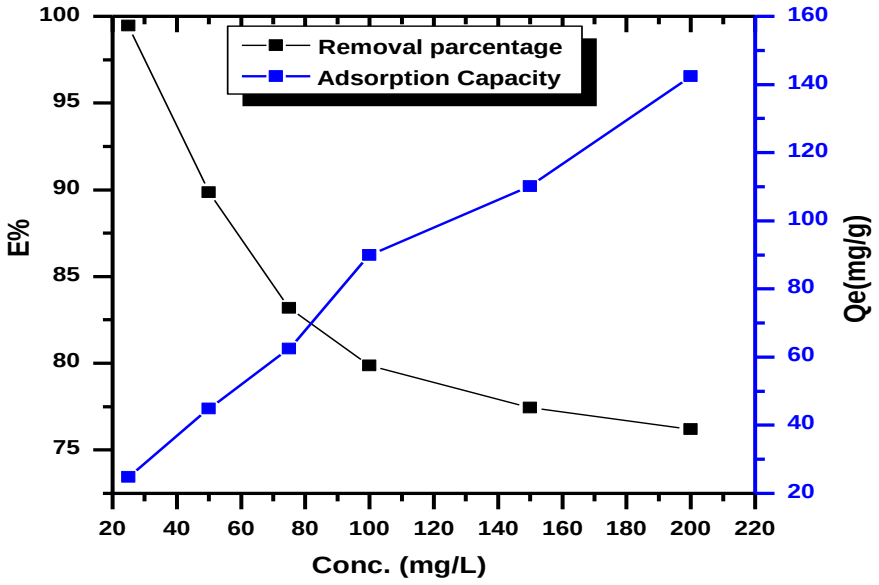

Figure (3-24): Effect of initial concentration on the percent removal and amount of adsorbed CHL drug onto hydrogel nanocomposite (Exp. Condition: Temp. = 25°C, contact time 1 h, and pH of solution 6 .1).

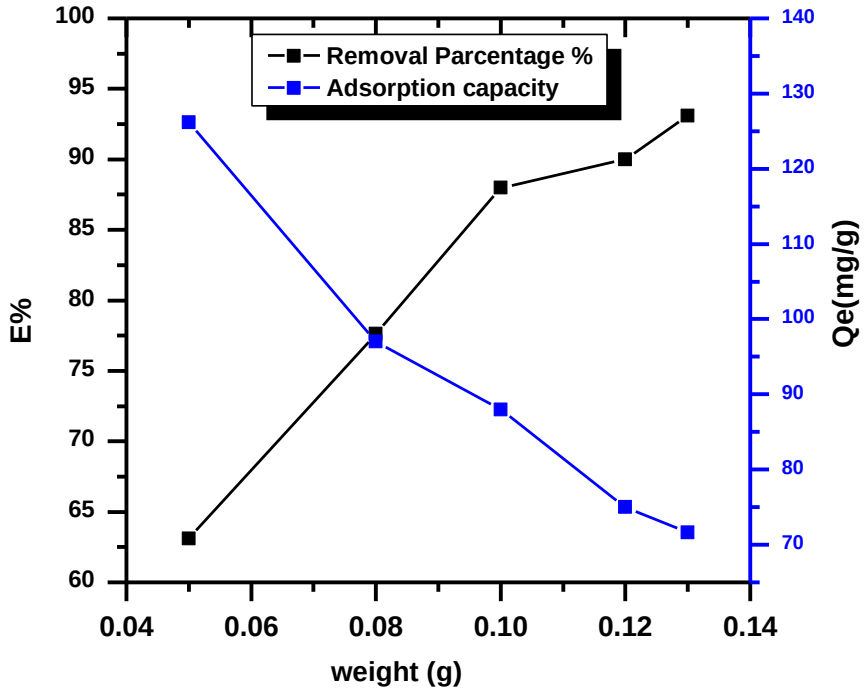

Figure (3-25): Effect of initial concentration on the percent removal and amount of adsorbed CLZ drug onto hydrogel nanocomposite (Exp. Condition: Temp. = 25°C, contact time 1 h, and pH of solution 6 .1).

3.3.4 pH solution :

Because of its impact on the surface characteristics of the adsorbent and the ionization/dissociation of the adsorbate molecule, the pH of an initial two drug solution has a significant impact on the adsorptive absorption of adsorbate molecules.[243], The degree of ionization and changes in structural and color stabilities for such an adsorbate are both influenced by the pH of the solution. The impact of acidity on the adsorption medium is thus one of the most crucial aspects in adsorption investigations. [244]. With starting drug concentrations of 100 mg.L^{-1}, the impact of pH on the adsorption of two medicines onto hydrogel nanocomposite was investigated. Figures 3-26 and 3-27 display the results, which are presented in Tables 3-13 and 3-14.

Table (3-13): Effect of solution pH on adsorption CLZ drug onto hydrogel nanocomposite

Co(mg/L)	pH	Ce(mg/L)	E%	Qe (mg/g)
100	2	46.54545	53.45455	53.45455
100	4	39.27273	60.72727	60.72727
100	6	12	88	88
100	9	10	90	90
100	11	6	94	94

Table (3-14): Effect of solution pH on adsorption CHZ drug onto hydrogel nanocomposite

Co(mg/L)	pH	Ce(mg/L)	E%	Qe (mg/g)
100	2	73.73034	26.26966	26.26966
100	4	58.89888	41.10112	41.10112
100	6	21.37079	78.62921	78.62921
100	9	16.31461	83.68539	83.68539
100	11	10.13483	89.86517	89.86517

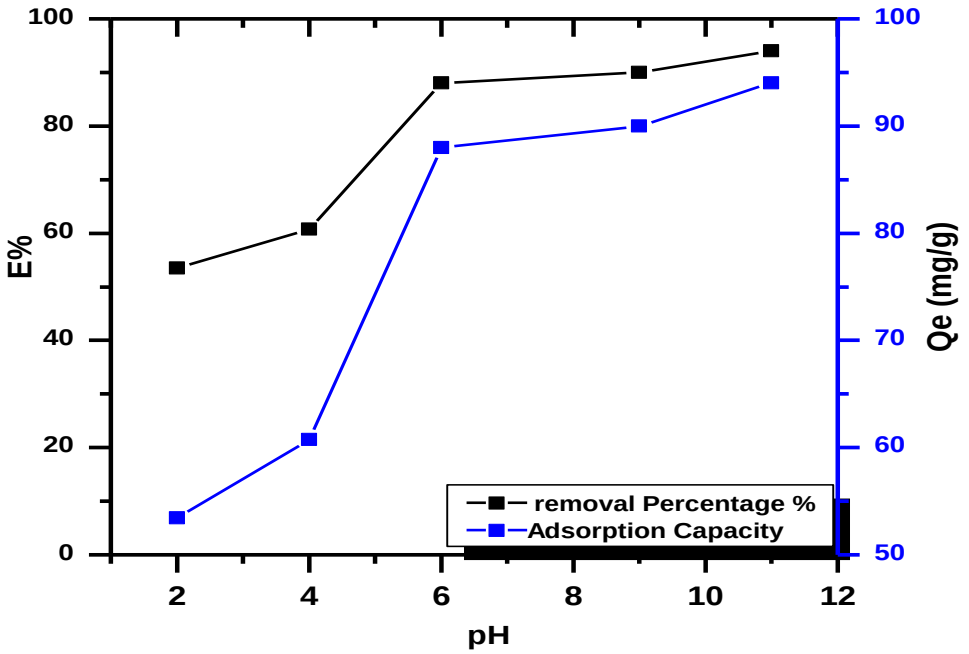

Figure (3-26): Effect of solution pH on the adsorption of CLZ drug on hydrogel nanocomposite . (Exp. Condition: Temp. = 25°C, contact time 1 hr).

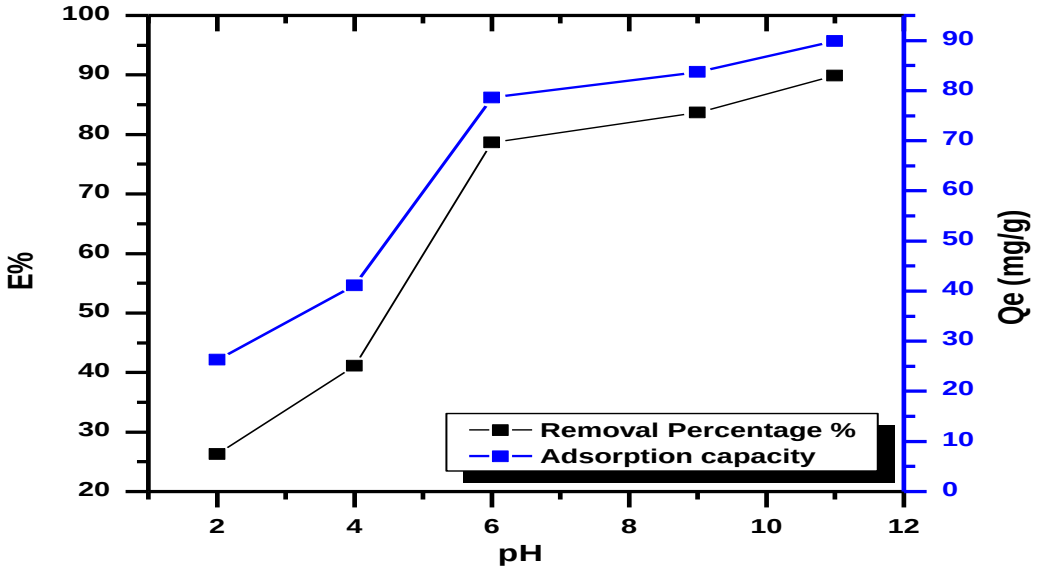

Figure (3-27): Effect of solution pH on the adsorption of CHZ drug on hydrogel nanocomposite . (Exp. Condition: Temp. = 25°C, contact time 1 hr).

3.3.5 Effect of Temperature:

Identify the exothermic or endothermic nature of the active adsorption process. For several drug-adsorbent systems, the adsorption isotherms were identified. The elimination of two medications has been investigated at different temperatures (15-35 C^o) with a range of beginning drug concentrations (10-200 mg L^{-1}). The results are shown in Tables (3-15 and 3-16) and displayed in Figures (3-28 and 3-29).

Table (3-15): Adsorption sotherm for adsorption of CLZ dye on the hydrogel nanocomposite at different temperatures. (pH 6.1, mass adsorbent 0.1 gm/ 100 ml, contact time 1h).

C_0 **mg. L^{-1}**	**15 C^o**		**25 C^o**		**35 C^o**	
	Q_e mg.g^{-1}	E %	Q_e mg.g^{-1}	E %	Q_e mg.g^{-1}	E %
25	24.45455	97.81818	24.45455	97.81818	24.63636	98.54545
50	47.54545	95.09091	48.54545	97.09091	49.09091	98.18182
75	69.90909	93.21212	69.90909	93.21212	70.81818	94.42424
100	84.90909	84.90909	88	88	90.36364	90.36364
150	119.4545	79.63636	126.7273	84.48485	134.9091	89.93939
200	153.0909	76.54545	153.0909	76.54545	173.0909	86.54545

Q : Adsorption capacity

E% : Removal percentage

C_o : Initial concentration

Table (3-16): Adsorption isotherm for adsorption of CHZ dye on the hydrogel nanocomposite at different temperatures. (pH 6.1, mass adsorbent 0.1 gm/ 100 ml, contact time 1h).

C_0 mg. L^{-1}	15 C°		25 C°		35 C°	
	Q_e mg.g^{-1}	E %	Q_e mg.g^{-1}	E %	Q_e mg.g^{-1}	E %
25	23.62921	94.51685	24.86517	99.46067	23.06742	92.26966
50	42.44944	84.89888	44.92135	89.8427	41.10112	82.20225
75	60.03371	80.04494	62.39326	83.19101	59.13483	78.84644
100	78.62921	78.62921	79.86517	79.86517	79.86517	79.86517
150	113.4607	75.64045	116.1573	77.4382	109.9775	73.31835
200	147.5056	73.75281	152.3933	76.19663	145.2584	72.62921

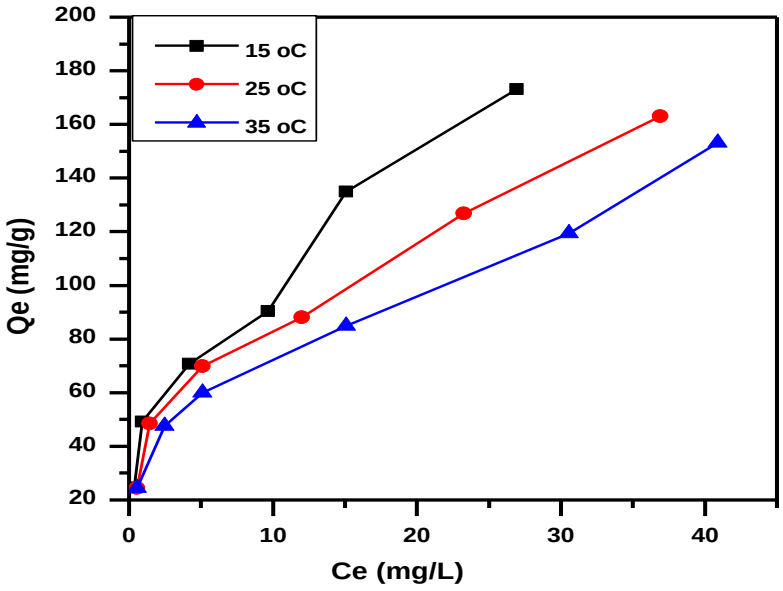

Figure (3-28) : Effect of temperature on the adsorption of CLZ on the surface of hydrogel nanocomposite (pH 6.1, mass adsorbent 0.1 gm/ 100 ml)

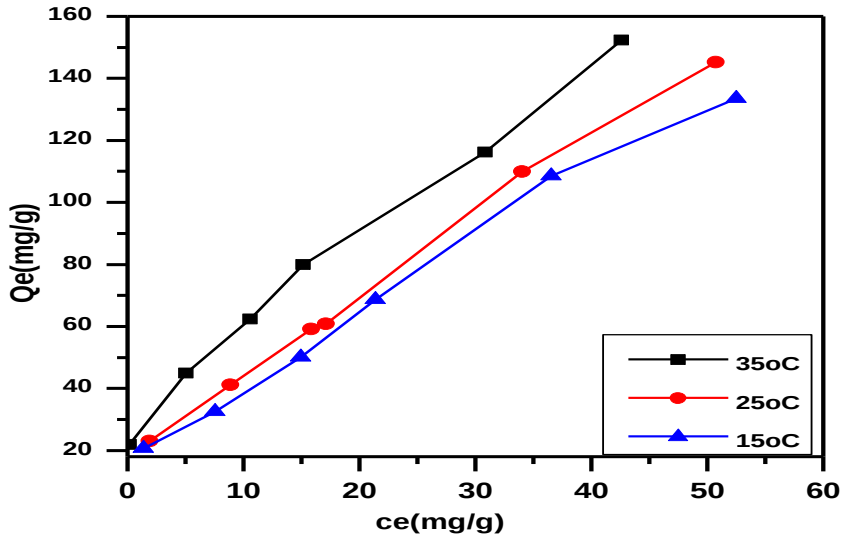

Figure (3-29) Effect of temperature on the adsorption of CHL on the surface of hydrogel nanocomposite. (pH 6.1, mass adsorbent 0.1 gm/ 100 ml)

The outcome demonstrates that, for all initial concentrations, the equilibrium adsorption capacity of the medicines CLZ and CHL has increased as the temperature of the solution has increased. As can be seen from Figures 3.28 and 3.29, the absorption capacity of hydrogel nanocomposite rises with rising temperature as a result of the mechanism's increased amplitude of the reverse (desorption) step. This may be a result of the environment's endothermic influence during the adsorption process [245].

Calculating the Gibbs free energy , change enthalpy , and change entropy , of the adsorption process will also be aided by the study of the impact of temperature on adsorption. From equations (3-2), the equilibrium constant (Ke) of the adsorption process at each temperature was determined [246]:

$$K_e = \frac{(Q_{max}) * Wt\ (0.1\ gm)}{(C_e) * V(0.1L)} \times 1000 \qquad 3-2$$

Where 0.1g stands for the weight of the hydrogel nanocomposite adsorbent that has been used, respectively, and 0.1L stands for the volume of the two drug solutions used in the adsorption process. Ce stands for the equilibrium concentration of the adsorbent expressed in ($mg.L^{-1}$).

The change in the free energy could be determined from the equation (3-3) [247]:

$$\Delta G=-RT \ln K_e \quad (3-3)$$

Where ΔG: Gibbs free energy ($J.K^{-1}.mol.^{-1}$), R is the gas constant (8.314 $J.K^{-1}.mole^{-1}$), T is the absolute temperature in Kelvin.

The enthalpy of adsorption may be obtained from the following equation (3-4) [247, 248]:

$$\ln X_m = -\frac{\Delta H}{RT} + Cons. \quad (3-4)$$

When Ce is a specific value of the equilibrium concentration (Ce) and Xm is the maximum amount of adsorption. Tables (3-17) and Table (3-18) provide Xm values for two medicines at various temperatures. As seen in Figures (3-30 and 3-31), plotting lnXm vs (1/T) should result in a line that is straight and has a slope of -H/R. The slope and intercept can be used to get the values of H and S, respectively.

Table (3-17) Maximum adsorption quantity Xm values of CLZ drug onto hydrogel nanocomposite surfaces at different temperatures.

T(K)	1000/T(K^{-1})	C_e = 26.5	
		X_m	ln X_m
288	3.472222	110	4.70048
298	3.355705	135	4.905275
308	3.246753	170	5.135798

Table (3-18) Maximum adsorption quantity Xm values of CHZ drug onto hydrogel nanocomposite surfaces at different temperatures.

T(K)	1000/T(K^{-1})	C_e = 40.12	
		X_m	ln X_m
288	3.472222	120	4.787492
298	3.355705	135	4.905275
308	3.246753	140	4.941642

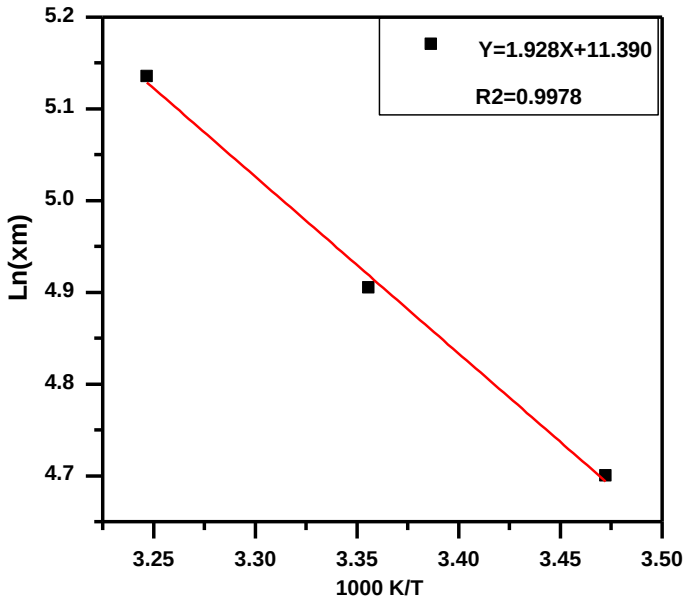

Figure (3-30) Plot ln X_m against the absolute temperature. of the adsorption (CLZ) onto hydrogel nanocomposite .

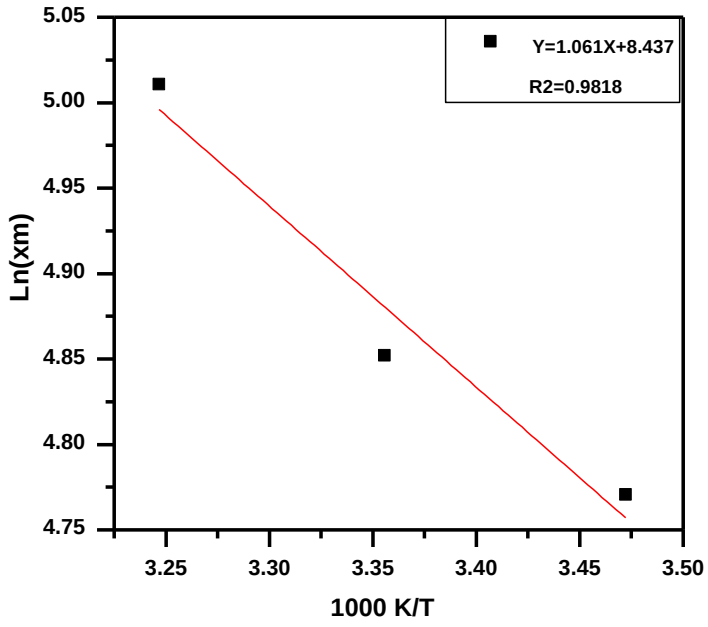

Figure (3-31) Plot ln X_m against the absolute temperature. of the adsorption (CHL) onto hydrogel nanocomposite

Tables 3.19 and 3.20 illustrate the quantitative thermodynamic effects of the medicines CLZ and CHZ on the hydrogel nanocomposite adsorbent surfaces. This table demonstrates that the ΔH values for the medicines CLZ and CHZ are positive, indicating an endothermic reaction during the adsorption process. All adsorption processes are taken into consideration to be spontaneous when ΔG is negative. While CLZ and CHZ medicines, which correspond to the random molecular interactions of the entire system, have positive values for ΔS [249, 250].

Table (3-19) : Thermodynamic parameter ΔS ΔG and, ΔH for CLZ drug adsorbed onto nanocomposite

Thermodynamic Factors			
ΔH(kJ/mol.)	**ΔG(kJ/mol.)**	**ΔS(J/K.mol.)**	**Equilibrium Constant(Ke)**
16.029	-4.311	94.11	5.47

Table (3-20): Thermodynamic parameter ΔS ΔG and, ΔH for CHZ drug adsorbed onto hydrogel nanocomposite

Thermodynamic Factors			
ΔH(kJ/mol.)	**ΔG(kJ/mol.)**	**ΔS(J/K.mol.)**	**Equilibrium Constant(Ke)**
8.8211	-3.311	70.144	3.36

3.4 Adsorption Isotherms

3.4.1 Freundlich Isotherm:

Equation 3.5 provides a definition for the Freundlich isotherm. [251] .

$$q_e = K_f C_e^{1/n} \quad (3.5)$$

q_e: Amount adsorbed per unit weight of the adsorbent at equilibrium (mg/g), (mol/g), Ce: Equilibrium concentration of the adsorbate in solution following adsorption (mg/L), (mol/L), Kf: Empirical Freundlich constant or capacity factor (L/g), or the amount of the drug adsorbed for one unit equilibrium concentration, 1/n: According to the Freundlich exponent, adsorption is linear if the value of n is equal to unity; if it is less than unity, the adsorption process is chemical; and if it is greater than unity, the adsorption process is physical [252].

3.4.2 Langmuir Isotherm:

The Langmuir isotherm is mostly employed for the adsorption of contaminants from liquid solutions. The Langmuir alternative equation 3.6 was used to determine the nature of the adsorption process [107]

$$q_e = \frac{q_m K_L C_e}{1 + K_L C_e} \qquad (3-6)$$

q_e: amount adsorbed per unit weight of adsorbent at equilibrium (mg/g), C_e: equilibrium concentration of adsorbent in solution after adsorption (mg/L), q_m: Empiricial Langmuir constant which represents maximum adsorption capacity (mg/g) or the total number of surface sites per mass of adsorbent and it may vary among different compounds because of differences in adsorbate sizes, K_L: empiricial Langmuir constant (L/mg) or the equilibrium constant of the adsorption reaction [253].

The values of KF and 1/n are derived from the intercept and slope of the linear regressions (Tables 3-21) and (Table 3-22), which are plotted as qe versus Ce in Figures 3-32 and 3-33.

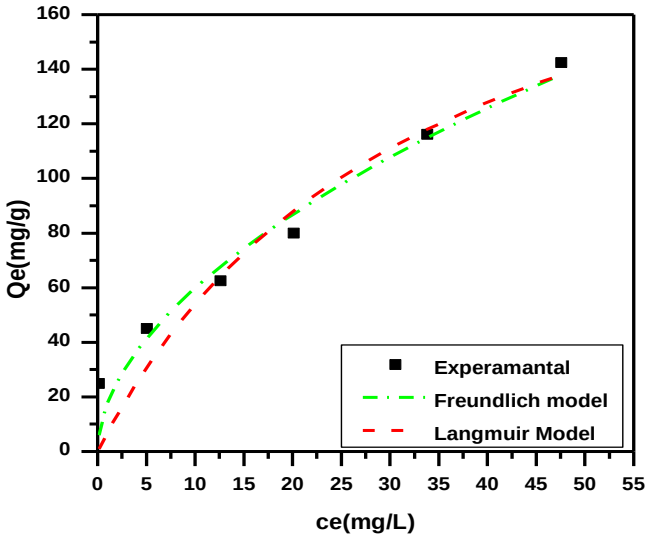

Figure (3-32): Nonlinear fit of different adsorption isotherm models for adsorption of CHL drug on hydrogel nanocomposite, initial concentration = 100 mg/L, Temp. = 25°C, contact time 1 h, and mass of adsorbent 0.1 g/L).

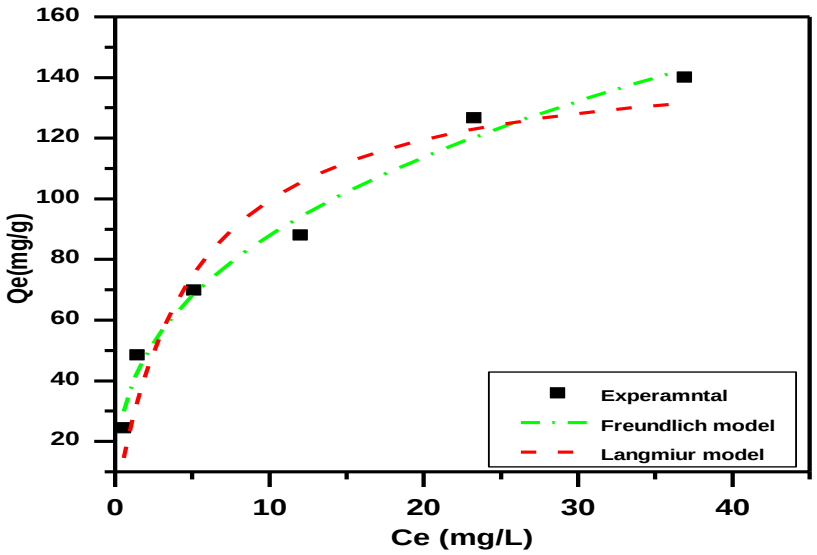

Figure (3-33): Nonlinear fit of different adsorption isotherm models for adsorption of CLZ drug on hydrogel nanocomposite, initial concentration = 100 mg/L, Temp. = 25°C, contact time 1 h, and mass of adsorbent 0.1 g/L).

Table (3-21): several factor isotherm for the adsorption study of CHL on to hydrogel nanocomposite

Hydrogel nanocomposite			
Freundlich	K_f	17.402	5.231±
	1/n	0.566	±0.084
	R^2	0.93899	
Langmuir	q_m (mg/g)	235.737	74.76±
	K_L (L/mg)	0.02	0.011±
	R^2	0.8891	

Table (3-22): several factor isotherms for the adsorption study of CLZ drug on to hydrogel nanocomposite

Hydrogel nanocomposite			
Freundlich	K_f	37.419	3.348±
	1/n	0.37	±0.084
	R^2	0.98814	
Langmuir	q_m (mg/g)	149.66	16.876±
	K_L (L/mg)	0.199	0.0811±
	R^2	0.9011	

3.5 Removal of Real Aqueous Pollutants by Using hydrogel nanocomposite

A given example In this study, 100 mL of pharmaceutical pollutants at a refry concentration were added to an Erlenmeyer conical flask along with 0.1 g of freshly prepared hydrogel nanocomposite. The mixture was then placed in a sonicated water bath for two hours, after which the supernatant was separated by centrifugation, and the remaining concentration was determined using a UV-Visible spectrophotometer at

the max nm [254] the outcome is depicted in figure (3-34)

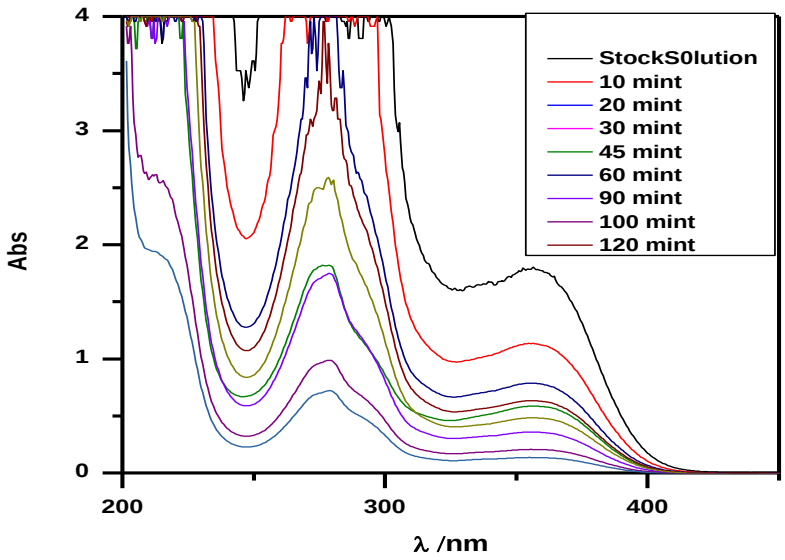

Figure (3-34): Spectra of removal pollutants by using hydrogel nanocomposite, (Exp. Condition: Temp. = 25°C, contact time 2 h, and mass absorbent 0.1 g).

3.6 A Comparative adsorption between different surfaces to removal two pharm. :

As adsorbents was, a comparison of CNT/ZnO, hydrogel, and hydrogel nanocomposite surfaces was conducted.The order of increasing hydrogel nanocomposite > hydrogel > CNT/ZnO produced the best percentage of elimination (E%) results for the two medicines (CLZ and CHL).The positive percentage of removal (E%) values for medications (CLZ and CHL) were 90.9%, 81.812%, and 1.818. seen in Figures (3–35).

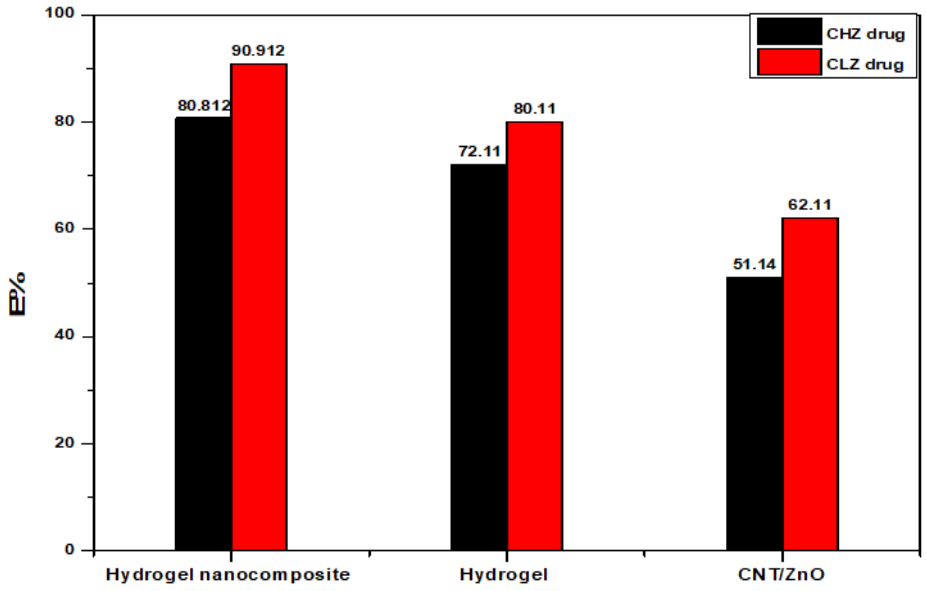

Figure (3-35): Comparative adsorption between different surfaces to removal two pharmaceutical .

3.7 Regeneration and Desorption of hydrogel nanocomposite.

One important economic factor for the treatment approach is the regeneration of the hydrogel nanocomposite after sorption. It aids in clarifying the process of removing the two pharmaceuticals CLZ and CHL from drug-loaded adsorbents, the mechanism of regeneration, and the recycling of used adsorbents, all of which may help to lower operating costs and safeguard the environment from secondary pollution. Utilizing various desorption agents at concentrations (0.01 N), including H_2SO_4, NaOH, H_3PO_4, HCl, HNO_3, and water, two medicines, CLZ and CHZ, were studied [255-258] . Utilizing water, the hydrogel nanocomposite was 100% regenerable. Under ideal circumstances, the effectiveness and reusability of hydrogel nanocomposite in the (CLZ and CHL medicines) adsorption process were tested up to 4 steps (Figures 3-36 and 3-37). Efficiency is still high (>80%) after three cycles of utilizing

hydrogel nanocomposite, indicating that it is likely a renewable adsorbed material. [257, 258].

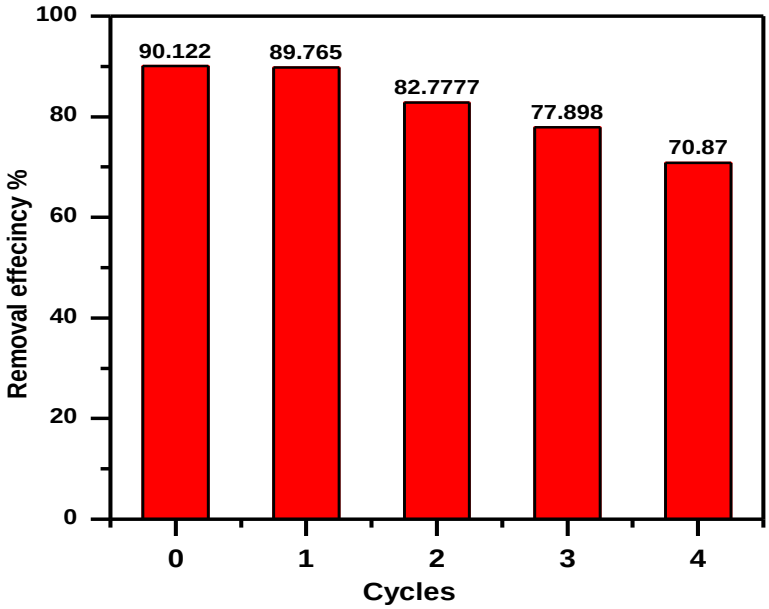

Figure 3-36: multi-cycle use of hydrogel nanocomposite for CLZ adsorption using water as desorption medium.

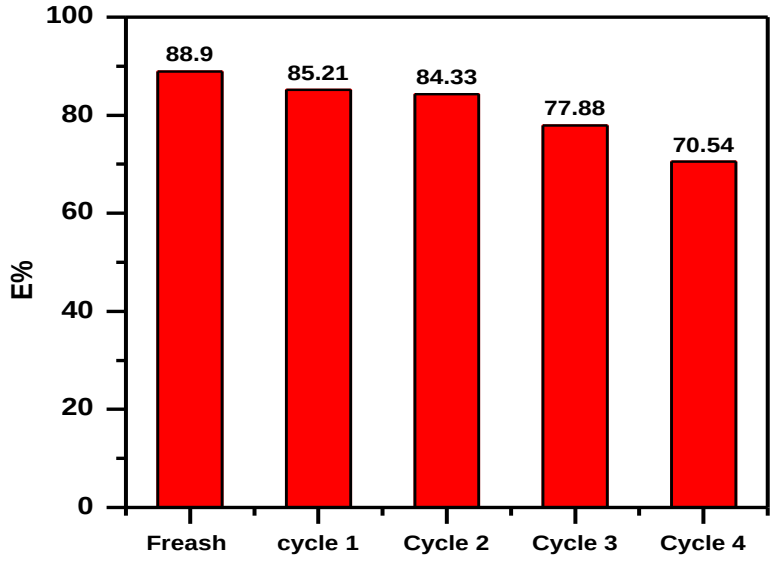

Figure 3-37: multi-cycle use of hydrogel nanocomposite for CHL drug adsorption using water as desorption medium.

Conclusion

Studies have been conducted to gain understandings and generic knowledge of the equilibrium aspects of adsorption of adsorbents (SA-g-P(Ac-co-AM)/ZnO-CNT) hydrogel nanocomposite, ((SA-g-P(Ac-co-AM) ,,ZnO /CNT surfaces. Removal of two pollutant (CLZ and CLH) from aqueous solutions by adsorption with (SA-g-P(Ac-co-AM)/ZnO-CNT) hydrogel nanocomposite surfaces have been experimentally determined. The best results have been found in temperature 25 oC, and adsorbent dosage 0.1gm of (SA-g-P(Ac-co-AM)/ZnO-CNT) hydrogel nanocomposite for both studying adsorption capacity and removal percentage" and the following observations are made:

1. The adsorption efficiency and removal parentage E% of two pollutant removal increase with increasing contact time, surface area, and temperature. But adsorption capacity has decreased with the increase of adsorbent dosage.
2. The optimum contact time for equilibrium to be achieved is found to be 2 hr.
3. The negative value of ΔG confirms the spontaneous nature adsorption process. The positive value of ΔS showed the increased randomness at the solid-solution interface during adsorption and the positive value of ΔH indicated the adsorption process was endothermic.
4. Adsorbent showed fits better to Freundlich isotherm which suggests that adsorption is heterogeneous.

5. (SA-g-P(Ac-co-AM)/ZnO-CNT) hydrogel nanocomposite had high antibacterial activity, That is, it had a higher effect on the Gram-positive bacteria than on the Gram-negative bacteria.
6. In two to seven days, according to the results, there is complete healing of the mice and the return of the skin to its natural color.

Reference

References

1. Shannon, M.A., et al., *Science and technology for water purification in the coming decades.* Nature, 2008. **452**(7185): p. 301-310.
2. Ai, L. and J. Jiang, *Removal of methylene blue from aqueous solution with self-assembled cylindrical graphene–carbon nanotube hybrid.* Chemical Engineering Journal, 2012. **192**: p. 156-163.
3. Walter, K. and M.R.W. Dodds, *Chapter 16 - Responses to Stress, Toxic Chemicals, and Other Pollutants in Aquatic Ecosystems*, in *Aquatic Ecology*. 2020. p. 453-502.
4. Nupur, N., et al., *Supercritical Extraction of Valued Components From Animals Parts.* Food Science, 2021. **1**: p. https://doi.org/10.1016/B978-0-08-100596-5.22673-5.
5. Bao, N., et al., *Adsorption of dyes on hierarchical mesoporous TiO2 fibers and its enhanced photocatalytic properties.* The Journal of Physical Chemistry C, 2011. **115**(13): p. 5708-5719.
6. Buonomenna, M., et al., *Preparation, characterization and use of PEEKWC nanofiltration membranes for removal of Azur B dye from aqueous media.* Reactive and Functional Polymers, 2009. **69**(4): p. 259-263.
7. Liu, C.-H., et al., *Removal of anionic reactive dyes from water using anion exchange membranes as adsorbers.* Water Research, 2007. **41**(7): p. 1491-1500.
8. Muruganandham, M. and M. Swaminathan, *TiO 2–UV photocatalytic oxidation of Reactive Yellow 14: effect of operational parameters.* Journal of hazardous materials, 2006. **135**(1): p. 78-86.
9. Arami, M., et al., *Equilibrium and kinetics studies for the adsorption of direct and acid dyes from aqueous solution by soy meal hull.* Journal of Hazardous Materials, 2006. **135**(1): p. 171-179.
10. Sahoo, S., S. Parveen, and J. Panda, *The present and future of nanotechnology in human health care.* Nanomedicine: Nanotechnology, Biology and Medicine, 2007. **3**(1): p. 20-31.

11. Weiss, J., P. Takhistov, and D.J. McClements, *Functional materials in food nanotechnology.* Journal of food science, 2006. **71**(9).
12. Whitesides, G.M., *Nanoscience, nanotechnology, and chemistry.* Small, 2005. **1**(2): p. 172-179.
13. Danner, M.-C., et al., *Antibiotic pollution in surface fresh waters: Occurrence and effects.* Science of The Total Environment, 2019. **664**: p. 793-804.
14. Quesada, H.B., et al., *Surface water pollution by pharmaceuticals and an alternative of removal by low-cost adsorbents: A review.* Chemosphere, 2019. **222**: p. 766-780.
15. Kumar, R., A.K. Sarmah, and L.P. Padhye, *Fate of pharmaceuticals and personal care products in a wastewater treatment plant with parallel secondary wastewater treatment train.* Journal of Environmental Management, 2019. **233**: p. 649-659.
16. Turk Sekulic, M., et al., *Surface functionalised adsorbent for emerging pharmaceutical removal: Adsorption performance and mechanisms.* Process Safety and Environmental Protection, 2019. **125**: p. 50-63.
17. Huber, M.M., et al., *Oxidation of Pharmaceuticals during Ozonation and Advanced Oxidation Processes.* Environ. Sci. Technol., 2003. **37**: p. 1016-1024.
18. Gagol, M., et al., *Effective degradation of sulfide ions and organic sulfides in cavitation-based advanced oxidation processes (AOPs).* Ultrasonics Sonochemistry, 2019. **58**: p. 104610.
19. Azuma, T., K. Otomo, M. Kunitou, M. Shimizu, K. Hosomaru, S. Mikata, Y. Mino, and T. Hayashi, *Removal of pharmaceuticals in water by introduction of ozonated microbubbles.* . Separation and Purification Technology, , 2019. **212**: p. 483-489.
20. Divyapriya, G., R. Srinivasan, I.M. Nambi, and J. Senthilnathan, , *Highly active and stable ferrocene functionalized graphene encapsulated carbon felt array - A novel rotating disc electrode for electro-Fenton oxidation of pharmaceutical compounds.* . Electrochimica Acta,

, 2018. **283**: p. 858-870.

21. Bora, N.S., et al., *Amelioration of UV radiation-induced photoaging by a combinational sunscreen formulation via aversion of oxidative collagen degradation and promotion of TGF-Smad-mediated collagen production.* European Journal of Pharmaceutical Sciences, 2019. **127**: p. 261-275.
22. Fabrao, R.M., et al., *Appraisal of photoelectrocatalytic oxidation of glucose and production of high value chemicals on nanotube Ti/TiO2 electrode.* Electrochimica Acta, 2019. **222**: p. 123-132.
23. Hernndez, R., et al., *Microwave-assisted sol-gel synthesis of an Au-TiO2 photoanode for the advanced oxidation of paracetamol as model pharmaceutical pollutant.* . Electrochemistry Communications, 2018. **96**: p. 42-46.
24. Dąbrowski, A., *Adsorption — from theory to practice.* Advances in Colloid and Interface Science, 2001. **93**(1): p. 135-224.
25. Ruthven, D.M., *Principles of Adsorption and Adsorption Processes*. 1984: Wiley.
26. Toth, J., *Adsorption*. 2002: Taylor & Francis.
27. Moosavi, S., et al., *Application of efficient magnetic particles and activated carbon for dye removal from wastewater.* ACS omega, 2020. **5**(33): p. 20684-20697.
28. Jarrige, F., et al., *The Contamination of the Earth: A History of Pollutions in the Industrial Age*. 2021: MIT Press.
29. Rehman, M.S.U., et al., *Global risk of pharmaceutical contamination from highly populated developing countries.* Chemosphere, 2015. **138**: p. 1045-1055.
30. Sell, N.J., *Industrial Pollution Control: Issues and Techniques*. 1992: Wiley.
31. Sen, T.K., *Air, Gas, and Water Pollution Control Using Industrial and Agricultural Solid Wastes Adsorbents*. 2017: CRC Press.
32. Thorsheim, P., *Inventing Pollution: Coal, Smoke, and Culture in Britain since 1800*. 2018: Ohio University Press.
33. Soloneski, S. and M. Larramendy, *Emerging Pollutants: Some Strategies for the Quality Preservation of Our Environment*. 2018: IntechOpen.
34. Rashid, R., et al., *A state-of-the-art review on wastewater treatment techniques: the effectiveness of adsorption method.*

Environmental Science and Pollution Research, 2021. **28**: p. 9050-9066.

35. C. P. Almeida, N.A. Debacher, A.J. Downs, L. Cottet, and A.D. Mello *Removal of methylene blue from colored effluents by adsorption on montmorillonite clay.* J. Collid Interface Sci., 2009. **332**(1): p. 46-53.
36. B.K.Nandi, R. Uppaluri, and M.K. Purkait, *Preparation and characterization of low cost ceramic membranes for micro-filtration applications.* Appl. Clay Sci., 2008. **42**: p. 102-110.
37. M. Alkan, M. Doğan, Y. Turhan, Ö. Demirbas, and P. Turanc, *Adsorption kinetics and mechanism of maxilonblue 5G dye on sepiolite from aqueous solutions.* Chem. Eng. J., 2008. **139**(2): p. 213-223.
38. S. Zhao, F. Zhou, L. Li, M. Cao, D. Zuo, and H. Liu, *Removal of anionic dyes from aqueous solutions by adsorption of chitosan-based semi-IPN hydrogel composites.* Composites: Part B 2012. **43** p. 1570-1578.
39. N. K.Amin, *Removal of direct blue-106 dye from aqueous solution using new activated carbons developed from pomegranate peel: Adsorption equilibrium and kinetics.* J.Hazard. Mater., 2009. **165**: p. 52-62.
40. M.C. S. Reddy, L. Sivaramakrishna, and A. V. Reddy, *The use of an agricultural waste material, Jujuba seeds for the removal of anionic dye (Congo red) from aqueous medium.* Journal of Hazardous Materials, 2012. **203-204**: p. 118-127.
41. G.Anaduria, R.S. Juang, and D.J. Lee, *Adsorption of Rhodamine 6G from aqueous solutions on activated carbon.* Environ.Sci.Health, 2001. **36**: p. 715-725.
42. T.A. Albanis, T.G. Danis, and M. Kourgiu *Adsorption-desorption studies of selected chlorphenols and herbicides and metal release in soil mixtures with fly ash and soil.* Environ.Technol. , 1998 **19**: p. 25-34.
43. Z. Wu, I. Ahn, C. Lee, J. Kim, Y. Shul, and K. Lee *Enhancing the organic dye adsorption on porous xerogels.* Colloids and Surfaces A: Physicochem. Eng. Aspects, 2004. **240**: p. 157-164.
44. S. Chowdhury, and P. Saha, *Sea shell powder as a new adsorbent to remove Basic Green 4 (Malachite Green) from aqueous*

solutions: equilibrium, kinetic and thermodynamic studies. Chem. Eng. J., 2010. **164**: p. 168-177.

45. A.Nemr, O. Abdelwahab, A. Khaled, and A. El Sikaily, *Biosorption of Direct Yellow 12 from aqueous solution using green alga Ulva lactuca.* Chemistry and Ecology, 2006. **22**(4): p. 253–266.
46. P. Vieira, A.A. Santana, W.B. Bezerra, Hildo A.S. Silva, A.P. Chaves, C.P. de Melo, C.da Silva Filho, and C. Airoldi *Kinetics and thermodynamics of textile dye adsorption from aqueous solutions using babassu coconut mesocarp.* J.Hazard.Mater., 2009. **166**: p. 1272-1278.
47. A.W. Adamson, *Physical Chemistry of Surface.* Wiley, New York, 2001. **3 ed.**
48. Viswanathan, V.K., et al., *Nanotechnology in Spine Surgery: A Current Update and Critical Review of the Literature.* World Neurosurgery, 2019. **123**: p. 142-155.
49. Zhang, W., D. Zhang, and Y. Liang, *Nanotechnology in remediation of water contaminated by poly- and perfluoroalkyl substances: A review.* Environmental Pollution, 2019. **247**: p. 266-276.
50. Fu, L.-H., et al., *Cellulose/vaterite nanocomposites: Sonochemical synthesis, characterization, and their application in protein adsorption.* Materials Science and Engineering: C, 2019. **96**: p. 426-435.
51. Teow, Y.H. and A.W. Mohammad, *New generation nanomaterials for water desalination: A review.* Desalination, 2019. **451**: p. 2-17.
52. Stone, V., et al., *Nanomaterials for environmental studies: classification, reference material issues, and strategies for physico-chemical characterisation.* Science of the total environment, 2010. **408**(7): p. 1745-1754.
53. Metanawin, S., et al., *The functionalization of hybrid titanium dioxide by miniemulsion polymerization technique.* Materials Today: Proceedings, 2018. **5**(3, Part 2): p. 9651-9657.
54. Lopez-Rubio, A., et al., *A novel approach for calculating starch crystallinity and its correlation with double helix content: A combined XRD and NMR study.* Biopolymers, 2008. **89**(9): p. 761-768.

55. Arivalagan, K., et al., *Nanomaterials and its potential applications.* Int. J. ChemTech Res, 2011. **3**(2): p. 534-538.
56. Cao, G., *Nanostructures and nanomaterials: synthesis, properties and applications*. 2004: World Scientific.
57. Larramendy, M.L. and S. Soloneski, *GREEN NANOTECHNOLOGY OVERVIEW AND FURTHER PROSPECTS.* J Nanotech Mater Sci, 2016. **3**(1): p. 1-7.
58. Nersisyan, H.H., et al., *Combustion synthesis of zero-, one-, two- and three-dimensional nanostructures: Current trends and future perspectives.* Progress in Energy and Combustion Science, 2017. **63**: p. 79-118.
59. Erol, O., et al., *Recent advances in bioactive 1D and 2D carbon nanomaterials for biomedical applications.* Nanomedicine: Nanotechnology, Biology and Medicine, 2018. **14**(7): p. 2433-2454.
60. Patra, S., et al., *2-Dimensional graphene as a route for emergence of additional dimension nanomaterials.* Biosensors and Bioelectronics, 2019. **89**: p. 8-27.
61. Lee, S.C., et al., *Hierarchically three-dimensional (3D) nanotubular sea urchin-shaped iron oxide and its application in heavy metal removal and solar-induced photocatalytic degradation.* Journal of Hazardous Materials, 2018. **354**: p. 283-292.
62. Yadav, T.P., R.M. Yadav, and D.P. Singh, *Mechanical milling: a top down approach for the synthesis of nanomaterials and nanocomposites.* Nanoscience and Nanotechnology, 2012. **2**(3): p. 22-48.
63. Joseph, D., Y.S. Huh, and Y.-K. Han, *A top-down chemical approach to tuning the morphology and plasmon resonance of spiky nanostars for enriched SERS-based chemical sensing.* Sensors and Actuators B: Chemical, 2019. **288**: p. 120-126.
64. Xie, K., et al., *Recent progress on fabrication methods of polymeric thin film gas separation membranes for CO2 capture.* Journal of Membrane Science, 2019. **572**: p. 38-60.
65. Pillar-Little, T.J., et al., *Superior photodynamic effect of carbon quantum dots through both type I and type II pathways: Detailed*

comparison study of top-down-synthesized and bottom-up-synthesized carbon quantum dots. Carbon, 2018. **140**: p. 616-623.

66. Ba Ryong An, G.-D.L., Dae Hee Son, Seung Ho Lee and Seong Soo Park, *Thermochromic Property of Tungsten Doped VO2 Prepared by Hydrothermal Method.* Journal of the Korean Industrial and Engineering Chemistry, 2019. **24**(6): p. 611-615.
67. Otromke, M.W., Robin J.;Sauer, Jrg, *Hydrothermal base catalyzed depolymerization and conversion of technical lignin : An introductory review.* Carbon Resources Conversion, 2019. **2**(1): p. 59-71.
68. Abdullah, T.A., et al., *Functionalized multi-walled carbon nanotubes for oil spill cleanup from water.* Clean Technologies and Environmental Policy, 2022. **24**(2): p. 519-541.
69. Agasti, N., et al., *Carbon nanotube based magnetic composites for decontamination of organic chemical pollutants in water: A review.* Applied Surface Science Advances, 2022. **10**: p. 100270.
70. Ahmaruzzaman, M., D. Mohanta, and A. Nath, *Environmentally benign fabrication of SnO2-CNT nanohybrids and their multifunctional efficiency as an adsorbent, catalyst and antimicrobial agent for water decontamination.* Scientific Reports, 2019. **9**(1): p. 12935.
71. Wang, Y., et al., *Environmental remediation applications of carbon nanotubes and graphene oxide: Adsorption and catalysis.* Nanomaterials, 2019. **9**(3): p. 439.
72. Wang, Z., et al., *The selective adsorption performance and mechanism of multiwall magnetic carbon nanotubes for heavy metals in wastewater.* Scientific Reports, 2021. **11**(1): p. 16878.
73. Dutra, F.V.A., et al., *Functional polyaniline/multiwalled carbon nanotube composite as an efficient adsorbent material for removing pharmaceuticals from aqueous media.* Journal of Environmental Management, 2018. **221**: p. 28-37.
74. Zhao, X., et al., *Aging of Carbon Nanotubes Increases Their Adsorption towards Tetracycline.* Water, 2022. **14**(17): p. 2731.
75. Purceno, A.D., et al., *Hybrid magnetic amphiphilic composites based on carbon nanotube/nanofibers and layered silicates fragments as efficient adsorbent for ethynilestradiol.* Journal of colloid and interface science, 2012. **379**(1): p. 84-88.

76. Shang, Y., et al., *Removal of sulfamethoxazole from water via activation of persulfate by Fe3C@ NCNTs including mechanism of radical and nonradical process.* Chemical Engineering Journal, 2019. **375**: p. 122004.
77. Yang, G., et al., *Surface oxidized nano-cobalt wrapped by nitrogen-doped carbon nanotubes for efficient purification of organic wastewater*. Separation and Purification Technology, 2021. **259**: p. 118098.
78. Wang, F., et al., *Adsorption of sulfamethoxazole and 17β-estradiol by carbon nanotubes/CoFe2O4 composites.* Chemical Engineering Journal, 2015. **274**: p. 17-29.
79. Chen, S., et al., *Preparation of MIL-100 (Fe) and multi-walled carbon nanotubes nanocomposite with high adsorption capacity towards Oxytetracycline from solution.* Journal of Environmental Chemical Engineering, 2021. **9**(2): p. 104780.
80. Xiong, W., et al., *Multi-walled carbon nanotube/amino-functionalized MIL-53 (Fe) composites: remarkable adsorptive removal of antibiotics from aqueous solutions.* Chemosphere, 2018. **210**: p. 1061-1069.
81. Zhao, W., et al., *Preparation and characteristics of a magnetic carbon nanotube adsorbent: Its efficient adsorption and recoverable performances.* Separation and Purification Technology, 2021. **257**: p. 117917.
82. Ma, J., et al., *Enhanced adsorption for the removal of antibiotics by carbon nanotubes/graphene oxide/sodium alginate triple-network nanocomposite hydrogels in aqueous solutions.* Chemosphere, 2020. **242**: p. 125188.
83. Zhang M, Chang L, and Zhao Y, *Fabrication of Zinc Oxide/ Polypyrrole Nanocomposites for brilliant green removal from aqueous phase.* Arabian J Sci Eng 2019. **44**(1): p. 111-121.
84. Stefaniuk I, Cieniek B, and Rogalska I, *Magnetic properties of ZnO:Co layers obtained by pulsed laser deposition method.* Mater Sci-Pol 2019. **36**(3): p. 439-444.
85. Khan TA, Nazir M, and Ali I, *Removal of Chromium (VI) from aqueous solution using guar gum-nano zinc oxide bio composite adsorbent.* Arabian J Chem 2018. **10**: p. S2388-S2398.

86. Vahidhabanu S, Karuppasamy D, and Adeogun AI, *Impregnation of zinc oxide modified clay over alginate beads: a novel material for the effective removal of Congo red from wastewater.* . RSC Adv 2018. **7**(10): p. 5669-5678.
87. Ćorković, I., et al., *Hydrogels: Characteristics and Application as Delivery Systems of Phenolic and Aroma Compounds.* Foods, 2021. **10**(6): p. 1252.
88. Sharma, S.S.A., et al., *The significance of graphene based composite hydrogels as smart materials: A review on the fabrication, properties, and its applications.* FlatChem, 2022: p. 100352.
89. Yavari Maroufi, L., et al., *Recent Advances of Macromolecular Hydrogels for Enzyme Immobilization in the Food Products.* Adv Pharm Bull, 2022. **12**(2): p. 309-318.
90. Zhou, Y. and L. Jin, *Hydrolysis-induced large swelling of polyacrylamide hydrogels.* Soft Matter, 2020. **16**(24): p. 5740-5749.
91. Peppas, N.A., et al., *Hydrogels in pharmaceutical formulations.* European journal of pharmaceutics and biopharmaceutics, 2000. **50**(1): p. 27-46.
92. Peppas, N.A., B.V. Slaughter, and M.A. Kanzelberger, *9.20 - Hydrogels*, in *Polymer Science: A Comprehensive Reference*, K. Matyjaszewski and M. Möller, Editors. 2012, Elsevier: Amsterdam. p. 385-395.
93. Zhou, P., et al., *A Human Umbilical Cord Mesenchymal Stem Cell-Conditioned Medium/Chitosan/Collagen/β-Glycerophosphate Thermosensitive Hydrogel Promotes Burn Injury Healing in Mice.* BioMed Research International, 2019. **2019**: p. 5768285.
94. Bahram, M., F. Keshvari, and P. Najafi-Moghaddam, *Development of cloud point extraction using pH-sensitive hydrogel for preconcentration and determination of malachite green.* Talanta, 2011. **85**(2): p. 891-896.
95. Ding, B., et al., *Fabrication of multi-functional porous microspheres in a modular fashion for the detection, adsorption, and removal of pollutants in wastewater.* Journal of Colloid and Interface Science, 2018. **522**: p. 1-9.

96. de Araujo, C.M.B., et al., *Continuous removal of pharmaceutical drug chloroquine and Safranin-O dye from water using agar-graphene oxide hydrogel: Selective adsorption in batch and fixed-bed experiments.* Environmental Research, 2023. **216**: p. 114425.
97. Adhikari, B., G. Palui, and A. Banerjee, *Self-assembling tripeptide based hydrogels and their use in removal of dyes from waste-water.* Soft Matter, 2009. **5**(18): p. 3452-3460.
98. Mohamed, A.K. and M.E. Mahmoud, *Encapsulation of starch hydrogel and doping nanomagnetite onto metal-organic frameworks for efficient removal of fluvastatin antibiotic from water.* Carbohydrate polymers, 2020. **245**: p. 116438.
99. Umbreen, N., et al., *Self-assembled three-dimensional reduced graphene oxide-based hydrogel for highly efficient and facile removal of pharmaceutical compounds from aqueous solution.* Journal of colloid and interface science, 2018. **527**: p. 356-367.
100. Mohamed, A.K. and M.E. Mahmoud, *Nanoscale Pisum sativum pods biochar encapsulated starch hydrogel: a novel nanosorbent for efficient chromium (VI) ions and naproxen drug removal.* Bioresource technology, 2020. **308**: p. 123263.
101. Dai, M., et al., *Preparation of thermoresponsive alginate/starch ether composite hydrogel and its application to the removal of Cu (II) from aqueous solution.* Bioresource technology, 2019. **294**: p. 122192.
102. Ehtesabi, H., Z. Bagheri, and M. Yaghoubi-Avini, *Application of three-dimensional graphene hydrogels for removal of ofloxacin from aqueous solutions.* Environmental nanotechnology, monitoring & management, 2019. **12**: p. 100274.
103. Godiya, C.B., Y. Xiao, and X. Lu, *Amine functionalized sodium alginate hydrogel for efficient and rapid removal of methyl blue in water.* International journal of biological macromolecules, 2020. **144**: p. 671-681.
104. Giuri, D., et al., *Water remediation from pollutant agents by the use of an environmentally friendly supramolecular hydrogel.* ChemNanoMat, 2022. **8**(4): p. e202200093.
105. Mondal, B., et al., *Peptide-based gel in environmental remediation: removal of toxic organic dyes and hazardous Pb2+*

and Cd2+ ions from wastewater and oil spill recovery. Langmuir, 2020. **36**(43): p. 12942-12953.

106. Saeed U J, A.A.K., Saad M, Iftikhar A, Guohua S, Cheng-Meng C, Rashid A, *Removal of azo dye from aqueous solution by a low-cost activated carbon prepared from coal: adsorption kinetics, isotherms study, and DFT simulation.* Environmental Science and Pollution Research, 2020. **1**: p. https://doi.org/10.1007/s11356-020-11344-4.
107. Langmuir, I., *The adsorption of gases on plane surfaces of glass, mica and platinum.* Journal of the American Chemical society, 1918. **40**(9): p. 1361-1403.
108. Del Mar Orta, M., Martn, Julia,Medina-Carrasco, Santiago,Santos, Juan Luis,Aparicio, Irene,Alonso, Esteban, *Adsorption of propranolol onto montmorillonite: Kinetic, isotherm and pH studies.* Applied Clay Science, 2019. **173**: p. 107-114.
109. Freundlich, H., *Over the adsorption in solution.* J. Phys. Chem, 1906. **57**(385471): p. 1100-1107.
110. Clement Yaw Efah, T.S., Shaohua Liu ,Yongjun Wu, *Klebsiella pneumoniae: an increasing threat to public health.* Ann Clin Microbiol Antimicrob 2020. **19**: p. 1.
111. V, N., *Streptococcal beta-hemolysins: genetics and role in disease pathogenesis.* Trends Microbiol 2020. **10**: p. 575-580.
112. Katz AR, M.D., *Severe streptococcal infections in historical perspective.* . Clin Infect Dis 2019. **12**: p. 14:298-307.
113. Akash, M.S.H. and K. Rehman, *Introduction to Spectrophotometric Techniques*, in *Essentials of Pharmaceutical Analysis*. 2020, Springer Nature Singapore: Singapore. p. 19-27.
114. Marczenko, Z. and M. Balcerzak, *Separation, preconcentration and spectrophotometry in inorganic analysis*. 2000: Elsevier.
115. Myers, D.N., *Chapter 10 - Innovations in Monitoring With Water-Quality Sensors With Case Studies on Floods, Hurricanes, and Harmful Algal Blooms*, in *Separation Science and Technology*, S. Ahuja, Editor. 2019, Academic Press. p. 219-283.
116. Germer, T., J.C. Zwinkels, and B.K. Tsai, *Spectrophotometry: Accurate measurement of optical properties of materials*. 2014: Elsevier.

117. Clark, B., T. Frost, and M. Russell, *UV Spectroscopy: Techniques, instrumentation and data handling*. Vol. 4. 1993: Springer Science & Business Media.
118. Skoog, D.A., et al., *Fundamentals of analytical chemistry*. 2013: Cengage learning.
119. Gavat, C., L. Vasilescu, and A. Marculescu, *Visible Spectrophotometric Analysis Method of Sodium Metamizole in Tablets.* Revista de Chimie -Bucharest- Original Edition-, 2019. **70**: p. 475-482.
120. Germer, T.A., J.C. Zwinkels, and B.K. Tsai, *Theoretical concepts in spectrophotometric measurements*, in *Experimental Methods in the Physical Sciences*. 2014, Elsevier. p. 11-66.
121. Shetty, P.R. and D.D. Patil, *Applications of simultaneous equation method and derivative method for the determination of rabeprazole sodium and levosulpiride in pharmaceutical dosage form and dissolution samples.* Journal of the Association of Arab Universities for Basic and Applied Sciences, 2014. **15**(1): p. 53-60.
122. Vyas, A.J., et al., *A brief review on q-absorption ratio method in UV-spectrophotometry.* Asian Journal of Pharmaceutical Analysis, 2022. **12**(4): p. 281-285.
123. Pandey, G. and B. Mishra, *A new analytical Q-absorbance ratio method development and validation for simultaneous estimation of lamivudine and isoniazid.* International Scholarly Research Notices, 2013. **2013**.
124. Abdelwahab, N.S., *Spectrophotometric methods for simultaneous determination of Carvedilol and Hydrochlorothiazide in combined dosage form.* Arabian Journal of Chemistry, 2016. **9**: p. S355-S360.
125. Kishore, P., *Validated Estimation of Silodosin in Pure, Pharmaceuticals and in Biological Sample by Uv-Spectroscopic and Rp-Hplc Method*. 2012, Adhiparasakthi College of Pharmacy, Melmaruvathur.
126. Pawar, S., et al., *Geometrical Correction Method For Simultaneous Estimation Of Azilsartan Medoxomil And Amlodipine Besylate From Biological Sample.* NVEO-NATURAL VOLATILES & ESSENTIAL OILS Journal| NVEO, 2021: p. 16787-16796.

127. Ojeda, C.B. and F.S. Rojas, *Recent developments in derivative ultraviolet/visible absorption spectrophotometry.* Analytica Chimica Acta, 2004. **518**(1-2): p. 1-24.
128. Owen, A., *Uses of derivative spectroscopy, application note, UV-visible spectroscopy.* Agilent Technologies, Waldbronn, 1995.
129. Vogt, F., *SPECTROPHOTOMETRY | Derivative Techniques*, in *Encyclopedia of Analytical Science (Second Edition)*, P. Worsfold, A. Townshend, and C. Poole, Editors. 2005, Elsevier: Oxford. p. 335-343.
130. Rote, A.R. and S.R. Bhalerao, *First-order derivative spectrophotometric estimation of nabumetone and paracetamol in tablet dosage form.* Pharmaceutical Methods, 2011. **2**(4): p. 260-263.
131. Acharjya, S.K., et al., *Spectrophotometric methods for the determination of letrozole in bulk and pharmaceutical dosage forms.* Journal of Advanced Pharmaceutical Technology & Research, 2010. **1**(3): p. 348.
132. Patel, H.B. and S. Patel, *Dual wavelength spectrophotometric method for simultaneous estimation of gatifloxacin sesquihydrate and Prednisolone acetate in combined dosage form.* 2013.
133. Hashem, E. and A.M. El-Zohry, *Simultaneous detection of dopamine and ascorbic acid in urine using the H-point standard addition method.* Journal of Applied Spectroscopy, 2012. **79**: p. 424-430.
134. Kamel, S.A. and F.M. Abdoon. *Spectrophotometric method for the simultaneous determination of pyridoxine hydrochloride & phenylephrine hydrochloride via H-point standard addition method*. in *AIP Conference Proceedings*. 2022. AIP Publishing LLC.
135. Safavi, A. and H. Abdollahi, *Simultaneous kinetic determination of Fe (III) and Fe (II) by H-point standard addition method.* Talanta, 2002. **56**(4): p. 699-704.
136. Sivasubramanian, L. and K. Lakshmi, *H-point standard addition method for simultaneous spectrophotometric determination of irbesartan, hydrochlorothiazide and telmisartan in tablets.* International journal of research in pharmacy and chemistry, 2014. **4**(2): p. 373-380.

137. Zaikin, V. and J.M. Halket, *A handbook of derivatives for mass spectrometry*. 2009: IM publications.
138. Worsfold, P., et al., *Encyclopedia of Analytical Science*. 2019: Elsevier Science.
139. Adegoke, O.A., *Chemical derivatization methodologies for UV-visible spectrophotometric determination of pharmaceuticals.* Int. J. Pharm. Sci. Rev. Res, 2012. **14**(2): p. 6-24.
140. Aboolla, A.A., S. El-ghadafi, and E.K.A. El-Swayah, *Spectrophotometric Determination of Nefidipine in Pharmaceutical Preparations by Coupling Reactions.* 2002.
141. Benkhaya, S., S. M'rabet, and A. El Harfi, *Classifications, properties, recent synthesis and applications of azo dyes.* Heliyon, 2020. **6**(1): p. e03271.
142. Dhamra, M.Y., *Spectrophotometric determination of tranexamic acid by azo-dye formation-application to pharmaceutical preparations.* Journal of Education and Science, 1999. **24**(3): p. 21-33.
143. Hunger, K., *Industrial Dyes: Chemistry, Properties, Applications*. 2007: Wiley.
144. Nikfar, S. and M. Jaberidoost, *Dyes and Colorants*, in *Encyclopedia of Toxicology (Third Edition)*, P. Wexler, Editor. 2014, Academic Press: Oxford. p. 252-261.
145. Revanasiddappa, H. and M. Veena, *Spectrophotometric determination of mosapride in pure and pharmaceutical preparations.* Eclética Química, 2007. **32**: p. 71-75.
146. Whitlock, L.R., S. Siggia, and J.E. Smola, *Spectrophotometric analysis of phenols and of sulfonates by formation of an azo dye*. Analytical Chemistry, 1972. **44**(3): p. 532-536.
147. Farges, J.-P., *Organic conductors: fundamentals and applications*. 2022: CRC Press.
148. Calatayud, J.M. and L.L. Zamora, *Spectrophotometry | Pharmaceutical Applications☆*, in *Encyclopedia of Analytical Science (Third Edition)*, P. Worsfold, et al., Editors. 2013, Academic Press: Oxford. p. 249-262.
149. McMurry, J.E., *Fundamentals of Organic Chemistry*. 2010: Cengage Learning.

150. Adegoke, O.A., et al., *Spectrophotometric determination of olanzapine after condensation with p-dimethylaminobenzaldehyde.* Journal of Taibah University for Science, 2014. **8**(3): p. 248-257.
151. Abdulghani, A.J., H.H. Jasim, and A.S. Hassan, *Determination of tetracycline in pharmaceutical preparation by molecular and atomic absorption spectrophotometry and high performance liquid chromatography via complex formation with Au (III) and Hg (II) ions in solutions.* International Journal of Analytical Chemistry, 2013. **2013**.
152. Niu, S. and M.B. Hall, *Theoretical studies on reactions of transition-metal complexes.* Chemical reviews, 2000. **100**(2): p. 353-406.
153. Cesme, M., D. Tarinc, and A. Golcu, *Spectrophotometric determination of metoprolol tartrate in pharmaceutical dosage forms on complex formation with Cu (II).* Pharmaceuticals, 2011. **4**(7): p. 964-975.
154. Zaręba, S., *Spectrophotometric determination of zinc in pharmaceutical multimineral preparations by azo-dye derivatives of benzimidazole and 1, 2, 4-triazole.* Pharmaceutica Acta Helvetiae, 1995. **70**(2): p. 195-198.
155. Jagleniec, D., et al., *Ion-pair induced supramolecular assembly formation for selective extraction and sensing of potassium sulfate.* Chemical Science, 2019. **10**(41): p. 9542-9547.
156. Parkinson, D.R., *Analytical Derivatization Techniques☆,* in *Reference Module in Chemistry, Molecular Sciences and Chemical Engineering*. 2014, Elsevier.
157. Passos, M.L.C., et al., *Spectrophotometry | Organic Compounds☆*, in *Encyclopedia of Analytical Science (Third Edition)*, P. Worsfold, et al., Editors. 2019, Academic Press: Oxford. p. 236-243.
158. Persson, B.A., *LIQUID CHROMATOGRAPHY | Ion Pair*, in *Encyclopedia of Analytical Science (Second Edition)*, P. Worsfold, A. Townshend, and C. Poole, Editors. 2005, Elsevier: Oxford. p. 157-164.
159. Sharmin, E. and F. Zafar, *Spectroscopic Analyses: Developments and Applications*. 2017: IntechOpen.
160. Phadungcharoen, N., et al., *Ion pair extraction coupled with digital image colorimetry as a rapid and green platform for*

pharmaceutical analysis: an example of chlorpromazine hydrochloride tablet assay. Talanta, 2020. **219**: p. 121271.

161. Yoshida, J.I. and F.W. Patureau, *Organic Redox Chemistry: Chemical, Photochemical and Electrochemical Syntheses*. 2022: Wiley.
162. Amin, A., et al., *Utility of oxidation–reduction reaction for the determination of ranitidine hydrochloride in pure form, in dosage forms and in the presence of its oxidative degradates.* Spectrochimica Acta Part A: Molecular and Biomolecular Spectroscopy, 2003. **59**(4): p. 695-703.
163. Abdel-Kader, D.A. and E.Y. Hashem, *Spectrophotometric determination of Metronidazole antibacterial drug via oxidation with alkaline potassium permanganate.* Spectrochimica Acta Part A: Molecular and Biomolecular Spectroscopy, 2021. **259**: p. 119858.
164. El-Didamony, A. and E. Erfan, *Cerimetric determination of four antihypertensive drugs in pharmaceutical preparations.* Journal of the Chilean Chemical Society, 2011. **56**(4): p. 875-880.
165. Castle, S.C., C.D. Morrison, and N.N. Barger, *Extraction of chlorophyll a from biological soil crusts: a comparison of solvents for spectrophotometric determination.* Soil Biology and Biochemistry, 2011. **43**(4): p. 853-856.
166. Ganesh, S., et al., *Spectrophotometric determination of trace amounts of phosphate in water and soil.* Water Science and Technology, 2012. **66**(12): p. 2653-2658.
167. Sharma, H., et al., *Diazotized reagent for spectrophotometric determination of glyphosate pesticide in environmental and agricultural samples.* Journal of the Indian Chemical Society, 2022. **99**(7): p. 100483.
168. Akter Mou, S., et al., *Determination of chloramphenicol in meat samples using liquid chromatography–tandem mass spectrometry.* Food Science & Nutrition, 2021. **9**(10): p. 5670-5675.
169. Vigh, G. and J. Inczédy, *Separation of some chloramphenicol intermediates by high-pressure liquid chromatography.* Journal of Chromatography A, 1976. **116**(2): p. 472-474.
170. Xiao, Z., et al., *Development of a subcritical water extraction approach for trace analysis of chloramphenicol, thiamphenicol,*

florfenicol, and florfenicol amine in poultry tissues. Journal of chromatography A, 2015. **1418**: p. 29-35.

171. Monogarova, O., A. Chaplenko, and K. Oskolok, *Identification and quantification of chloramphenicol in medicines by multisensory digital colorimetry.* Moscow University Chemistry Bulletin, 2020. **75**: p. 1-7.
172. Hamoudi, T.A. and W.A. Bashir, *Spectrophotometric determination of chloramphenicol in pharmaceutical preparations.* مجلة دراسات موصلية, 2018: p. 19-35.
173. Li, X., et al., *Comparison of the determination of chloramphenicol residues in aquaculture tissues by time-resolved fluoroimmunoassay and with liquid chromatography and tandem mass spectrometry.* Food and agricultural immunology, 2006. **17**(3-4): p. 191-199.
174. van Rossum, H., P. Kootstra, and S. Sterk, *Determination of chloramphenicol in bovine urine, meat and shrimp by GC-MS. Method validation according to Commission Decision 2002/657/EC.* 2004.
175. Zhang, Q.-J., et al., *Determination of chloramphenicol residues in aquatic products using immunoaffinity column cleanup and high performance liquid chromatography with ultraviolet detection.* Journal of AOAC International, 2013. **96**(4): p. 897-901.
176. Ali, I., et al., *Analysis of chloramphenicol in biological samples by SPE-HPLC.* Analytical Chemistry Letters, 2013. **3**(3): p. 181-190.
177. Zeng, S., L. Lin, and C. Yang. *Rapid Determination of Chloramphenicol in Tilapia by ultra-high performance liquid chromatography-mass spectrometry*. in *E3S Web of Conferences*. 2019. EDP Sciences.
178. Ozcan, N. and O. Aycan, *Determination of chloramphenicol in honey, milk, and egg by liquid chromatography/mass spectrometry: single-laboratory validation.* Journal of AOAC International, 2013. **96**(5): p. 1158-1163.
179. Neuhaus, B.K., J.A. Hurlbut, and W. Hammack, *LC/MS/MS analysis of chloramphenicol in shrimp.* Laboratory Information Bulletin, 2002. **4290**: p. 1-13.
180. do Rego, E.C.P., et al., *The validation of a new high throughput method for determination of chloramphenicol in milk using liquid–*

liquid extraction with low temperature partitioning (LLE-LTP) and isotope-dilution liquid chromatography tandem mass spectrometry (ID-LC-MS/MS). Analytical Methods, 2015. **7**(11): p. 4699-4707.

181. Bogialli, S. and A. Di Corcia, *Recent applications of liquid chromatography–mass spectrometry to residue analysis of antimicrobials in food of animal origin.* Analytical and bioanalytical chemistry, 2009. **395**: p. 947-966.
182. Novković, S., et al., *The validation of a method for the determination of chloramphenicol in milk.* Journal of Agronomy, Technology and Engineering Management, 2022. **5**(1): p. 697-703.
183. Tyagi, A., et al., *Determination of chloramphenicol in shrimp by liquid chromatography-electrospray ionization tandem mass spectrometry (LC-ESI-MS-MS).* Food additives and contaminants, 2008. **25**(4): p. 432-437.
184. Calvarese, S., et al., *Chloramphenicol in royal jelly: analytical aspects and occurrence in Italian imports.* Apidologie, 2006. **37**(6): p. 673-678.
185. Ashraf, S.A. and Z.A.A. Azad, *Validation of an analytical methodology for the determination of chloramphenicol residues in honey using UPLC-MS/MS.* Oriental Journal of Chemistry, 2018. **34**(2): p. 723.
186. Jung, H.-N., et al., *Simultaneous quantification of chloramphenicol, thiamphenicol, florfenicol, and florfenicol amine in animal and aquaculture products using liquid chromatography-tandem mass spectrometry.* Frontiers in Nutrition, 2022. **8**: p. 1181.
187. Rizzo, S., et al., *Determination of chloramphenicol in honey using salting-out assisted liquid-liquid extraction coupled with liquid chromatography-tandem mass spectrometry and validation according to 2002/657 European Commission Decision.* Molecules, 2020. **25**(15): p. 3481.
188. Kikuchi, H., et al., *Total determination of chloramphenicol residues in foods by liquid chromatography-tandem mass spectrometry.* Food chemistry, 2017. **230**: p. 589-593.
189. Li, Y., et al., *Analysis of chloramphenicol in drinking water using an evaporation preparative step and isotope dilution liquid chromatography–tandem mass spectrometry.* Acta Chromatographica, 2018. **30**(1): p. 17-20.

190. Kawano, S.-i., et al., *Analysis of chloramphenicol in honey by on-line pretreatment liquid chromatography–tandem mass spectrometry.* Chinese Chemical Letters, 2015. **26**(1): p. 36-38.
191. Hosain, M.Z., S.S. Islam, and M.M. Kamal, *Analytical Method Validation for Quantification of Chloramphenicol Residues in Poultry Meal Using a Liquid Chromatography-Tandem Mass Spectrometry.* American Journal of Chemical and Biochemical Engineering, 2022. **6**(2): p. 44-50.
192. Kalia, B. and U.S. Baghel, *Method development and validation of stability indicating RP-HPLC method for simultaneous estimation of escitalopram oxalate and clonazepam in bulk and its pharmaceutical formulations.* Journal of Drug Delivery and Therapeutics, 2019. **9**(1-s): p. 265-274.
193. Mitić, S.S., et al., *Development and Application of Ligand-Exchange Reaction Method for the Determination of Clonazepam.* Tropical Journal of Pharmaceutical Research, 2012. **11**(1): p. 91-98.
194. Jing, D., S. Yintao, and W. Junwei, *Qualitative and Quantitative Analysis of Clonazepam and its Metabolite 7-aminoclonazepam in Blood by LC-tandem QTOF/MS and LC-MS/MS.* FORENSIC SCI SEM, 2014. **4**(1): p. 45-52.
195. Perchalski, R.J. and B. Wilder, *Determination of benzodiazepine anticonvulsants in plasma by high-performance liquid chromatography.* Analytical Chemistry, 1978. **50**(4): p. 554-557.
196. Albishri, H.M., N.A. Aldawsari, and D. Abd El-Hady, *A Simple and Reliable Liquid Chromatographic Method for Simultaneous Determination of Five Benzodiazepine Drugs in Human Plasma.* Analytica, 2022. **3**(2): p. 251-265.
197. Bares, I.F., F. Pehourcq, and C. Jarry, *Development of a rapid RP–HPLC method for the determination of clonazepam in human plasma.* Journal of pharmaceutical and biomedical analysis, 2004. **36**(4): p. 865-869.
198. Hadi, H., *Spectrophotometric determination of clonazepam in pure and dosage forms using charge transfer reaction.* Iraqi Journal of Pharmaceutical Sciences (P-ISSN 1683-3597 E-ISSN 2521-3512), 2015. **24**(1): p. 25-32.

199. Diniz, M.E.R., et al., *Development and validation of method for the determination of the benzodiazepines clonazepam, clobazam and N-Desmethylclobazam in serum by LC-MS/MS and its application in clinical routine.* Br. J. Anal. Chem, 2017. **4**(14): p. 8-16.
200. de Araujo, F.G., et al., *Development and validation of an analytical method for the detection and quantification of bromazepam, clonazepam and diazepam by UPLC-MS/MS in surface water.* Bulletin of environmental contamination and toxicology, 2019. **103**: p. 362-366.
201. Shaw, W., G. Long, and J. McHan, *An HPLC method for analysis of clonazepam in serum.* Journal of analytical toxicology, 1983. **7**(3): p. 119-122.
202. Cavedal, L.E., et al., *Clonazepam quantification in human plasma by high-performance liquid chromatography coupled with electrospray tandem mass spectrometry in a bioequivalence study.* Journal of mass spectrometry, 2007. **42**(1): p. 81-88.
203. Gu, J., et al., *LC–MS Method for the Quantification of Clonazepam in Rat Plasma.* Chromatographia, 2009. **70**: p. 1709-1713.
204. Fadhel, S.R. and N.M. Khamees, *Development of spectrophotometric method for estimating clonazepam in its pure form and pharmaceutical tablets.* Orient J. Chem, 2018. **34**(1): p. 1604-1610.
205. Shiri, S., K. Alizadeh, and N. Abbasi, *A novel technique for simultaneous determination of drugs using magnetic nanoparticles based dispersive micro-solid-phase extraction in biological fluids and wastewaters.* MethodsX, 2020. **7**: p. 100952.
206. Soroush, S., et al., *Potentiometric determination of clonazepam using carbon paste electrode based on Molecular Imprinted Polymer (MIP) in solution and in a biological fluid model.* Pharmaceutica Analytica Acta, 2016. **7**(7): p. 2.
207. Badcock, N. and A. Pollard, *Micro-determination of clonazepam in plasma or serum by electron-capture gas—liquid chromatography.* Journal of Chromatography B: Biomedical Sciences and Applications, 1982. **230**(2): p. 353-361.
208. Salem, A., B. Barsoum, and E. Izake, *Spectrophotometric and fluorimetric determination of diazepam, bromazepam and clonazepam in pharmaceutical and urine samples.* Spectrochimica

Acta Part A: Molecular and Biomolecular Spectroscopy, 2004. **60**(4): p. 771-780.

209. Patel, J.U. and U.K. Chhalotiya, *A Synchronous fluorescence spectrofluorometric method for the simultaneous determination of clonazepam and paroxetine hydrochloride in combined pharmaceutical dose form.* Turkish Journal of Pharmaceutical Sciences, 2017. **14**(3): p. 251.
210. Khan, M.A.A., et al., *NOVEL RP-HPLC METHOD FOR THE QUANTIFICATION DETERMINATION OF CLONAZEPAM AND PROPRANOLOL IN BULK FORM AND MARKETED FORMULATION.*
211. Förster, H., *UV/Vis spectroscopy.* Characterization I, 2004: p. 2734-2734.
212. Reichelt, R., *Scanning electron microscopy*, in *Science of microscopy*. 2007, Springer. p. 133-272.
213. Reimer, L., *Transmission electron microscopy: physics of image formation and microanalysis*. Vol. 36. 2013: Springer.
214. Jenkins, R. and R.L. Snyder, *Introduction to X-ray Powder Diffractometry, Volume 138.* Chemical analysis, a series of monographs on analytical chemistry and its applications, 1996.
215. Hameed Mahmood, Z., et al., *Magnetic Nanoparticles Supported Copper Nanocomposite: A Highly Active Nanocatalyst for Synthesis of Benzothiazoles and Polyhydroquinolines.* Polycyclic Aromatic Compounds, 2022.
216. M. Doğan, M. Alkan, O. Demirbas, Y. Ozdemir, and C. Ozmetin, *Adsorption kinetics of maxilon blue GRL onto sepiolite from aqueous solutions.* Chem. Eng. J., 2006. **124**: p. 89-101.
217. R. Ahmad, *Studies on adsorption of crystal violet dye from aqueous solution onto coniferous pinus bark powder (CPBP).* J. Hazard. Mater., 2009. **171**: p. 767-773.
218. Alidadi, H., et al., *Enhanced removal of tetracycline using modified sawdust: Optimization, isotherm, kinetics, and regeneration studies.* Process Safety and Environmental Protection, 2018. **117**: p. 51-60.
219. Rifaqat Ali Khan Rao , M.K., *Adsorption studies of Cd(II) on ball clay: Comparison with other natural clays.* Arabian Journal of Chemistry, 2016. **9**: p. S1233-S1241.

220. A.Bashir, T.A.H.W., *Spectrophotometric Determination of Chloramphenicol in Pharmaceutical Preparations.* Journal of Education and Science, 2018. **27**(3): p. 19-35.
221. Aljeboree, A.M., et al. *Role of Selenium dioxide in Spectrophotometric determination of Tetracycline in pure and pharmaceutical formulations*. in *Journal of Physics: Conference Series*. 2021.
222. Al-Rimawi, F. and M. Kharoaf, *Analysis of chloramphenicol and its related compound 2-amino-1-(4-nitrophenyl) propane-1, 3-diol by reversed-phase high-performance liquid chromatography with UV detection. Chromatography Research International*, 2011. **2011**.
223. Mbodi, F.E., et al., *Determination of chloramphenicol residues in commercial chicken eggs in the Federal Capital Territory, Abuja, Nigeria.* Food Additives & Contaminants: Part A, 2014. **31**(11): p. 1834-1839.
224. Mehdizadeh, S., H.R. Kazerani, and A. JAMSHIDI, *Screening of chloramphenicol residues in broiler chickens slaughtered in an industrial poultry abattoir in Mashhad, Iran.* 2010.
225. Zhao Ying, C.Y., Zhao Jian, Tong Zongrui, Jin Shaohua, *Preparation of SA-g-(PAA-co-PDMC) polyampholytic superabsorbent polymer and its application to the anionic dye adsorption removal from effluents.Ultrasonics Sonochemistry* 2020. **25**: p. 12-18.
226. Banerjee, S. and M.C. Chattopadhyaya, *Adsorption characteristics for the removal of a toxic dye, tartrazine from aqueous solutions by a low cost agricultural by-product.* Arabian Journal of Chemistry, 2017. **10**: p. S1629-S1638.
227. Saeed Ullah Jan, A.A., Adnan Ali Khan1, Saad Melhi, Iftikhar Ahmad, Guohua Sun, Cheng-Meng Chen, Rashid Ahmad, *Removal of azo dye from aqueous solution by a low-cost activated carbon prepared from coal: adsorption kinetics, isotherms study, and DFT simulation.* Environmental Science and Pollution Research, 2020. **1**: p. https://doi.org/10.1007/s11356-020-11344-4.
228. Hemant Mittal , A.A.A., Pranay P. Morajkar , Saeed M. Alhassan, *Graphene oxide crosslinked hydrogel nanocomposites of xanthan gum for the adsorption of crystal violet dye.* ournal of Molecular Liquids 2021. **323**: p. 115034.

229. V. Srivastava, D.G., Y.C. Sharma *Synthesis, characterization and application of zinc oxide nanoparticles.* Ceram. Int, 2013. **39**(8): p. 9803-9808.
230. Giphin George, M.P.S., *Facile synthesis of carbon-coated layered double hydroxide and its comparative characterisation with Zn–Al LDH: application on crystal violet and malachite green dye adsorption—isotherm, kinetics and Box-Behnken design.* Environmental Science and Pollution Research, 2019. **1**: p. https://doi.org/10.1007/s11356-018-3001-3.
231. R. Saravanan, V.K.G., T. Prakash, V. Narayanan, A. Stephen, *Synthesis, characterization and photocatalytic activity of novel Hg doped ZnO nanorods prepared by thermal decomposition method.* J. Mol. Liq., 2013. **178**: p. 88-93.
232. Ali M. El Shafey, M.K.A.-L., H.M. Abd El-Salam, *The facile synthesis of poly(acrylate/acrylamide) titanium dioxide nanocomposite for groundwater ammonia removal.* Desalination and Water Treatment, 2021. **212** p. 61–70.
233. M. Akhond, G.A., H. Ershadifar, *Highly sensitive colorimetric determination of amoxicillin in pharmaceutical formulations based on induced aggregation of gold nanoparticles.* Spectrochim. Acta A, , 2015. **143**: p. 223-229.
234. Soulaima Chkirida , N.Z., Redouane Achour , Hicham Hassoune , Adil Lachehab ,Abou el kacem Qaiss , Rachid Bouhfid, *Highly synergic adsorption/photocatalytic efficiency of Alginate/Bentonite impregnated TiO2 beads for wastewater treatment.* Journal of Photochemistry & Photobiology, A: Chemistry 2021. **412** p. 113215.
235. Arif Chowdhury, S.K., Afaq Ahmad Khan, M. Ravi Chandra, and Sahid Hussain, *Activated carbon loaded with Ni-Co-S nanoparticle for Superior Adsorption Capacity of Antibiotics and Dye from Wastewater: Kinetics and Isotherms.* Journal Pre-proof, 2020. **1**: p. https://doi.org/10.1016/j.colsurfa.2020.125868.
236. V.O. Njoku , K.Y.F., M. Asif , B.H. Hameed, *Preparation of activated carbons from rambutan (Nephelium lappaceum) peel by microwave-induced KOH activation for acid yellow 17 dye adsorption.* Chemical Engineering Journal 2014. **250**: p. 198-204.

237. C.F. Iscen, I. Kiran, and S. Ilhan *Biosorprion of Reactive Black 5 dye by Penicillium restrictum: The Kinetic study.* J.Hazard. Mater. , 2007. **143**: p. 335-338.
238. M. Zhu, L. Lee, H. Wang, and Z.Wang, *Removal of an anionic dye by adsorption/precipitation processes using alkaline white mud.* J. Hazard. Mater., 2007. **149**: p. 735-741.
239. Aljeboree, A.M., *Adsorption and Removal of pharmaceutical Riboflavin (RF) by Rice husks Activated Carbon. International* Journal of Pharmaceutical Research 2019. **11**(2): p. 255-261.
240. Cardoso NF, L.E., Pinto IS, Amavisca CV, Royer B, Pinto RB, Alencar WS, Pereira SFP *Application of cupuassu shell as biosorbent for the removal of textile dyes from aqueous solution.* J Environ Manage 2011. **92**: p. 1237-1247.
241. Ahmed M. Kamil, H.T.M., Ayad F. Alkaimand Falah H. Hussein *Adsorption of Congo red on multiwall carbon nanotubes: Effect of operational parameters* Journal of Chemical and Pharmaceutical Sciences 2016. **9**(3): p. 1128-1133.
242. Alkaim, A.F. and M.B. Alqaragully, *Adsorption of basic yellow dye from aqueous solutions by Activated carbon derived from waste apricot stones (ASAC): Equilibrium, and thermodynamic aspects.* international journal of chemical sciences, 2013. **11**(2): p. 797-814.
243. L.Wang, *Application of activated carbon derived from 'waste' bamboo culms for the adsorption of azo disperse dye: Kinetic, equilibrium and thermodynamic studies.* Journal of Environmental Management, 2012. **102**: p. 79-87.
244. A. Saeed, M. Sharif, and M. Iqbal, *Application potential of grapefruit peel as dye sorbent: kinetics, equilibrium and mechanism of crystal violet adsorption.* J. Hazard. Mater, 2010. **179**: p. 564-572.
245. Amer M. Alshamri, A.M.A., Mohammed B. Alqaragully, Ayad F. Alkaim, *Removal of toxic textile dyes from aqueous solution through adsorption onto coconut husk waste: Thermodynamic and isotherm studies.* Caspian J. Environ. Sci. , 2021. **19**(3): p. 513~522
246. A. F. AlKaim, A. N. AlShirifi, and A. H. AlDujaili, *Kinetic study of adsorption of phenol on the novel polymer prepared AUFP from*

aqueous solution. National Journal of Chemistry, 2007. **27**: p. 428-455.

247. I. Mobasherpour, E. Salahi, and M.Pazouki, *Removal of nickel (II) from aqueous solutions by using nano-crystalline calcium hydroxyapatite.* Journal of Saudi Chemical Society, 2011. **15**(2): p. 105-112.
248. A. Jain, A. K. Gupta, V. K. Bhatnagar, and A.Suhas, *Utilization of industrial waste products as adosrbents for the removal of dyes.* J. Hazard. Mater. B 2003. **101**: p. 31-42.
249. Abdalghaffar M. , O.A.H., Tawfik A.S *Simultaneous adsorption of dye and toxic metal ions using an interfacially polymerized silica/polyamide nanocomposite: Kinetic and thermodynamic studies.* Journal of Molecular Liquids, 2020. **314**(15): p. 113640.
250. Adheem, H.M., Jasim, L.S., *Preparation and Characterization of a three-component hydrogel composite and study of kinetic and thermodynamic applications of adsorption of some positive and negative dyes from their aqueous solutions.* IOP Conference Series: Materials Science and Engineering, 2020. **928**(5): p. 052027.
251. Freundlich H, W., *The Adsorption of cis- and trans-Azobenzene* J Am Chem Soc, 1939. **61**: p. 2228-2230.
252. Kim, Y.-S. and J.-H. Kim, *Isotherm, kinetic and thermodynamic studies on the adsorption of paclitaxel onto Sylopute.* The Journal of Chemical Thermodynamics, 2019. **130**: p. 104-113.
253. Zaheer, Z., A. Al-Asfar, and E.S. Aazam, *Adsorption of methyl red on biogenic Ag@Fe nanocomposite adsorbent: Isotherms, kinetics and mechanisms.* Journal of Molecular Liquids, 2019. **283**: p. 287-298.
254. Xiong, J., et al., *Hexagonal boron nitride adsorbent: Synthesis, performance tailoring and applications.* Journal of Energy Chemistry, 2020. **40**: p. 99-111.
255. Zhang, G., Feizbakhshan, Mohammad,Zheng, Shuilin,Hashisho, Zaher,Sun, Zhiming,Liu, Yangyu, *Effects of properties of minerals adsorbents for the adsorption and desorption of volatile organic compounds (VOC).* Applied Clay Science, 2019. **173**: p. 88-96.
256. Hoppen, M.I., Carvalho, K. Q.,Ferreira, R. C.,Passig, F. H.,Pereira, I. C., Rizzo-Domingues, R. C. P.,Lenzi, M. K.,Bottini, R. C. R., *Adsorption and desorption of acetylsalicylic acid onto activated*

carbon of babassu coconut mesocarp. Journal of Environmental Chemical Engineering, 2019. **7**(1): p. 102862.

257. Al-Bayati, R.A., *Adsorption-desorption isotherm of one of antidibetic drug from aqueous solutions on some pharmaceutical adsorbents.* Eur. J. Sci. Res., 2020. **40**: p. 580-588.
258. Sevda Pashaei-Fakhri , S.J.P., Rauf Foroutan ,Nasser Arsalani , Bahman Ramavandi, *Crystal violet dye sorption over acrylamide/graphene oxide bonded sodium alginate nanocomposite hydrogel, 2021.* Chemosphere **270**: p. 129419.
259. Asmaa H. Hammadi, S.A.H., Lena Fadhil Al-Jibouri, Falah H. Hussien, *Synthesis, Characterization and Biological Activity of Zinc Oxide Nanoparticles (ZnO NPs).* Sys Rev Pharm 2020. **11**(5): p. 431 439.
260. Dehui Xu, S.W., Bing Li, Miao Qi, Rui Feng, Qiaosong Li, Hao Zhang, Hailan Chen, and Michael G Kong, *Effects of Plasma-Activated Water on Skin Wound Healing in Mice.* Microorganisms, 2020. **7**(8): p. 1091.
261. Evelina Vågesjö, E.Ö., Anneleen Mortier, Hava Lofton, Fredrik Huss, Paul Proost, Stefan Roos, Mia Phillipsona,, *Accelerated wound healing in mice by on-site production and delivery of CXCL12 by transformed lactic acid bacteria.* National Center for Biotechnology Information, 2018. **7**(8): p. 1-9.
262. Samia Afrin , M.S., Papia Haque , Md. Sazedul Islam , Shafiul Hossain ,Taslim Ur Rashid , Tanvir Ahmed , Makoto Takafuji , Mohammed Mizanur Rahman *Advanced CNC/PEG/PDMAA Semi-IPN Hydrogel for Drug Delivery Management in Wound Healing.* Gels, 2022. **8**: p. 340.

الخلاصة

تنقسم الدراسة الحالية إلى قسمين . يتضمن القسم الأول تطوير وتحديد طريقة طيفية بسيطة وسريعة وحساسة لتقدير اثنين من العقارات كلونازيبام (CLZ) والكلورامفينيكول (CHL) في مستحضراتهما الصيدلانية. تعتمد الطريقة على تفاعل اقتران ازو بين الدواء المؤزوت مع كاشف مولد للون (فيتامين B6) في محلول قلوي لتكوين صبغة ازو ذات لون وردي محمر والذي اعطى أقصى امتصاص عند الطول الموجي λ_{max} 453nm و 532 nm لـ CHL وCLZ على التوالي تم فحص المتغيرات التي تؤثر على استقرار وتطوير منتج التفاعل بدقة وتحسينها. كانت التراكيز التي تطاوع قانون لامبر بير(17-0.5) و (26-1.2) ميكروغرام مل$^{-1}$ مع معامل الارتباط R (09982) و (0.9989). وجد بان حساسية ساندل هي 0.013 و 0.0184 ميكروغرام سم^{2} مع معامل الامتصاص المولاري 357 × 10^4 و 256 × 10^4 لتر مول$^{-1}$ سم$^{-1}$ كذلك اظهرت النتائج بأن حدود الكشف (LOD) هي 0.117 و 0.299 ميكروغرام مل$^{-1}$ مع حدود كم (LOQ) 0.355 و 0.908 ميكروغرام مل$^{-1}$ ثم تطبيق الطريقة المقترحة بنجاح التقدير الأدوية المدروسة في بعض المستحضرات الصيدلانية

يهدف الجزء الثاني إلى تحضير وتشخيص هلام مائي جديد(هيدروجل) محمل (CNT/ZnO) SA- g-P(Ac-co-AM) / ZnO-CNT يخضع التحضير لميكانيكية بلمرة الجذور الحرة لحمض الأكريليك باستخدام (MBA) (N.N-Methylenebisacrylamide) كعامل ارتباط تم إجراء تشخيص الهيدروجيل القائم على CNT/ZnO باستخدام التحليل الحراري الوزني (TGA) ، ومسح المجهر الإلكتروني (SEM) ، والمجهر الإلكتروني النافذ (TEM) ، وانحراف الأشعة السينية (XRD) وتحليل EDS تم استخدام هيدروجيل النانوي لإزالة الأدوية من عينة حقيقية لأنها تتمتع بقدرة امتزاز عالية. تمت دراسة وتحسين المتغيرات العملية مثل تركيز الدواء الأولي ، ودرجة الحموضة ، وجرعة الممتزات ، وزمن الاتزان) التي تؤثر على كفاءة الامتزاز أظهرت نتائج ايزوثيرمات الامتزاز ان هناك توافق كبير في عملية الامتزاز مع ايزوثيرم فريندلش مع معامل الارتباط (R= 0.999) بالمقارنة مع ايزوثيرم لنكماير وجد ان الهيدروجيل النانوي ذو قدرة امتزاز جيدة في حدود 78-83 % لإزالة الدوائين . كما تم شرح ميكانيكيات التخليق والامتزاز بالتفصيل مع بيان اعادة التنشيط والاسترداد وإعادة استخدام المواد المازة. لذلك, قد يوفر الهيدروجيل كماده فعاله من حيث التكلفة وسهل التعديل وذو كفاءة عالية لإزالة الأدوية.

بسم الله الرحمن الرحيم

اقرأ باسم ربك الذي خلق (1)خلق الانسان من علق (2) اقرا وربك الاكرم (3) الذي علم بالقلم (4) علم الانسان مالم يعلم (5)

صدق اللع العظيم

سورة العلق

الآيات1-5

وزارة التعليم العالي والبحث العلمي
جامعة بابل/ كلية العلوم
قسم الكيمياء

تقدير وامتزاز الكلورامفينيكول والكلونازيبام على سطح
النانو المتراكب هايدروجل/Zno/CNT

أطروحة مقدمة

إلى مجلس كلية العلوم – جامعة بابل

وهي جزء من متطلبات نيل درجة الدكتوراه فلسفه في العلوم/ الكيمياء

تقدمت بها

لبنى عبد الحسين عبد الأمير الشيخ

بكالوريوس علوم كيمياء/ جامعة النهرين 2004

ماجـــستير علوم كيمياء/ جامعة النهرين 2007

بإشراف

أ.د. عباس نور محمد الشريفي

أ.د. اياد فاضل محمد القيم

1444 هـ 2023 م